



UNIVERSIDADE DE BRASÍLIA
CAMPUS DE PLANALTINA – FUP
PROGRAMA DE PÓS-GRADUAÇÃO EM CIÊNCIAS AMBIENTAIS

**Mineral formation and element release from aluminosilicate rocks
promoted by maize rhizosphere**

Luise Lottici Krahl

Brasília, DF - Brazil
January 2020



UNIVERSIDADE DE BRASÍLIA
CAMPUS DE PLANALTINA – FUP
PROGRAMA DE PÓS-GRADUAÇÃO EM CIÊNCIAS AMBIENTAIS

**Mineral formation and element release from aluminosilicate rocks
promoted by maize rhizosphere**

Luise Lottici Krahl

Thesis presented at the University of Brasília as
a requirement for earning the degree of Doctor
in Environmental Sciences.

Advisor: Prof. Dr. Éder de Souza Martins
Co-advisor: Dr. Giuliano Marchi

Brasília, DF - Brazil
January 2020



UNIVERSIDADE DE BRASÍLIA
CAMPUS DE PLANALTINA – FUP
PROGRAMA DE PÓS-GRADUAÇÃO EM CIÊNCIAS AMBIENTAIS

**Formação de minerais e liberação de elementos de rochas
aluminossilicáticas promovidas pela rizosfera do milho**

Luise Lottici Krahl

Tese apresentada à Universidade de Brasília
como requisito para obtenção do título de
Doutora em Ciências Ambientais.

Orientador: Prof. Dr. Éder de Souza Martins
Coorientador: Dr. Giuliano Marchi

Brasília, DF
Janeiro de 2020

Ficha catalográfica elaborada automaticamente,
com os dados fornecidos pelo(a) autor(a)

KK89m Krahl, Luise Lottici
Mineral formation and element release from
aluminosilicate rocks promoted by maize rhizosphere / Luise
Lottici Krahl; orientador Éder de Souza Martins; co
orientador Giuliano Marchi. -- Brasília, 2020.
104 p.

Tese (Doutorado - Doutorado em Ciências Ambientais) --
Universidade de Brasília, 2020.

1. Agromineral. 2. Biointemperismo. 3. Rochas
silicáticas. 4. Troca catiônica. 5. Química do solo. I.
Martins, Éder de Souza , orient. II. Marchi, Giuliano , co
orient. III. Título.

ACKNOWLEDGMENTS

Dr. Éder de Souza Martins, the main advisor in this research, for his trust and commitment to developing this project, even in the midst of many challenges - and for sharing his knowledge, friendship, and extreme kindness.

Dr. Giuliano Marchi, co-advisor of this research, for his knowledge and partnership, that were essential for the concretion of this project. I appreciate the time and effort you put into mentoring me.

Dr. José Carlos Sousa-Silva, a remarkable researcher that shared his time and knowledge in very important discussions about the content and the appropriate evolution of this work.

The team of researchers integrated by Dr. Leonardo Fonseca Valadares, Dr. Simone Patrícia Aranha da Paz, and Dr. Rômulo Simões Angélica, for their help with the fundamental lab analyses and results discussions.

University of Brasília, Embrapa Cerrados, Embrapa Agroenergia, and Federal University of Pará, for hosting me during this stage of personal and professional enhancement and enrichment.

CAPES e FAPDF for their financial support.

Juaci Vitória Malaquias for his support during the development of the statistical analyses.

Professor Antônio Felipe Couto Júnior for his support to successfully conclude my doctorate studies.

My colleagues Maria Inês, Mariana Gabos, Douglas Mendes, and Amanda Gonçalves for helping me conducting all the experiments and lab analyses.

My friend Javier Santiago for proof-reading the texts.

My family, for their support, affection, and comprehension.

I specially dedicate this work to:

My husband Herberth, for his partnership, his patience, unconditional support, and love;

My mother Mara Flora, for her example and for encouraging me to follow my dreams;

My fathers, Jones and Sivaldo, for believing in my competence and skills as a researcher and as a professional;

To Manuela, my inspiration and biggest love, as I hope she can find inspiration in this work.

TABLE OF CONTENTS

	Page
RESUMO	i
ABSTRACT	iii
CHAPTER 1. INTRODUCTION	1
Theoretical framework	2
Thesis structure.....	15
CHAPTER 2. SUCCESSIVE OFFTAKE OF ELEMENTS BY MAIZE GROWN IN PURE BASALT POWDER	18
Introduction	19
Material and methods	21
Results and discussion.....	23
Conclusions	29
Tables and figures	30
CHAPTER 3. SILICATE MINERALS AS A SOURCE OF NUTRIENTS TO MAIZE GROWN SUCCESSIVELY	36
Introduction	37
Material and methods	38
Results and discussion.....	41
Conclusions	46
Tables and figures	47
CHAPTER 4 . RHIZOSPHERE OF MAIZE INCREASES WEATHERING RATES AND CHARGE OF SILICATE ROCKS.....	55
Introduction	56
Material and methods	58
Results and discussion.....	61
Conclusions	67
Tables and figures	68
CHAPTER 5 . REMARKS AND FUTURE RESEARCH DIRECTIONS.....	76
Evaluation of the work	76
Future research directions	77
REFERENCES	81
SUPPLEMENTARY MATERIAL	94

RESUMO

A liberação de macro e micronutrientes de aluminossilicatos contribui significativamente para a nutrição das plantas e algumas rochas silicáticas podem, assim, atuar como fertilizantes de liberação lenta. O intemperismo desses minerais pode ocorrer em poucos dias sob a influência da rizosfera e alguns minerais primários formam minerais do tipo 2:1, como vermiculita e esmectita. Esses minerais apresentam características como alta carga permanente e superfície específica, e podem contribuir para a qualidade do solo, especialmente aumentando sua capacidade de troca catiônica. No entanto, a seleção de rochas silicáticas para uso agrícola não depende apenas do teor absoluto de nutrientes, mas da taxa de dissolução dos minerais e liberação dos nutrientes para as plantas. A atividade radicular é um fator determinante nesse contexto pois afeta as taxas de dissolução dos minerais das rochas, mas as taxas de intemperismo dependem do tipo e da proporção de minerais presentes. A maioria das pesquisas sobre rochas silicáticas como agrominerais concentra-se na avaliação agrônômica do rendimento das culturas, porém são necessários novos estudos sobre o processo de intemperismo e a solubilização dos elementos sob a influência das plantas. O objetivo deste trabalho é investigar as taxas de liberação de elementos e os minerais neoformados pelo processo de biointemperismo promovidos pela rizosfera de milho nas rochas basalto, biotita xisto e biotita sienito. Experimentos em vasos foram realizados sob condições ambientais controladas em casa de vegetação. Amostras das rochas puras foram colocadas em vasos de 500 mL e duas plantas de milho foram cultivadas por vaso em conjuntos de três vasos, repetidos por sete ciclos de crescimento sucessivos de 45 dias cada, totalizando 315 dias de ação das raízes. As rochas e as plantas foram avaliadas após cada ciclo de crescimento.

As rochas forneceram nutrientes às plantas em um curto período e as taxas de absorção dos elementos foram descritas por equações. Os elementos K, Ca, Mg, Al, B, Cu, Fe, Mn e Zn foram analisados na matéria seca e associados ao intemperismo dos minerais constituintes de cada rocha. A caracterização mineralógica e química das rochas, incluindo a capacidade de troca catiônica, foi discutida e relacionada à liberação e acúmulo de nutrientes pelas plantas.

No estudo do basalto, a análise de difração de raios-X revelou diopsídio e andesina como os principais minerais da rocha. A esmectita presente no basalto contribuiu para a alta capacidade de troca catiônica. A mineralogia da rocha não se modificou durante o experimento e não foram detectados minerais cristalinos secundários após os sete ciclos

de crescimento do milho. Os resultados indicaram que a dissolução dos minerais do basalto pela rizosfera de milho foi congruente ou formou novas fases precipitadas como amorfos e minerais de baixa cristalinidade. Imagens de microscopia eletrônica de varredura evidenciaram novos componentes amorfos resultantes do intemperismo induzido pela rizosfera. O crescimento do milho e o acúmulo de elementos diminuiu ao longo dos ciclos, provavelmente devido ao intemperismo de superfície e à dissolução de partículas muito pequenas nos ciclos iniciais, onde os nutrientes foram facilmente extraídos.

Embora o biotita xisto tenha apresentado consideravelmente menos K em sua composição que o biotita sienito, as plantas cultivadas no biotita xisto produziram uma quantidade maior de matéria seca e acumularam mais K e Mg. Isso reflete o processo de intemperismo da biotita, condicionado pelos teores de Mg e Fe. O intemperismo da biotita no biotita xisto e no biotita sienito resultou em alterações mineralógicas na difração de raios-X. A mudança mais significativa nos difratogramas ocorreu na fração de tamanho de partícula $< 53 \mu\text{m}$, mas a fração entre $53 - 300 \mu\text{m}$ também apresentou alterações. Uma biotita-vermiculita interestratificada (hidrobiotita) foi observada nas duas rochas, como resultado do intemperismo da biotita e perda de K. Mas nas amostras de biotita sienito, a formação de hidrobiotita foi menor que no biotita xisto. O conteúdo de Mg e Fe(II) na estrutura do mineral biotita no biotita sienito, com alta relação Fe/Mg no sítio octaédrico, explica a menor taxa de formação de hidrobiotita pois a oxidação do Fe(II) da biotita no biotita sienito gerou um ambiente de intemperismo estável, impedindo a continuidade da liberação de K e a formação de cargas.

No biotita xisto, o processo de intemperismo foi responsável por um aumento na capacidade de troca catiônica nas frações de tamanho $< 300 \mu\text{m}$. Esses materiais com maior capacidade de troca catiônica são particularmente importantes para o manejo de solos com pequena capacidade de retenção de cátions, como os Latossolos em ambientes tropicais.

Palavras-chave: agromineral, biointemperismo, disponibilidade de nutrientes, basalto, biotita, troca catiônica.

ABSTRACT

The release of macro and micronutrients from aluminosilicate significantly contribute to plant nutrition. Thus, some silicate rocks could work as slow-release fertilizers. The weathering of these minerals can occur in a few days under the influence of the rhizosphere, and some primary minerals form new 2:1 type minerals, such as vermiculite and smectite, These minerals present characteristics such as high permanent charge and surface area, thus it could contribute to the increase of the soil quality, especially on building up of cation exchange capacity. However, the selection of sources for agricultural use does not depend only on the absolute nutrient content, but rather on the rate minerals dissolve and nutrients are available for plants. The root activity is a determining factor affecting dissolution rates of silicate minerals, but the weathering rates depend on the kind and proportion of minerals it contains. Most of the research on silicate rocks as agrominerals focuses on agronomic evaluation on crop yield, but investigations are required to understand the weathering process and the elements solubilization in a plant growth environment. The objective of this work is to investigate the release rates of elements and the newly formed minerals during the bioweathering of pure crushed rocks – basalt, biotite schist, and biotite syenite – promoted by maize rhizosphere. Pot tests were carried out under controlled environmental conditions in a greenhouse experiment. The pure rocks samples were placed into 500 mL pots, and two plants of maize per pot were grown in sets of three pots, repeated for seven 45-day growth cycles, totaling 315 days of root action. Rock materials and plants were evaluated at each successive growing cycle. The studied rocks provided nutrients to plants in the short term, and the offtake rates of elements were described by equations. The elements K, Ca, Mg, Al, B, Cu, Fe, Mn, and Zn were measured in the dry mass and associated with the weathering of minerals. Mineralogical and chemical characterization of the rocks, including cation exchange capacity, were discussed and were related to the release and offtake of nutrients by plants. In the basalt study, the X-ray powder diffraction analysis showed diopside and andesine as the main minerals of basalt. An amount of smectite was also present and contributed to the high cationic exchange capacity. Basalt mineralogy did not modify during the experiment and there were detected no secondary crystalline minerals after seven maize growth cycles. The dissolution of basalt minerals by maize rhizosphere was congruent or formed new phases precipitated as amorphous phases and low crystallinity minerals. Scanning electron microscopy images evidenced new amorphous components resulting

from rhizosphere-induced weathering. The maize growth and the offtake of elements decreased over the cycles, probably due to the weathering of surfaces and dissolution of very small mineral particles in the initial cycles, where nutrients were easily extractable. In the subsequent cycles, a higher effort seems to be made to extract and acquire nutrients from basalt minerals.

Although biotite schist presented considerably less K in its composition than biotite syenite, plants grown in biotite schist produced a higher amount of dry mass and accumulated more K and Mg. It reflects the weathering process of the biotite mineral, conditioned by Mg and Fe content. The weathering of biotite mineral in biotite schist and biotite syenite resulted in mineralogical changes. The most significant changes in X-ray diffraction patterns occurred in $< 53 \mu\text{m}$ particle size fraction, but the $53 - 300 \mu\text{m}$ fractions also changed. An interstratified biotite-vermiculite mineral (hydrobiotite) was observed for both rocks as a result of biotite weathering and loss of K. For the biotite syenite samples, the formation of hydrobiotite was lower than with biotite schist. The Mg and Fe(II) contents on biotite mineral structure of the biotite syenite, with high Fe/Mg in octahedral site, explain the slow pace of hydrobiotite formation rate because the Fe(II) oxidation in the mineral of biotite in the biotite syenite has generated a stable weathering environment, preventing further K release and the formation of charge.

In the biotite schist, the weathering process was responsible for an increase in the cation exchange capacity in the $< 300 \mu\text{m}$ size fractions. These materials with permanent cation exchange capacity are particularly important for the management of soils presenting small cation retention capacity, such as tropical Oxisols.

Keywords: agromineral, bioweathering, nutrient availability, basalt, biotite, cation exchange.

CHAPTER 1: INTRODUCTION

Selected crushed silicate rocks as agrominerals, in the first moment, is regarded as a primary source of nutrients for plants (Li et al., 2015; Manning et al., 2010; Nunes et al., 2014; van Straaten, 2006). For some highly weathered soils, however, which present low natural fertility and low cation exchange capacity, such as Brazilian Oxisols, the application of these crushed rocks has a broader meaning.

Some silicate rocks contain primary minerals that, after weathering, form new 2:1 type minerals, including vermiculite and smectite (Churchman and Lowe, 2012; Pozzuoli et al., 1992; Schulze, 2002; Wilson, 2004); amorphous phases, and low crystallinity minerals (Singh et al., 2018; Tamrat et al., 2018; Yu et al., 2017). These minerals present characteristics such as high permanent charge and surface area, thus it could contribute to the increase of the soil quality, especially on building up of cation exchange capacity.

For agricultural systems, time is a determinant factor for the broad application of these agrominerals. New evidences (Anda et al., 2015; Basak et al., 2018; Burghilea et al., 2015; Ciceri et al., 2019; Hinsinger et al., 1991; Manning et al., 2017; Mohammed et al., 2014; Naderizadeh et al., 2010; Norouzi and Khademi, 2010) have been showed that, depending on the environmental conditions, some silicate minerals were weathered in a few days and not in hundreds of years as it was believed before. It has been shown that plants have a major role in weathering of primary minerals in the soil, known as bioweathering, by modifying its environment, absorbing and releasing elements, releasing organic substances, and promoting microbial population growth (Hinsinger et al., 1993; Jones, 1998; Uroz et al., 2009; Wang et al., 2011; Yu, 2018). Nevertheless, the dissolution rates of primary minerals under systems containing plants have not been systematically investigated.

The knowledge about the dissolution of these minerals during the bioweathering can lead to a better understanding of the nutrient release rates, the physicochemical characteristics, and the processes involved in mineral transformation under such conditions. This work aims to study the release rates of elements and the newly formed minerals during the bioweathering of pure crushed rocks – basalt, biotite schist, and biotite syenite – promoted by maize rhizosphere.

Theoretical framework

Main characteristics of temperate and tropical agricultural soils

Different mineral weathering processes and rates in temperate and tropical regions occur during the soil formation, depending on factors such as parent rock mineralogy, its reactive surface area, moisture, temperature, abundance of organic compounds, and time of weathering conditions (Berner and Berner, 1997; Wilson, 2004; West et al., 2005). The weathering stage of soils is determined by the mineralogy and the type of minerals which they contain influences its inherent fertility and resilience (Figure 1). As environmental conditions are diverse over time and location, soils formed from similar parent rock would often weather differently, resulting in different characteristics (Schaeztl and Anderson, 2005). Thus, the weathering and climate conditions in temperate and tropical regions promoted different soils which have distinct properties (Berner and Berner, 1997; Burke et al., 2007; West et al., 2005), reflecting on different models of agricultural development (Hartemink, 2002; Figure 2).

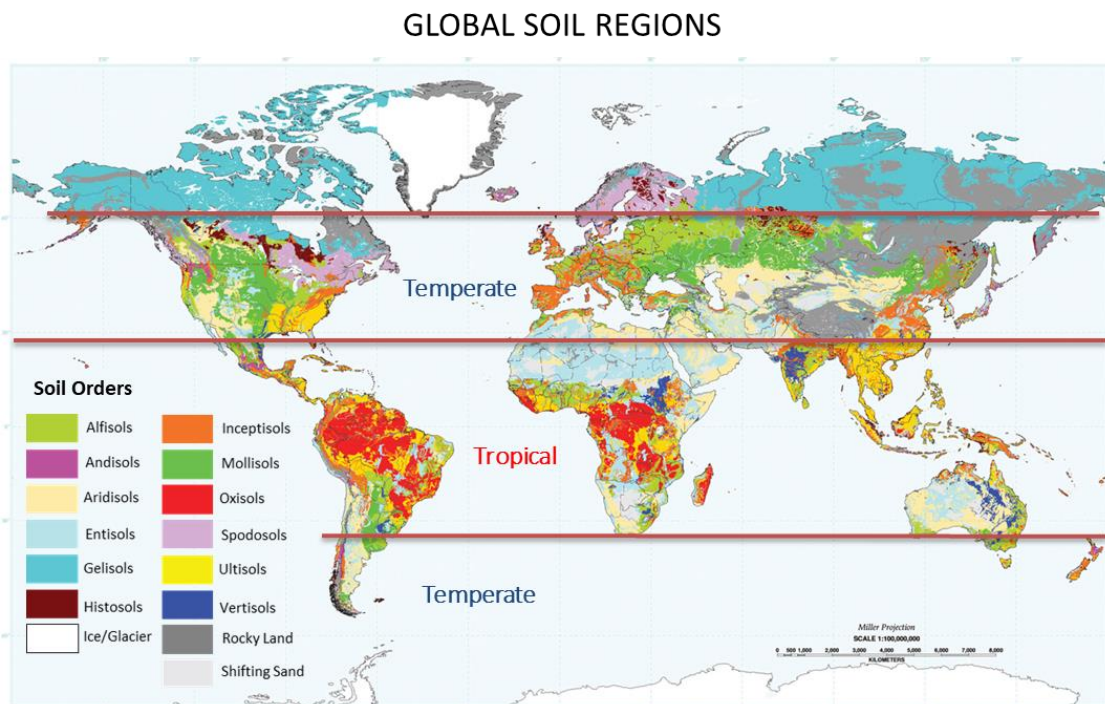


Figure 1. Global soil distribution according USDA system of Soil Taxonomy (Adapted from United States Department of Agriculture – USDA, 2006).

Soils under temperate climate environments were formed from glacial and fluvial-lacustrine deposits developed during Quaternary, on the time scale of 10^3 and 10^4 years.

Extensive temperate agricultural lands are occupied by Mollisols (Figure 1; USDA, 2006), intensively used for agricultural crop because of its high fertility and resilience (Figure 2). The natural areas of occurrence of these soils are the prairies and steppes of the temperate lands. The major part of the 899 million ha of Mollisols in the world occurs in the mid-latitudes of North America, Eurasia, and South America (Liu et al., 2012).

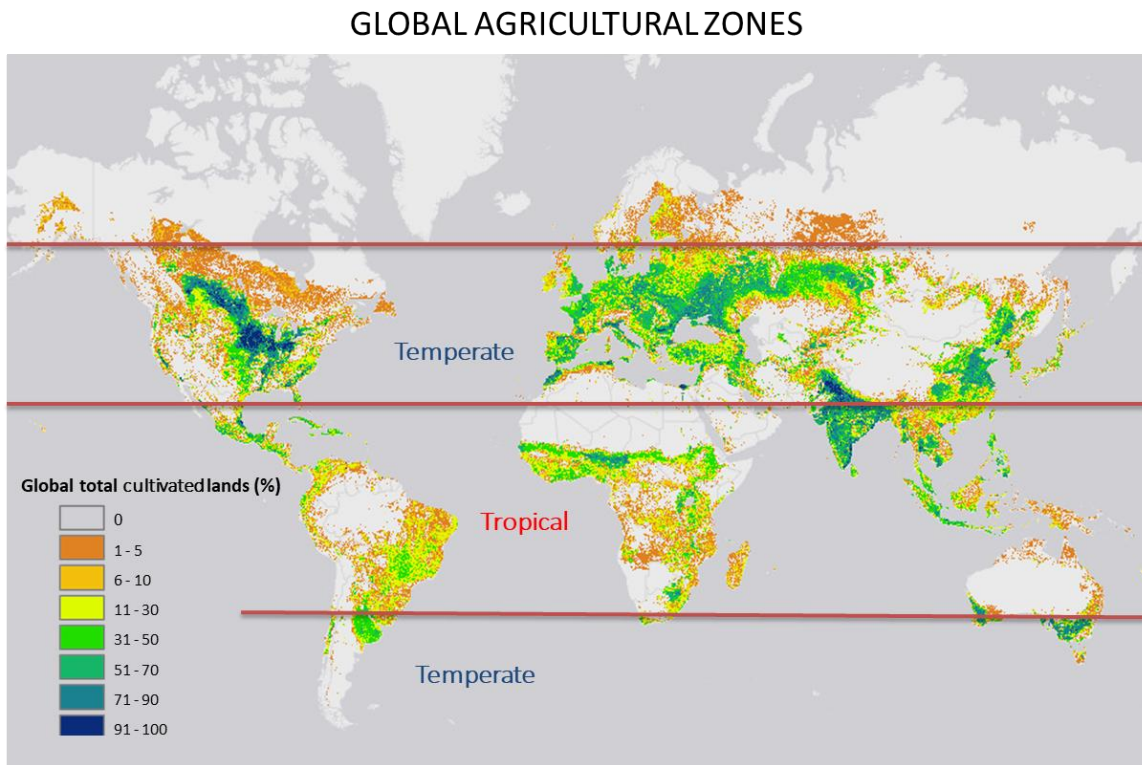


Figure 2. Worldwide agricultural use intensity. (Adapted from Fischer et al., 2008; Land Use Change and Agriculture Program, International Institute for Applied Systems Analysis - IIASA).

The temperate soils have a mineral composition with a predominance of 2:1 clay minerals, which provide a high cation exchange capacity (CEC), associated with high organic matter contents and available cations (Ca^{2+} , Mg^{2+} , K^+) (Figure 3). The 2:1 layer minerals present permanent negative charges due to the isomorphous substitution of silicon or aluminum ions for the lower valence ions. The layers are bonded to the adjacent layer by ionic interactions between the negatively charged layers and interlayer cations (between the 2:1 layers). The interlayer surfaces are accessible to water molecules and ions, and as the interlayer cations are not tightly held in the mineral structure, they are exchangeable and can be displaced. The CEC of the upper profile is derived from organic

matter with pH-dependent charge and clay-sized phyllosilicates having permanent charge (Table 1; Churchman and Lowe, 2012; Sarkar et al., 2018; Singh et al., 2018). In the lower soil profile, the CEC is nearly exclusively from clay-sized phyllosilicates such as smectite, vermiculite, or illite (Liu et al., 2012).

Table 1. Properties of some common soil minerals.

Group Name	Type	Name	Effective Surface Area (m² g⁻¹)	Cation Exchange Capacity (cmol_ckg⁻¹)
Kaolinite	1:1	Kaolinite	6 – 40	0 – 8
Mica	2:1	Illite	55 – 195	10 – 40
Vermiculite	2:1	Vermiculite	600 – 800	120 – 150
Smectite	2:1	Montmorillonite	650 – 800	80 – 120
Al–Si	Noncrystalline	Imogolite and allophane	700 – 1500	pH variable
Al hydroxide, oxyhydroxide, oxide	Non-silicates	Gibbsite	unknow	pH variable
Fe oxyhydroxide, oxide	Non-silicates	Goethite	14 – 77	pH variable
		Hematite	35 – 45	pH-variable
		Ferrihydrite	200 – 500	pH-variable

*Adapted from Churchman and Lowe (2012).

In contrast, most of the soils under tropical conditions were formed by strong weathering process (total hydrolysis) and intense base leaching under moist and warm conditions since Tertiary, within a scale of 10⁶ to 10⁷ years (Figure 1). Silicate clay minerals within these soils are resistant secondary minerals, depleted of available cations and silica (Buol and Eswaran, 2000). The weathering under such conditions typically involves loss of silica from primary and secondary silicate minerals, forming 1:1 type minerals like kaolinite, and iron (Fe) and aluminum (Al) oxides and hydroxides like hematite, gibbsite and goethite (Figure 3).

The structure of the 1:1 layer mineral is composed of a tetrahedral sheet of covalently bonded oxygen ions and an octahedral sheet, with a minimal isomorphic substitution and low CEC (Table 1). These minerals also exhibit a very small charge, as the isomorphic substitution of Si⁴⁺ by Al³⁺ in the tetrahedral layer, or Al³⁺ by Mg²⁺ or

vice versa in the octahedral layer, is minor (Essington, 2003). The Fe and Al oxides and hydroxides present pH-dependent charge and a high anion exchange capacity (AEC) (Uehara and Gillman 1981). Therefore, these soils exhibit high phosphorus absorption capacity (Withers et al., 2018), as well as leaching losses of nutrient cations (Schaefer et al., 2008; Wilcke and Lilienfein, 2005). Besides, the moisture conditions and the high temperatures favor the oxidation of soil organic matter (SOM) (Ogle et al., 2005; Zech et al., 1990), which is responsible for the most of the cation retention in these soils.

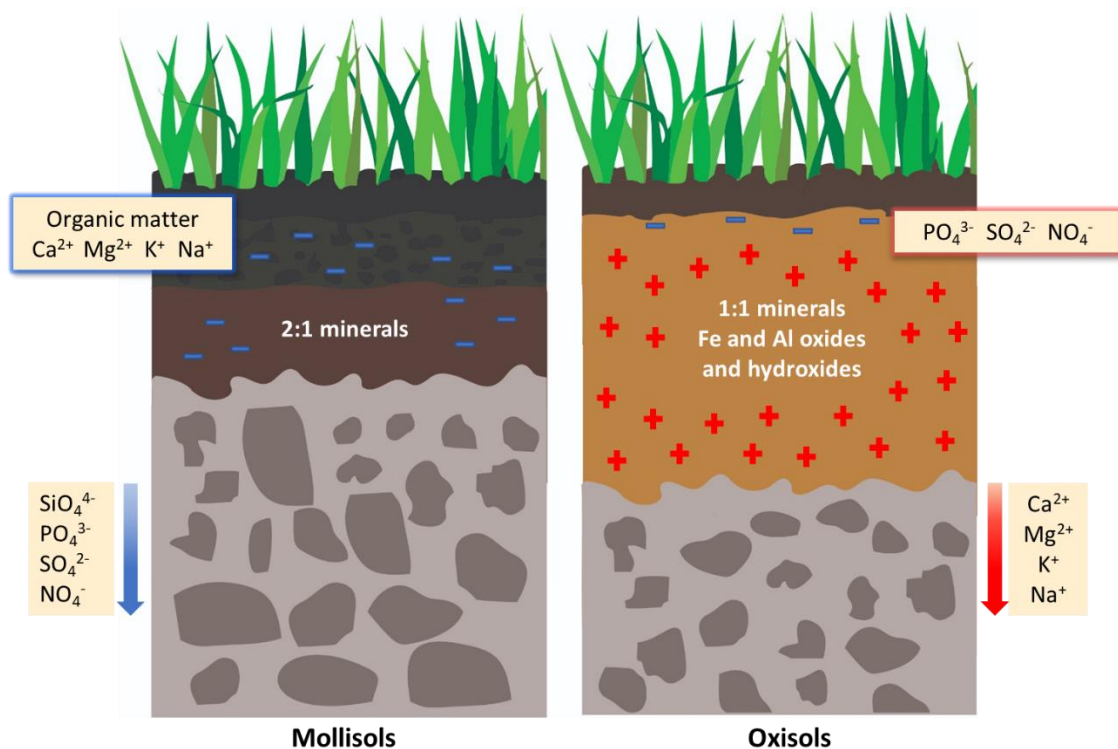


Figure 3. Main characteristics of agricultural soils under temperate climate (Mollisols) and tropical (Oxisols).

One of the most important agricultural soils in tropical regions are the Oxisols. These soils comprise 916 million ha of the tropical land area, typically on low sloping land surfaces of great age that have been stable for a long time (Sanchez, 2019) confers high resilience but low productivity (Figure 2). They represent the most extensive areas of Cerrado, a savannah-like environment. Although most of these soils present inherent low fertility, they are highly productive under correct management (Reatto and Martins, 2005; Wilcke and Lilienfein, 2005). Managing the soil by lime application and adopting practices that avoid organic matter oxidation, increase soil pH and CEC. (Azevedo et al.,

1996; Carvalho et al., 2000; Fageria and Stone, 1999; Goedert, 1983; Kamprath, 1984; Miranda et al., 2005; Resk et al., 2008; Souza et al., 2009; Souza and Lobato, 2002).

Due to the high leaching rates, which are mainly related to monovalent cations like potassium (K^+), repeated applications of nutrients are essential to agricultural productivity, exposing the need for a higher cation exchange capacity to increase production performance.

Farming with silicate agrominerals: existing knowledge and gaps

Large areas of Oxisols in Brazil are now productive grain-growing areas with the development of soil management technology in the late-twentieth-century (Goedert, 1983; Rada, 2013). In spite of tropical soil fertility management was responsible for advances in agriculture in Brazilian Oxisols, it is still necessary strategies to increase CEC in these soils and to improve the efficiency of fertilizers. The use efficiency of K soluble fertilizers in tropical environments is approximately 40% (Baligar et al., 2001). Besides, over 80% of the global potash production is dominated by a few countries - Belarus, Canada, China, Germany, and Russia (Manning, 2015), and Brazil depends on 96% of imported potassium for agricultural development (Gameiro et al., 2019).

A new alternative would be to make use of local natural resources, such as the silicate agrominerals (Basak, 2018; Ciceri and Allanore, 2019; Li et al., 2015; Manning et al., 2017; van Straaten, 2006).

Silicate agrominerals refer to a broad category of primary rocks and minerals that bear elements of agronomic values (Ciceri and Allanore, 2019). These are defined as materials derived from silicate minerals to produce soil remineralizers or fertilizer for agricultural production (Martins et al., 2014). These materials can also be subjected to biological, chemical and/or, physical treatments, which increase the nutrient availability.

Among these materials, one can highlight the silicates to correct acidity and provide nutrients for crops (Anda et al., 2015; Basak et al., 2018; Burghelea et al., 2015, 2018; Ciceri et al., 2019; Madaras et al., 2012; Manning et al., 2017; Mohammed et al. 2014; Norouzi and Khademi, 2010; Nunes et al., 2014; Ramos et al., 2019). Those materials containing phlogopite, biotite or feldspars minerals, also contain potassium in their composition, like some schists and syenites (Basak et al., 2018; Burghelea et al., 2015; Ciceri and Allanore, 2019; Manning et al., 2017), which are widely available in tropical environments (Ciceri et al., 2019; Manning et al., 2017; Navarro et al., 2013). Basic rocks, rich in Fe, Si, Ca, and Mg, such as basalt, are globally available in large quantities and

present a relatively rapid weathering rate (Anda et al., 2015; Lefebvre et al., 2019; Nunes et al., 2014).

Some crushed silicate rocks are known as soil remineralizers because their primary minerals can form new minerals that benefit the physicochemical characteristics of agricultural soils. These include a range of clay minerals such as vermiculite and smectite (Hinsinger et al., 1991; Norouzi and Khademi, 2010), amorphous phases and low crystallinity minerals (such as ferrihydrite) (Colombo et al., 2014; Yu et al., 2017), with large specific surface area (SSA), and higher charge (CEC). The weathering process and the amounts applied along the time can modify soil properties, as a regulator of soil carbon storage, inclusive carbon stabilization and sequestration process in the long term (Kleber et al., 2015; Singh et al., 2017; Beerling et al., 2018, Hartmann et al. 2013).

The investigation of the agricultural potential of silicate agrominerals, however, have almost been guided by the release of nutrients to the soil and by the effects on the production of cultivated plants.

The use of silicate agrominerals in tropical environments, compared to application in temperate environments (Ramezani et al., 2013), can be a viable alternative because the high temperature and moisture of tropical environments increase the rate of mineral dissolution and nutrient release to the soil solution (Bakker et al., 2019; Leonardos et al., 2000; Shirale et al., 2019; van Straaten, 2006). The effects of these rocks depend on diverse factors associated with its mineralogical and chemical composition and particle size, as well as to their interaction with soil and agricultural system components that interfere in the nutrient release process (Harley and Gilkes, 2000; Manning et al., 2010; Zhang et al., 2018).

The greatest part of the waste rock in Brazil is generated as a by-product of mining activities (Lefebvre et al., 2019; Ramos et al., 2015), considered as an environmental liability if left uncleaned or unused. The use of these materials as powder in agriculture could reduce fertilizer costs and the damage to the environment, contributing to sustainable production.

The disadvantage of many rock materials is that they generally contain low nutrient concentrations and low solubility, which can negatively affect the agronomic effectiveness of short term crops, mainly in temperate climates (Ramezani et al., 2013). As the application rate is commonly in the range of several tons per hectare, shipping large amounts of silicate rock fertilizers over large distances is likely uneconomical and environmentally not sustainable (van Straaten, 2006). Therefore, they should be applied

regionally (Leonardos et al., 2000). With the right choice of locally available rock materials for the right soils, these materials have shown to be of benefit to local agriculture (Ciceri and Allanore, 2019; van Straaten, 2006).

Silicates as rock-forming minerals

The weathering of rocks and minerals is a fundamental process in the geochemical cycle, especially for soil formation and its fertility (Wilson, 2004; Hartmann et al., 2013). The knowledge about mineralogy and the dissolution mechanisms of these minerals can contribute to the understanding of the natural distribution of nutrients in the soil and their physicochemical characteristics.

The origin of primary minerals influences their structure and chemical composition and stability against altering (Figure 4). However, environmental factors can affect the chemical reactions and play a decisive role in the rate of the weathering process and products of their alteration (Karathanasis, 2002).

Chemical weathering involves changes related to mineral dissolution and nucleation and the emergence of new phases by chemical and mineralogical changes. The new mineral phases are formed from the residues of the alteration process, with chemical and mineralogical compositions depending on the parent material and the weathering environment (Loughnan, 1969).

The silicate mineral class is a large and fundamental group of minerals. Nearly 90% of the exposed crust of the earth are silicates (Schulze, 2002). Silicates comprise the bulk of most soils, occurring as both primary minerals inherited from igneous or metamorphic rock, and as secondary minerals formed from the weathering products of primary minerals (Churchman and Lowe, 2012; Schulze, 2002; Wilson, 2004). The presence of primary minerals – olivine, pyroxenes, feldspars, micas, and others - is determined by the parent material and could be employed to establish the weathering stage of soil and provide a non-labile pool of some nutrients (Wilson, 2004).

Secondary minerals are those formed through weathering and provide cation and anion exchange sites that control plant nutrients in soil solution (Sanchez, 2019). They result from changes in the primary mineral structure (incongruent reaction), neoformation through precipitation or recrystallization of dissolved constituents into a more stable structure (congruent reaction) (Karathanasis, 2002). These secondary minerals are often referred to as secondary silicates and Fe and Al oxides and hydroxides.

The aluminosilicates and ferromagnesian silicates are major rock-forming minerals and they may be a primary source of many nutrients required for plant growth. Nutrient elements have diverse associations with minerals and are released by a variety of weathering reactions (Harley and Gilkes, 2000).

The main weathering reactions which promote chemical changes and, consequently, changes in the structure and mineralogy of minerals are hydrolysis, hydration, dissolution, and oxidation (Churchman and Lowe, 2012; Wilson, 2004). Regarding the dynamics of silicates, the hydrolysis is the major important dissolution reaction of these minerals. Most silicate dissolution reactions depend on interactions between ions on the mineral surface (Kalinowski and Schweda, 1996). The hydrolysis reactions commonly occur with the release of more soluble components from the mineral. This removal may leave a solid residue which differs in composition from the original mineral, or with a solid alteration product precipitates out of the solution. The solid precipitate will most likely have a different composition and perhaps also a different crystal structure from its antecedent (partly or completely) dissolved mineral (Churchman and Lowe, 2012).

Some elements of the silicate framework can greatly influence the weathering rates and products, being iron (Fe) a key element in this process (Gilkes et al., 1973; Murakami et al., 2003). The most important weathering reactions involve Fe, a component of many of the primary minerals that generally occurs in its reduced form - Fe(II). This is easily converted to their oxidized form - Fe(III) - sets up a charge imbalance, leading to a loss of other ions from the mineral structure, which can destabilize the minerals (Tombolini et al., 2012). It occurs in ferromagnesian minerals such as biotite, amphiboles, pyroxenes, and olivine (Wilson, 2004).

The crystallization order of minerals in igneous or metamorphic rock generally determines their susceptibility to weathering (Figure 4). Olivine is one of the primary minerals of several igneous, basic and ultramafic rocks, coexisting with plagioclases and pyroxenes (Oelkers et al., 2018). Olivine dissolution mechanism is less complex than most other naturally occurring multi-oxide silicates and it is rapidly altered by weathering (Figure 4; Table 2). In the surface environment, unstable olivines easily lose Mg^{2+} , Fe(II) (or Mn^{2+}) and could originate a variety of secondary mineral products, including smectite, kaolinite, halloysite, and various oxides, hydroxides, and oxyhydroxides of Fe (Churchman and Lowe, 2012; Wilson, 2004).

Pyroxenes and amphiboles, which are slightly more stable than olivine, tend to weather similarly to the olivine, with an initial loss of their divalent cations, typically Mg^{2+} , Ca^{2+} and $Fe(II)$ (Table 2; Churchman and Lowe, 2012; Schulze, 2002). Pyroxenes form the most important group of ferromagnesian minerals in rocks. They occur in almost all types of igneous rocks and in metamorphic rock varieties, such as basalts. The susceptibility of basalt minerals to weathering generally follows the sequence, according to Bowen reaction series: glass > olivine > pyroxene > amphibole > plagioclase > K-feldspar > quartz (Bowen, 1928; Eggleton et al., 1987), and the changes resulting from the loss of Ca^{2+} , Mg^{2+} , and Si^{4+} , oxidation of $Fe(II)$ and hydration. Ultimately, all these minerals can alter to a mixture of allophane, iron oxide-hydroxide, and clay minerals such as smectites (Deer et al., 2013). The ferromagnesian minerals present in basaltic rocks form pseudomorphs of trioctahedral smectite, whereas plagioclase alters to pseudomorphous dioctahedral smectite.

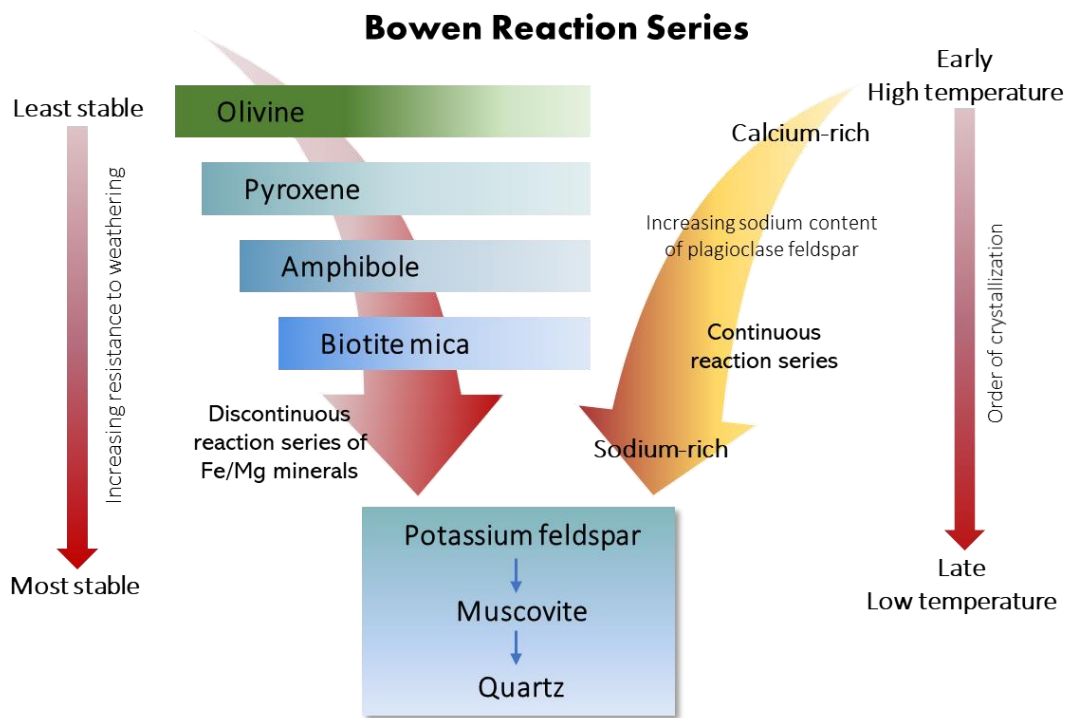


Figure 4. Illustration of the Bowen reaction series (Bowen, 1928), which shows the order of mineral crystallization, indicating that minerals formed at low magma temperatures are more stable in the terrestrial environment than minerals formed at high magma temperatures.

The feldspars minerals are the most abundant constituents of silicate rocks (Deer et al., 2013), and they are classified as the potassium feldspars - orthoclase and microcline, and the plagioclase series - albite, oligoclase, andesine, labradorite, bytownite, and anorthite. Potassium feldspar is a K-bearing mineral widely found in soils and rocks (Table 2). But it is regarded as inert on the short timescale given its resistance to weathering, as determined by the mineral structure with a 3-dimensional network of Si and Al coordinated tetrahedrally with oxygen (Harley and Gilkes, 2000; Schulze, 2002).

Table 2. Structure and chemical formula of common primary silicate minerals, in order of decreasing stability.

Minerals	Group name	Structural type	General formula
Olivines	Isolated tetrahedra	Nesosilicates	(Mg,FeII) ₂ SiO ₄
Pyroxenes	Single chains	Inosilicates	(Ca,Na)(Mg,Al,Fe)(Si,Al) ₂ O ₆
Amphiboles	Double chains	Inosilicates	(Ca,Na) _{2.3} (Mg,Fe,Al) ₅ (Si,Al) ₈ O ₂₂ (OH) ₂
Micas	Layer	Phyllosilicates	Muscovite KAl ₂ (AlSi ₃)O ₁₀ (OH) ₂ Biotite K(Mg,FeII) ₃ AlSi ₃ O ₁₀ (OH,F) ₂
Feldspars	Framework	Tectosilicates	Plagioclases (Na,Ca)(Si,Al) ₄ O ₈ K-feldspar KAlSi ₃ O ₈
Quartz	Framework	Tectosilicates	SiO ₂

*Modified from Churchman and Lowe (2012).

A huge amount of work has been done on the weathering of mica minerals because of their importance as a potential source of K in the soil for plants. Trioctahedral micas, such as biotite and phlogopite, are more susceptible to weathering than dioctahedral micas (Table 2), including muscovite and most illite (Figure 4).

Biotite is commonly found in granitic rocks and metamorphic rock. This mineral is a 2:1 trioctahedral mica with a high degree of isomorphic substitution - Si⁴⁺ by Al³⁺ and Fe³⁺ in tetrahedron site or Al³⁺ by Mg²⁺ in octahedron sites, and K⁺ in the interlayer region. Biotite weathering occurs both by solid-state alteration and dissolution/precipitation mechanisms. The chemical composition of biotite, especially the Fe and Mg content, lead to different weathering rates (Gilkes et al., 1973; Murakami et al., 2003). Biotite weathering occurs both by solid-state alteration and dissolution/precipitation mechanisms. The products of these weathering reactions are

hydrobiotite, vermiculite, smectite, chlorite, hydroxy-interlayered vermiculite, gibbsite or kaolinite, depending on the alteration conditions (Pozzuoli et al., 1992; Wilson, 2004; Schulze, 2002). The main mechanism is the oxidation and loss of Fe(II) and other small cations like Mn^{2+} and Mg^{2+} , with subsequent release of K from the interlayers to form hydrobiotite and subsequently vermiculite, which involves only a structural adjustment. Fe- and Al-minerals can precipitate between altered biotite layers and at the edge (Murakami et al., 2003).

Changing time scales: the bioweathering

Rock dissolution and soil formation in natural systems occur on a geological time scale, depending on the intensity of soil formation factors (Hartmann et al., 2013; White and Brantley, 1995). The dissolution kinetics in laboratory diluted aqueous solutions is very low, ranging from 10^4 to 10^7 years for the transformation of primary to secondary minerals (Lasaga, 1995; Palandri and Kharaka, 2004). Experimental weathering rates for silicate minerals are commonly two to four orders of magnitude faster than natural field-derived rates (White and Brantley, 2003). At these rates, aluminosilicates would have no effect on agricultural processes.

However, newly emerging evidence indicates that these rocks may present relatively fast dissolution rates as affected by plants, being able to release nutrients for crops (Basak et al., 2018; Burghelea et al., 2015; Li et al., 2015; Manning et al., 2017; Wang et al., 2000). The weathering of silicate minerals by the action of rhizosphere and their associated organisms, named biological weathering or *bioweathering*, in addition to releasing nutrients, has the potential to form 2:1 clay minerals and low crystallinity minerals during the annual crop cycle time scale, from 10^0 to 10^1 years (Hinsinger et al., 1991; Mohammed et al. 2014; Naderizadeh et al., 2010; Norouzi and Khademi, 2010).

The term *rhizosphere* is defined as the volume of soil influenced by root activity (Uroz et al., 2015). It is a biogeochemical hotspot with microbial activity, soil organic matter production, mineral weathering, and secondary phase formation. According to this broad definition, the size of the rhizosphere may extend well beyond the first millimeters of soil adhering to plant roots when one considers the uptake of water and mobile nutrients (Jones, 1998; Uroz et al., 2015; van Dam and Bouwmeester, 2016; White et al., 2017).

Plant-induced weathering rates of silicate rocks depend on the type and proportion of minerals the rock contains. The recent literature suggests that minerals, in soils and elsewhere, favors the development of specific microbial communities according to their

mineralogy, nutritive content, and weatherability (Uroz et al., 2015). In the soil environment, plants rhizosphere and their associated soil microbial populations increases dissolution rates of minerals, particularly through their effects in generating acidity, absorbing and releasing elements and low molecular weight organic acids (Hinsinger et al., 1993; Jones, 1998; Kong et al. 2014; Uroz et al., 2009; White et al., 2017; Yu, 2018). These root activities result in either the accumulation or depletion of the ions contained in the soil solution in the rhizosphere. The nature and intensity of the changes in ionic concentrations depend on the requirements by the plant and the supply by the soil.

Besides, root exudates of organic acids and enzymes, for instance, can contribute a significant proportion of the supply of major nutrients for plants, acting as important drivers of silicate weathering (Bray et al., 2015; Kong et al., 2014; Li et al., 2014; Machado et al., 2016). The secretion of organic acids by plants and microorganisms can alter the structure of some minerals, such as potassium feldspar and biotite (Figure 5), releasing elemental nutrients and altering the environmental chemistry.

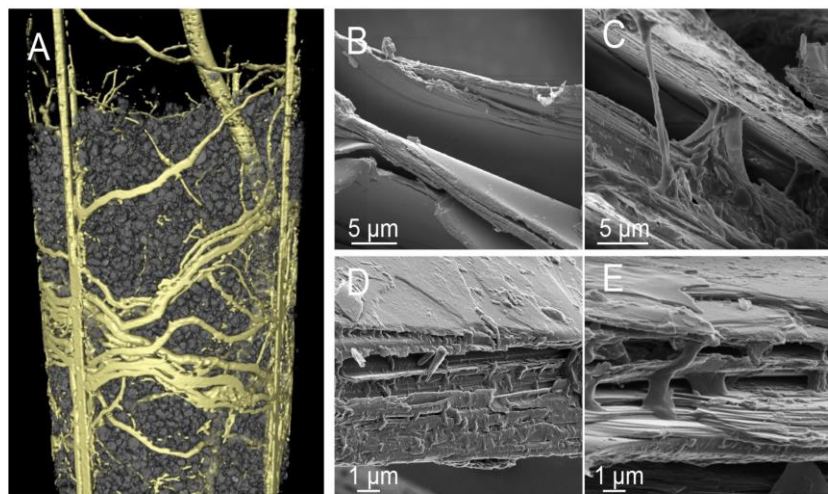


Figure 5. (A) X-ray computed tomography image of a reconstructed column with roots and minerals reconstruction. (B) Image of microscopy from biotite edge: the starting material without any organic residue. (C,D,E) with freshly formed organic material that originated from the root exudates and microbial activity. Notice the bacterially-produced amorphous organic material intercalated between the phyllosilicate layers, facilitating the mineral weathering (Source: Dohnalkova et al., 2017).

Typically roots contain many organic acids varying in chain length with lactate, acetate, oxalate, succinate, fumarate, malate, citrate, isocitrate, and aconitate being the primary anion components. Concentrations of organic acids in soil solution normally range from 0,1 $\mu\text{mol L}^{-1}$ to 0,1 mmol L^{-1} but can exceed 50 mmol L^{-1} at the root surface (Jones et al., 1996). Similarly, the exudation of phytosiderophores by roots, especially of some grass species, plays a significant role in the acquisition of poorly mobile micronutrients such as iron and many other metals (Burghelea et al., 2015).

Some attempts have been made to investigate the effect of plant types on rock and minerals in field and laboratory experiments as: muscovite and/or biotite (Basak et al., 2018; Burghelea et al., 2015; Hinsinger et al., 1991; Mohammed et al. 2014; Naderizadeh et al., 2010; Norouzi and Khademi, 2010); glauconite (Franzosi et al. 2014; Rudmin et al. , 2018); K-feldspar (Ciceri et al., 2019; Manning et al., 2017; Ramos et al., 2019); waste micas (Madaras et al. 2013; Singh et al., 2014); basalt powder (Akter and Akagi, 2005; Anda et al., 2015; Hinsinger et al., 2001; Shafar et al., 2017) and gneiss (Wang et al. 2000). Most of these researches focus on nutrient release from rocks and minerals and plant response.

The importance of silicate sources, however, extends beyond nutrient availability alone (Anda et al., 2015). Plant-induced weathering rates depend on the rocks mineralogy, soil characteristics and crop species (Burghelea et al., 2015; Harley and Gilkes, 2000; Mohammed et al. 2014; Wang et al; 2000). These determine the type and proportion of newly formed minerals. One complication in the agrominerals dissolution study is that some minerals are subject to a variety of possible transformation into other minerals (chlorite, vermiculite, smectite, amorphous phases, and low crystallinity minerals) or dissolution of the bulk mineral. Besides, the rocks are heterogeneous and have complex and relatively unknown compositions, especially regarding their behavior in agricultural systems (Harley and Gilkes, 2000; Li et al., 2015; Nunes at al., 2014; Ramos et al., 2015; Zhang et al., 2018).

Chemical and mineralogical characterization of silicate rocks as agrominerals, therefore, is essential for understanding its potential benefits to agricultural soils and crops, as well as the evaluation of the rhizosphere effects of the cultivated plants on nutrient release and the structural transformation processes in these minerals.

The understanding of the mechanism of silicate dissolution by rhizosphere remains incomplete, as well as their bioweathering products (Basak et al., 2017; Li et al., 2014). Minimal information is available regarding chemical alteration and negative charges by

weathering from the perspective of plant nutrition. The influence of different size fractions on the elements release pattern for meeting the plant demands is also not fully understood (Harley and Gilkes, 2000). Considering that the formation of new mineral stages can increase negative charge (CEC), the proposition is that the successive application of silicate agrominerals and the rhizosphere weathering process by cultivated plants generate emergent properties. That could improve soil physical and chemical properties throughout time, especially in highly weathered soils, devoid of nutrients, such as Oxisols. From medium to long term, this practice could lead to the development of resilient, sustainable, and high productivity anthropogenic soils.

Thesis structure

Most of the silicate agrominerals research focuses in agronomic evaluation on crop yield. Further investigations are required to understand the weathering process and the solubilization of elements in a plant growth environment and whether this process can produce crystalline or amorphous secondary minerals with potential benefits to soils.

The objective of this work is to investigate the bioweathering process promoted by rhizosphere in pure silicate rocks and the newly formed materials, a subject not yet well elucidated. The focus lies on the mineral changes, particularly crystalline phases, and the elements offtake by plants after successive crops of maize (*Zea mays* L.). We also characterized the rock materials.

The rocks used in the study were: basalt, biotite schist (BSC), and biotite syenite (BSY). The basalt sample was collected from piles located at Araguari, Minas Gerais State, Brazil (Moraes et al., 2018). It is a by-product that originated from the production of gravel for civil construction. The BSC was collected from residue piles in quarries located at Abadiânia, state of Goiás, Brazil (Navarro et al., 2013), and BSY was collected at Ceraíma massif, in the southeastern of the state of Bahia, Brazil (Cruz et al., 2016).

A single experiment was conducted under controlled environmental conditions in a greenhouse at Embrapa Cerrados, Planaltina – Brazil (Figure 6), starting in April 2016. The pure rocks samples were placed into 500 mL pots, and two plants of maize per pot were grown in sets of three pots, repeated for seven growth cycles, totaling 63 pots (21 pots of each rock). Seven extra pots of each rock without plants were prepared as a control treatment. Each growth cycle was 45 days.

At the end of each 45 days cycle, whole plants from all pots were harvested and analyzed. The rock content from one set of three pots of each rock previously grown with plants, and another, from one pot of the control set, were removed from the greenhouse. The pots content was used for the laboratory analyses. The remaining sets were re-sown for a new growth cycle.

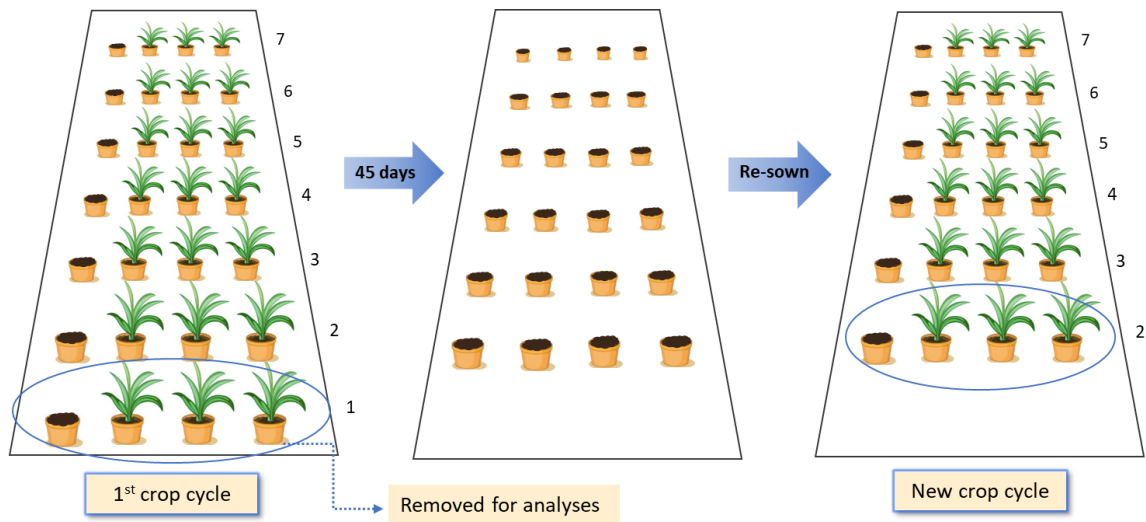


Figure 6. Design of the greenhouse experiment at Embrapa Cerrados, Planaltina - Brazil.

The rocks materials were characterized before and after every crop cycle. The mineralogical composition of samples was analyzed by X-ray diffraction analysis (XRD). The main chemical elements in the rocks were analyzed using wavelength dispersive X-ray fluorescence (XRF) spectroscopy and by inductively coupled plasma-optical emission spectrometry (ICP-OES). The morphology of the samples was examined by scanning electron microscopy (SEM), and the CEC was determined by BS EN ISO 11260 (2011) method.

Major (K, Ca, Mg, Al and Fe) and minor elements (B, Cu Mn, and Zn) in maize dry biomass (total dry mass comprising shoots and roots) were determined by ICP-OES.

The results are organized and presented in three independent chapters as they were submitted as articles to the journals (Chapters 2, 3 and 4). The specifications of the equipment and the detailed analytical conditions are described in the papers.

The Chapter 2 presents the treatment with basalt, an igneous rock with the potential to supply calcium and magnesium and with very different mineralogy from the other studied rocks. Chapters 3 and 4 are devoted to the biotite bearing rocks BSC and

BSY. They are rocks with biotite from metamorphic and igneous origins, respectively, both having potential to provide especially potassium.

These results chapters are presented according to the subject as:

CHAPTER 2. “Successive offtake of elements by maize grown in pure basalt powder”. In this chapter the chemical and mineralogical composition of the basalt is investigated, as well as the elements offtake by maize during the successive crop cycles. The offtake rate of elements from basalt is described by equations. The chemical and mineralogical characteristics of basalt are also discussed and related to both nutrient release and offtake by plants. The results indicate that the basalt provides nutrients to the plants and exhibits cation exchange capacity, especially important for highly weathered soils presenting low cation exchange capacity like Oxisols.

CHAPTER 3. “Silicate minerals as a source of nutrients to maize grown successively”. The chapter addresses the characterization of BSC and BSY, and the extraction of elements by maize plants. This approach begins by discussing the chemical and mineralogical composition of rocks and the implication for the weathering process. The remainder of the chapter describes the offtake rate of macro and micronutrients by maize in the successive crops, allowing to identify the weathering process of minerals and to relate to the composition of each rock. The potential of rocks as a source of nutrients is identified.

CHAPTER 4. “Rhizosphere of maize increases weathering rates and charge of silicate rocks”. The chapter focuses on the mineralogical transformations and weathering products of BSC and BSY, as affected by the rhizosphere of maize. The distinction among biotite minerals of each rock is drawn. Differences in the weathering processes of rocks are evaluated, addressing the magnesium and iron contents of each type of biotite. The study provides knowledge about the newly formed mineralogical stages and the impact of bioweathering on cation exchange capacity. The increased cation exchange capacity is demonstrated experimentally, and the results support the use of silicate minerals as soil remineralizer.

The aluminosilicates studies developed here indicate research directions for the future as the use as agrominerals (Chapter 5). The outlined strategy here connects research in agriculture, mineralogy, and environmental sciences which can collaborate to the successful implementation of the silicate agrominerals in the soil quality context.

CHAPTER 2. SUCCESSIVE OFFTAKE OF ELEMENTS BY MAIZE GROWN IN PURE BASALT POWDER

Luise Lottici Krahl^{a*}, Simone Patrícia Aranha da Paz^b, Rômulo Simões Angélica^b, Leonardo Fonseca Valadares^c, José Carlos Sousa-Silva^d, Giuliano Marchi^d, Éder de Souza Martins^d

^a Universidade de Brasília, Área Universitária, 01, Vila Nossa Senhora de Fátima, CEP: 73345-010 - Planaltina - DF, Brazil. E-mail: luisekrahl@yahoo.com.br

^b Universidade Federal do Pará, Instituto de Geociências, Caixa Postal 1611, CEP: 66075-110, Belém - PA, Brazil. E-mail: paz@ufpa.br, angelica@ufpa.br

^c Embrapa Agroenergia, Parque Estação Biológica - PqEB s/n°. Caixa Postal 40.315, CEP: 70770-901 - Brasília - DF, Brazil. E-mail: leonardo.valadares@embrapa.br

^d Embrapa Cerrados, Rodovia BR-020, Km 18, Caixa Postal 08223, CEP: 73310-970 – Planaltina - DF, Brazil. E-mail: jose.sousa-silva@embrapa.br, giuliano.marchi@embrapa.br, eder.martins@embrapa.br

*Corresponding author.

E-mail address: luisekrahl@yahoo.com.br (L.L. Krahl).

Chapter published as an article in *African Journal of Agricultural Research*.

Abstract - Basalt powder wastes from mining activities have potential to be used as a natural fertilizer. Basalt minerals in agricultural soils may release plant nutrients and increase soil negative charge. In this work, the weathering of a basalt promoted by maize rhizosphere was investigated. We studied the chemical and mineralogical composition of basalt, including cation exchange capacity, as well as the rate of elements offtake by maize grown in a pure basalt powder during seven successive growth cycles. A pot experiment was carried out under controlled environmental conditions; plant and rock materials were evaluated at the end of successive growth cycles. X-ray powder diffraction analysis showed diopside and andesine as main minerals of basalt, and smectite. Scanning electron microscopy images evidenced new amorphous components resulting from rhizosphere-induced weathering. The elements K, Ca, Mg, Al, B, Cu, Fe, Mn and Zn were measured in plant tissue, and related to the weathering of basalt minerals. The studied

basalt, therefore, provides nutrients to plants and exhibits physicochemical properties, such as cation exchange capacity, especially important for highly weathered soils presenting low cation exchange capacity, such as Oxisols.

Keywords: bioweathering, natural fertilizer, mining waste, basalt minerals, cation exchange, nutrient availability.

Introduction

Some silicate minerals contain high concentration of nutrients, which are required by plants for growth. These minerals have been used as agricultural fertilizers, releasing its nutrients slowly (Ciceri and Allanore, 2019; Manning et al., 2017; Zorb et al., 2014). In the recent years, many studies where mining by-products were applied to soils have emerged, turning mining waste in products as a soil fertilizer or remineralizer. The approach is an attempt to reduce agricultural costs and dependence on imported fertilizers. Many works showed positive results for crop productivity and increases in soil quality, whereby basalt powder, for its composition and abundance in spread areas over the world, may assist massively in quality building of soils (Anda et al., 2015; Nunes et al., 2014; Silva et al., 2017). In Brazil, an existing network of basalt quarries, already producing construction aggregates at low cost, has the potential to supply crushed material to agricultural regions (Lefebvre et al., 2019).

Basalts are among the most studied rocks because it provides nutrients for plants, especially calcium (Ca), magnesium (Mg), potassium (K) and micronutrients, such as boron (B), copper (Cu), manganese (Mn) and zinc (Zn) (Anda et al., 2015; Chaturika et al., 2015; Ramos et al., 2015). Plants rhizosphere and their associated microbial populations play a major role in the silicate minerals weathering (bioweathering) by increasing acidity, absorbing and releasing elements and organic ligands, as well as siderophores (Burghelea et al., 2015). Plant roots, ultimately, contribute to increase the dissolution rates of Ca and Mg silicates present in basaltic minerals (Akter and Akagi, 2005; Anda et al., 2015; Hinsinger et al., 2001; Silva et al., 2017).

Basalt minerals undergo a congruent dissolution whenever its bulk chemical composition is rich in iron (Fe), and alkaline earth elements, such as Mg and Ca (Silva et al., 2017). The susceptibility of basalt minerals to weathering, generally follows the sequence: glass > olivine > pyroxene > amphibole > plagioclase > K-feldspar (Eggleton et al., 1987). The Fe(II) oxidation is a driving force in primary mineral weathering

(Essington, 2003). As an intermediate step, at an early stage of weathering of basic silicate minerals, the rapid oxidation of Fe(II) can form amorphous phases and low crystallinity minerals, such as ferrihydrite (Colombo et al., 2014; Yu et al., 2017), which is formed from solution precipitates. In time, the weathering of these minerals may become a mixture of ferrihydrite, iron oxide-hydroxides and clay minerals. Some phases may be slowly recrystallized forming secondary minerals. During weathering some of the basalt minerals may be converted into smectites. Ferromagnesian minerals form trioctahedral smectite, whereas plagioclase alters to dioctahedral smectite.

In weathered basalts, pyroxenes also weather via a mechanism involving a high degree of structural inheritance. The mechanism can be induced by grinding particles to an ultra-fine size (Berner and Schott, 1982). When the surface of these particles, in diopside, suffers cation depletion followed by deprotonation, an incongruent dissolution takes place, and secondary minerals, normally smectite, are formed (Berner and Schott, 1982).

The application of a finely ground basalt in a highly weathered soil increases its cation exchange capacity. Anda et al. (2015) verified, after a high dose (80 t basalt ha⁻¹) was applied in a Malaysian Oxisol, a sharp increase in the soil's net negative charge from 1.5 to 6.3 cmol_c kg⁻¹ in a 12-month incubation period, and to 10.1 cmol_c kg⁻¹, after 24 months. The increasing net negative charge rate suggest that smectite like minerals or low crystallinity minerals, which is a source of permanent negative charge, were formed. An increase in permanent negative charge in Oxisols is an invaluable gain for its quality. However, basalt composition is very dissimilar among different source locations and its charge contribution to soils, as well as rate of transformation or dissolution will depend on the basalt composition and texture, and on abiotic and biotic conditions.

Most natural tropical soils - such as Brazilian Oxisols - due to the strong weathering and intense leaching processes, become acidic, with low fertility and low cation exchange capacity. Thus, the management of these soils with crushed rocks should be focused on increases surface charge characteristics and cation retention. We believe that crushed basalt applied to agrosystems release beneficial elements for crop growth and generate new negative charge sites in the soil. Hence, the knowledge of physicochemical properties of basalt powder and how the rhizosphere of cultivated plants affects the weathering of basalt minerals, is a requirement to understand its potential benefits to agricultural soils. The aim of this work is to investigate changes in the

chemical and mineralogical composition of basalt powder, including cation exchange capacity, as affected by the rhizosphere of maize, as well as the rate of elements offtake.

Material and methods

Sampling

A basalt sample was collected from piles located at Araguari, Minas Gerais State, Brazil (Moraes et al., 2018). This is a by-product originated from the production of gravel for civil construction. The sample was air-dried and was homogenized using the cone-and-quartering reduction method (Campos and Campos, 2017). This procedure was repeated several times to ensure complete homogenization of material, forming the bulk sample.

Greenhouse experiment

The pure bulk basalt sample was placed into 500 mL pots under controlled environmental conditions in a greenhouse. Two plants of maize (*Zea mays* L.) per pot were grown in sets of three pots, repeated for seven growth cycles, totaling 21 pots. Each growth cycle was 45 days. Seven extra pots without plants were prepared, as a control treatment. At every two days, all pots were watered with deionized water. Pots were fertilized with nutrient solution ($92.76 \text{ mg pot}^{-1} \text{ NH}_4\text{H}_2\text{PO}_4$) in the 15th and 30th days of growth of each cycle.

At the end of each 45-days cycle, whole plants from all pots were harvested. The basalt content from one set of three pots previously grown with plants, and another, from one pot of the control set were removed from the greenhouse. The pots content was used for the laboratory analyses. The remaining sets were re-sown for a new growth cycle.

Plant analyses

The harvested plants were oven dried at 65 °C until constant weight. The dry biomass was taken. Major (K, Ca, Mg, Al, Fe) and minor elements (B, Cu, Mn e Zn) in dry biomass (total dry mass comprising shoots and roots) were extracted by $\text{HNO}_3:\text{HClO}_4$ in a digestion block, according to Embrapa (2017) and determined by inductively coupled plasma-optical emission spectrometry (ICP-OES).

Elements offtake (plant element concentration x dry mass) along the cycles were modelled and the equations were selected according to the analysis of variance (ANOVA)

(Supplementary material; Figures S1 and S2; p-values for the coefficients: ** $p < 0.01$) and, thereafter, were tested for normality (Shapiro-Wilk) and constant variance test (homoscedasticity), considering p-values < 0.05 significant. These statistical analyses were performed using Sigma Plot 12.0 software (Sigma Plot Software; San Jose, California, USA).

Dry mass and elements offtake from all crop cycles were analyzed by Principal Component Analysis (PCA), using standardized scores. The RStudio software (version 3.4.0) was used along with its PCA packages FactoMineR and factoextra.

Rock material analyses

The basalt pots removed from the glasshouse at the end of each growth cycle were dismantled and its contents were wet sieved to obtain four size fractions: $< 53 \mu\text{m}$, 53-300 μm , 300-1000 μm and $> 1000 \mu\text{m}$.

The main chemical elements of basalt were analyzed using the multi-acid solution method, where: 500 mg of sample was digested in 2:3:2:1 ratio of HCl:HNO₃:HF:HClO₄; 10:15:10:5 mL, respectively, and determined by ICP-OES (SGS Geosol Laboratórios Ltda). Major elements were determined by wavelength dispersive X-Ray Fluorescence (XRF) spectroscopy, on fused glass discs, 40 mm-diameter, prepared from 0.8 g of sample powder mixed with 4.5 g lithium tetraborate flux and fused in Pt-5% Au crucibles at 1120 °C (SGS Geosol Laboratórios Ltda) (Supplementary material; Table S1). The analysis was handled according to certified quality management system ABNT NBR ISO 9001:2008. The loss on ignition was determined after heating samples overnight at 105 °C to remove water. The weight loss was measured after calcination of samples at 1,000 °C for approximately 2 hours.

The mineralogical composition of fractions $< 53 \mu\text{m}$ was analyzed by X-ray diffraction analysis (XRD) using a PANalytical Empyrean (PW3050/60) diffractometer, using the powder method in the range of $5^\circ < 2\theta < 75^\circ$. CoK α radiation (40 kV; 40 mA) was applied, and the 2θ scanning speed was set at $0.02^\circ \text{ s}^{-1}$. Data was acquired using the software X'Pert Data Collector 4.0 and the data were treated on X'Pert HighScore 3.0 (PANalytical). Minerals were identified by comparing the obtained diffractogram with the ICDD-PDF (International Center for Diffraction Data) database.

The X-ray diffraction patterns of the clay fraction (oriented sample) were obtained three times: the first was air-dried, the second was after treatment with ethylene glycol,

and the third was after heating at 550 °C for 2 h. The information obtained provided the types of clay minerals.

The mineralogical composition in each basalt size fraction was estimated by the stoichiometric method, also known as rational calculation, which is based on the relationship of the experimental chemical composition with the chemical formulas of the minerals, establishing logical considerations based on the qualitative (XRD) and quantitative (XRF) analytical data. An already well-known software used to perform the rational calculation is the ModAn (Paktunk, 1998), which was used in this work.

The morphology of the basalt bulk samples was examined by scanning electron microscopy (SEM) using a Zeiss field emission microscope model SIGMA HV using the InLens detector. A thin conductive layer of gold (10 nm) was deposited over the samples using the Q150T-ES sputter (Quorum Technologies). The chemical composition of selected mineral particles was evaluated by Energy-dispersive X-ray spectroscopy (EDS).

Cation exchange capacity on the fractions < 53 µm was determined by magnesium sorption (BS EN ISO 11260, 2011). Measurements of the CEC followed the methodology: 3.5 g of sample were placed in 50 mL polyethylene tubes, and leached with 30 mL 0.1 mol L⁻¹ barium chloride dihydrate for 1 h. Tubes were centrifuged and the supernatant was removed. The procedure was repeated three times. Samples were, then, equilibrated with 30 mL 0.01 mol L⁻¹ barium chloride solution, and shaken for 12 h. Tubes were centrifuged and the supernatants were removed. Subsequently, 30 mL 0.02 mol L⁻¹ magnesium sulfate heptahydrate was added and shaken for 12 h. Tubes were centrifuged and supernatant was collected for analysis. The excess magnesium was determined by flame atomic absorption spectrometry (FAAS AA-6300 Shimadzu). Triplicates were used.

Results and discussion

The X-ray fluorescence (XRF) analysis showed that the chemical composition in basalt fractions (Table 1) was nearly uniform (Tables 2 and 3). The amount of SiO₂ and Al₂O₃ reflects the presence of minerals such as andesine [(Ca,Na)(Al,Si)₄O₈], a plagioclase feldspar, and diopside [MgCaSi₂O₆], a monoclinic pyroxene. A high content of Fe₂O₃ comes from diopside and ilmenite [FeTiO₃]. Significant concentration of CaO and MgO was found in all grain sizes, when compared to the basalt composition applied

as fertilizers in another studies (Nunes et al., 2014; Ramos et al., 2015), even though basalt chemical composition varies widely.

Basalt mineralogy is dominated by andesine and diopside (Figure 1). After 315 days in presence or absence of plants, basalt mineralogy remained unchanged. The reflections of andesine and diopside minerals showed little changes in the X-ray patterns and there were detected no secondary crystalline minerals after seven maize growth cycles.

The XRD analysis of the clay fraction as analyzed on oriented mount (Figure 2) revealed the typical shift of the d_{001} peak from 15.9 Å (in the air-dried state) to 17.7 Å (in the ethylene glycol state), indicating the presence of smectite, which was found in different proportions among the basalt fractions (Table 3). After heating, the typical collapse to 9.9 Å is observed.

An important parameter in the dissolution rate and nutrient release of primary minerals is the grain size and its relationship with the exposed reactive surface of minerals and with the chemical composition. The smallest grain sizes are the most reactive fractions (Basak, 2018; Bray et al., 2015).

The crystalline phases on < 53 µm size fraction of the mineral were composed of 48.2% of andesine, that has also calcium in its structure (Table 3; Figure 3). However, andesine has high structural stability and it is not easily weathered as it presents a great proportion ($Al/Si = 0.5 - 0.66$) of Al in its structure. It would be expected that the dissolution of andesine was incongruent, releasing alkalis and alkaline earths relative to silica and alumina.

Diopside represents 20.5% of < 53 µm sample. Depending on milling size, and environmental conditions, the diopside is, relatively, an easily weatherable mineral, and after applied to agricultural soils, may become a source of Ca and Mg for crops in diopside rich basalts (Figure 3). Moreover, diopside is unstable under acidic conditions and may dissolve congruently by weathering in such conditions (Wilson, 2004). The rhizosphere is the environment where diopside dissolution is likely to occur. The dissolution of pyroxenes is controlled by reactions at the mineral surface. By structural reasons, Ca, Mg and Fe are released preferentially at the beginning, and, lately, the dissolution becomes congruent and linear, as the weathering proceeds. The dissolution products could be precipitated as amorphous compounds, not detectable by XRD (Berner and Schott, 1982).

Diopside and ilmenite (18% of <53 μm fraction) comprise the major iron-containing minerals in the basalt sample (Figures 1 and 3). Iron rich minerals are also rich in micronutrients such as Mn, B, Cu, and Zn.

A representative amount of a smectite (13.2%), mainly in the < 53 μm fraction was present in the basalt. Smectite is an expansive clay that has a high cationic exchange capacity (CEC). As particle size increases, the presence of smectite decreases (Table 3). Probably the weakest cleavage faces on basalt particles are those richer in smectite. Non-weathered samples from basalt presented 24.85 (± 1.16) $\text{cmol}_c \text{ kg}^{-1}$ on < 53 μm size fraction. The smectite is a secondary mineral of the phyllosilicate class responsible for most of the reactivity of the studied basalt. As a matter of comparison, the CEC values of the montmorillonites range between 70 and 120 $\text{cmol}_c \text{ kg}^{-1}$, while the CEC values for the vermiculites range between 130 and 210 $\text{cmol}_c \text{ kg}^{-1}$ (Essington, 2003). Also, Oxisols from Cerrado present CEC $\sim 9.4 \text{ cmol}_c \text{ kg}^{-1}$ (STD = 3.9), and some are as low as 4.1 $\text{cmol}_c \text{ kg}^{-1}$ at pH 7.0 (Marchi et al., 2015). These soils present variable charge and natural pH is lower than 5, with effective CEC to even lower values. Therefore, inputs materials containing elevated surface area, permanent negative charge in these soils, may represent a great gain in quality.

Total plant biomass production decreased along each successive cycle (Equation 1), with highest production in the first crop cycle (4.15 g of dry matter) and the lowest in the last cycle (1.22 g of dry matter; Figure 4). Although plants were grown in pure rock, they were able to grow and take up some macro and micronutrients from basalt in its natural pH (9.04 – 6.99).

$$\text{Dry mass (g per pot)} = 4.54^{**} - 0.44^{**}(\text{cycle}), R^2 = 0.96 \quad [\text{Eq.1}]$$

The amount of nutrients taken up from basalt by plants varied over each crop cycle (Figure 4). These differences in element mobilization were related to dissolution kinetics of specific minerals. Potassium uptake showed a diverse dynamic than the other elements (Figure 5). Probably K was extracted by plant roots from non-exchangeable sites from interlayers of smectite minerals, other than by dissolution, such as Ca and Mg. Slowly available potassium, which is fixed and non-exchangeable, is trapped between the layers or sheets of K-rich 2:1 minerals. The idea was clarified statistically by the principal component analysis (PCA) where K, with similar statistical contribution than the other elements to describe results, pulls up toward the y axis, pulling dry matter in between (Figure 6). The PCA indicated that K presents a different mechanism of release from rock and it reflects on the interaction among the other nutrients.

After applied to soils, the layers from 2:1 minerals may adsorb and release cations, but their efficacy will also depend on the mineral particle size. Indeed, several studies show the presence of 2:1 clay size minerals, even in subsidiary quantities, increases effectively the retention of cations in soil (Raheb and Heidari, 2011).

Plants have developed several highly specific mechanisms to acquire K from minerals (Samal et al., 2010). Wang et al. (2000) investigated the ability of plant types to extract and uptake K from slightly weathered gneiss of differing particle sizes. The authors showed that, among the studied plant species, maize was the one that extracted the highest amount of K.

Concentrations of K in maize dry mass varied from 2.6 to 15 g K kg⁻¹ of dry weight. The results demonstrate that the plants were able to access some K from basalt to sustain growth. The K requirement for optimal maize growth range is 17.5 to 22.5 g kg⁻¹ in vegetative parts (Malavolta et al., 1997). K offtake were in range between 0.03 g pot⁻¹ from the first cycle to 0.004 g pot⁻¹ to the last cycle (Figure 4; Equation 2).

$$K_{\text{offtake}} (\text{g per pot}) = 0.03^{**} - 0.0049^{**}(\text{cycle}), R^2 = 0.81 \quad [\text{Eq. 2}]$$

Contents of Ca, Mg, Al and Fe in the maize tissue along the seven growth cycles indicated that nutrients were released from basalt minerals, and that basalt minerals were dissolved, partly due to a preferential dissolution of diopside.

The weathering of diopside and andesine in maize rhizosphere provided calcium and magnesium for plants. The nutrient concentration in dry mass ranged from 2.3 to 5.3 g Ca kg⁻¹ and from 1.3 to 6.6 g Mg kg⁻¹. Calcium and magnesium requirement for maize growth was reached as concentration in maize leaves for optimum growth varies from 2.5 to 4.0 g Ca kg⁻¹ (Malavolta et al., 1997), and from 2.5 to 4.0 g Mg kg⁻¹ (Hawkesford et al., 2012). Calcium offtake was from 0.015 to 0.005 g pot⁻¹ and Mg was from 0.016 to 0.004 g pot⁻¹, from the first to the last cycle, respectively (Figure 4, Equations 3 and 4).

$$Ca_{\text{offtake}} (\text{g per pot}) = 0.015^{**} - 0.0042^{**} \ln(\text{cycle}), R^2 = 0.85 \quad [\text{Eq. 3}]$$

$$Mg_{\text{offtake}} (\text{g per pot}) = 0.014^{**} - 0.0046^{**} \ln(\text{cycle}), R^2 = 0.80 \quad [\text{Eq. 4}]$$

The decay in maize growth and in the offtake of elements is probably due to the weathering of surfaces and dissolution of very small mineral particles in the initial cycles, where nutrients were easily extractable, while in the subsequent cycles a higher effort seems to be made to extract and acquire nutrients from basalt minerals. The rhizosphere has an intrinsic role in basalt dissolution and release of elements. Akter and Akagi (2005) evaluated the active role of rhizosphere in basalt and showed that maize increased the Ca and Mg extraction by a factor of 3 - 4 and 15 - 75, respectively, when compared with the

control pots with no plants. According to Hinsinger et al. (2001), the amounts of Ca, Mg and Na released from basalt under leaching conditions in the laboratory increased by a factor ranging from 1 to 5 in the presence of crop plants.

The Al concentration in dry mass ranged from 0.2 to 3.5 g Al kg⁻¹. Aluminum offtake along the cycles, although in a different scale, presented the same rate of Fe offtake (Figures 4 and 5). The Fe concentration ranged from 0.8 to 21.5 mg Fe kg⁻¹ and the concentration in maize leaves for optimum growth varies from 50 – 250 mg Fe kg⁻¹ (Malavolta et al., 1997). In the course of the experiment, the offtake of these elements decayed (Equations 5 and 6). It suggests ilmenite and diopside dissolution starts from iron oxidation during weathering, mainly from small particles and surfaces of lower crystallinity. As dissolution of easily weatherable minerals proceeds, along the cycles, Al, and Fe offtake decreases. Silva (2016) compared the dissolution of basalt at different grain sizes, despite not verifying the formation of new solid phases, confirmed the idea that the finer fractions are responsible for faster dissolution, while the coarser fractions dissolved slowly.

$$\text{Al}_{\text{offtake}} \text{ (g per pot)} = 0.01^{**} e^{(-0.47^{**}\text{cycle})}, R^2= 0.91 \quad [\text{Eq. 5}]$$

$$\text{Fe}_{\text{offtake}} \text{ (g per pot)} = 0.047^{**} e^{(-0.45^{**}\text{cycle})}, R^2= 0.91 \quad [\text{Eq. 6}]$$

The dissolution of small inclusions of ilmenite and diopside in basalt releases Fe. Strains of Fe-oxidizing bacteria are able to grow using the Fe(II) derived from ilmenite of basaltic rocks (Navarrete et al., 2013). This effect may be strongly influenced by the presence of organic acids from plants rhizosphere (Dontsova et al., 2014).

The water solubility of minerals containing Fe in soil is usually very low; however, plant and microbes, in the presence of organic substances, may work together for the oxidation and extraction Fe(II) complexes, increasing Fe availability for plant growth (Colombo et al., 2014). In particular, gramineous species may have evolved, developing a very efficient mechanism to mobilize Fe (Broadley et al., 2012). According to Hinsinger et al. (2001), the amount of Fe released from basalt under leaching conditions using maize plants reached a maximum increase of about 100-500 times the release without plants (control). Non-absorbed iron ions in solution are, then, precipitated as low crystallinity iron oxides (especially ferrihydrite and amorphous ferric hydroxide) (Silva et al., 2017).

Images of basalt samples obtained by SEM after the last crop cycle show the interaction between roots and mineral particles, including low crystalline structures (Figure 7). These structures are known as short-range ordered (SRO) minerals, such

ferrihydrite. Long-term field studies conducted by Yu et al. (2017) demonstrated that the presence of roots significantly increased Al and Fe availability from soils.

This result challenges the conceptual view that the weathering and the formation of SRO minerals are very slow processes and cannot be detected in the short-term (Colombo et al., 2014; Yu et al., 2017). It suggests that the dissolution of minerals can be accelerated by plant roots.

Offtake of manganese, boron, copper, and zinc showed a similar trend when normalized (Figures 4 and 5), although were taken up in different proportions by plants. The micronutrients Mn, B and Zn are present indistinctively in all primary minerals that compose this basalt, especially diopside (Moraes et al., 2018), while Cu is accumulated in smectite structure, formed by hydrothermal process (Baggio et al., 2016).

Manganese undertakes a similar oxidation process than Fe in mineral structures during weathering, releasing other elements. Manganese concentration values in maize tissue varied from 35 to 159 mg Mn kg⁻¹, while the sufficiency range for maize is from 50 to 150 mg Mn kg⁻¹ (Malavolta et al., 1997). The Mn offtake varied from 0.35 to 0.07 mg pot⁻¹, from the first to the last cycle, respectively (Figure 4), and decayed according to the Equation 7.

$$Mn_{\text{offtake}} \text{ (mg per pot)} = 0.32^{**} - 0.12^{**} \ln(\text{cycle}), R^2 = 0.92 \quad [\text{Eq. 7}]$$

Boron concentration values in maize ranged between 13.5 to 76.7 mg B kg⁻¹, while the adequate level for maize is from 15 to 20 mg B kg⁻¹ (Malavolta et al., 1997). For maize, the critical toxicity concentrations in leaves are in the range of 100 mg kg⁻¹ (Broadley et al., 2012), therefore, in the case the basalt is applied to soils, it does not represent any risk of soil contamination with B, but a source of nutrient. In the course of experiment, B offtake ranged from 0.13 to 0.04 mg pot⁻¹ from first and the last cycle (Figure 4) and decayed according to the Equation 8.

$$B_{\text{offtake}} \text{ (mg per pot)} = 0.13^{**} - 0.049^{**} \ln(\text{cycle}), R^2 = 0.92 \quad [\text{Eq. 8}]$$

Copper offtake was higher in the first cycle, media of 120 mg pot⁻¹, and decreased to 20 mg pot⁻¹ in the last (Figure 4; Equation 9) but shows an adequate Cu concentration in all cycles (mean 23.5 mg Cu kg⁻¹). The critical level concentration of Cu in maize is generally between 6 to 20 mg Cu kg⁻¹ (Malavolta et al., 1997) no visible toxicity symptoms of Cu were noticed.

$$Cu_{\text{offtake}} \text{ (mg per pot)} = 0.11^{**} - 0.041^{**} \ln(\text{cycle}), R^2 = 0.79 \quad [\text{Eq. 9}]$$

Zinc concentration in maize dry matter were below the critical level [15 – 50 mg Zn kg⁻¹, (Broadley et al., 2012)]. Zinc offtake was the lowest among micronutrients,

reflecting the content of the element in the basalt. Zinc offtake decayed from 0.04 to 0.08 mg pot⁻¹, from the first to the last cycle (Figure 4), following the Equation 10.

$$\text{Zn}_{\text{offtake}} \text{ (mg per pot)} = 0.04^{**} - 0.016^{**} \ln(\text{cycle}), R^2 = 0.97 \quad [\text{Eq. 10}]$$

Conclusions

The basalt mineralogical composition did not change throughout the experiment because part of the dissolution of basalt minerals by maize rhizosphere was congruent and/or formed new phases precipitated as amorphous phases and low crystallinity minerals. The smectite present in the basalt contributed to the high cationic exchange capacity, indicating a possible ability to change cations into the soil environment. Therefore, applications of basalt in Cerrado Oxisols can improve soil quality by adding permanent charge, by increasing its overall CEC. Basalt was able to provide nutrients to maize plants in a short period. Additionally, the offtake rate of elements from basalt was described by equations, which may be used for estimating nutrients release from basalt after applied in agricultural soils.

Tables and figures

Table 1. Particle size distribution of the basalt powder used in the experiment.

Sample	Particle size distribution (μm)				Total (g pot ⁻¹)
	< 53	53 - 300	300 - 1000	> 1000	
	-----%-----				
Basalt powder	10.67	12.44	26.5	50.39	663.69

Table 2. Chemical composition of the basalt powder (fractions and bulk) determined by XRF and ICP-OES.¹

Fraction (μm)	SiO ₂	Al ₂ O ₃	Fe ₂ O ₃	CaO	MgO	TiO ₂	P ₂ O ₅	Na ₂ O	K ₂ O	MnO	BaO	Cr ₂ O ₃	Cu	Mo	Zn	LOI ²
	-----%-----												----- mg kg ⁻¹ -----			
< 53	49.4	12	16.5	7.38	6.35	2.74	0.35	1.72	0.97	0.16	0.06	<0,01	206	<3	116	2.57
53 - 300	49	11.3	16.2	7.91	5.91	2.84	0.36	1.73	0.95	0.19	0.06	0.01	196	<3	131	1.55
300 - 1000	49.4	12.2	15.5	8.53	5.4	3.24	0.4	1.95	0.98	0.19	0.06	0.01	194	<3	134	0.93
> 1000	49.4	12.7	15.1	8.85	4.9	3.38	0.4	2.46	0.93	0.2	0.05	0.01	211	<3	149	0.58
Content bulk ³	49	12.6	15.4	8.73	5.28	3.2	0.43	2.06	0.9	0.2	0.06	<0,01	208	<3	139	1.32

¹SGS Geosol Laboratórios Ltda; ²Loss on ignition; ³Original sample.

Table 3. Mineralogical composition of the basalt powder (fractions and bulk).

Fractions (μm)	Andesine	Diopside	Ilmenite	Smectite
	-----%			
< 53	48.2	20.5	18.0	13.2
53 - 300	47.0	24.5	18.3	10.2
300 - 1000	50.7	24.9	18.0	6.3
> 1000	53.1	25.7	17.9	3.3
Content bulk ¹	51.9	25.7	18.1	4.3

¹Original sample.

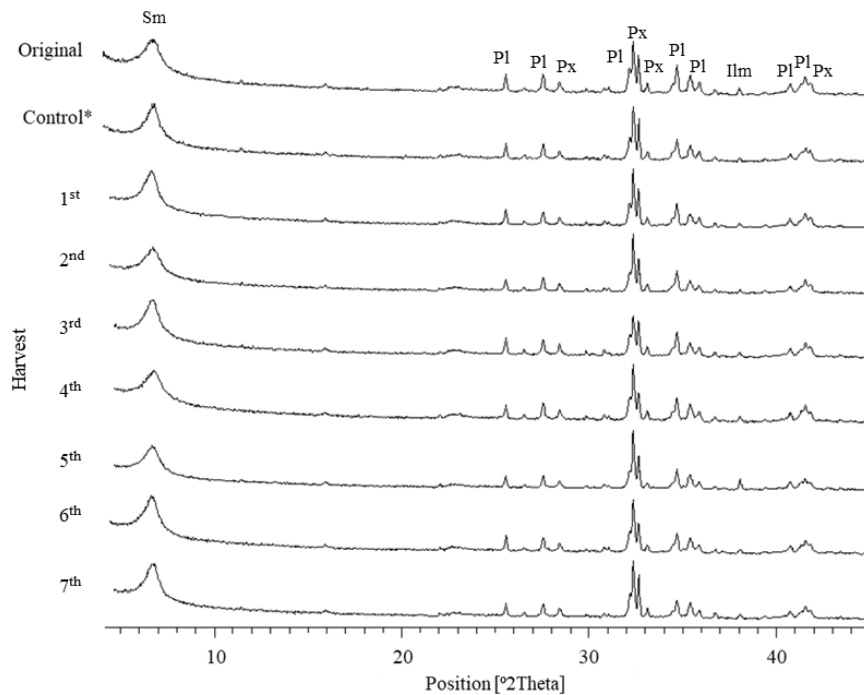


Figure 1. X-ray diffraction patterns of <math><53\ \mu\text{m}</math> size particles of basalt after interaction with maize rhizosphere evidencing andesine (Pl), diopside (Px), smectite (Sm) and ilmenite (Ilm) minerals during 7 harvest crops; *Control is the basalt collected from the pot without plants at the end of the experiment.

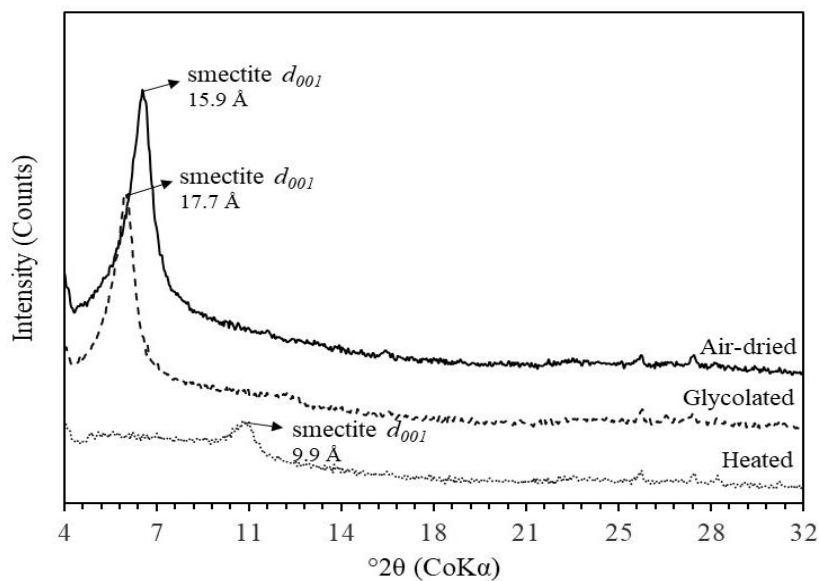


Figure 2. X-ray diffraction patterns of the clay fraction (oriented sample) obtained three times: air-dried, after treatment with ethylene glycol, and heated at $550\ ^\circ\text{C}$.

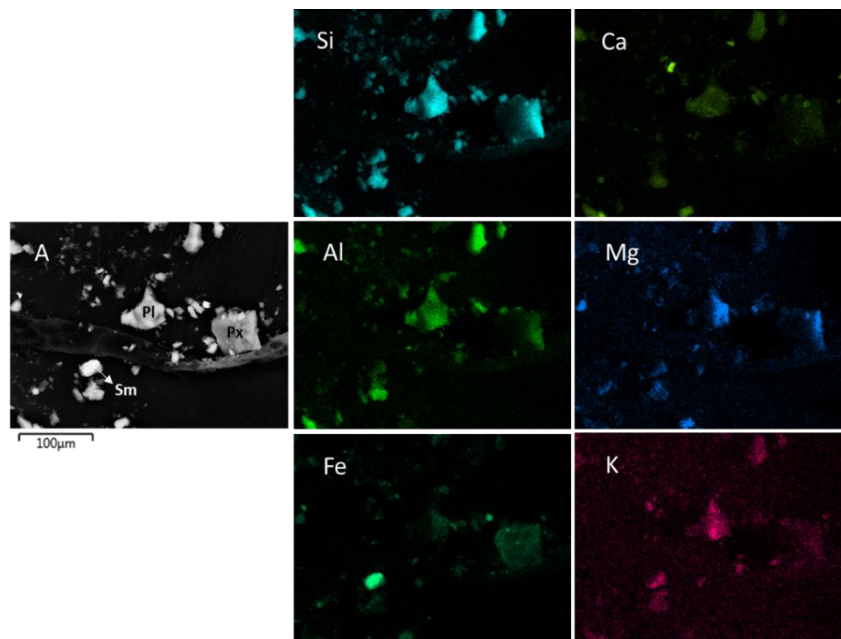


Figure 3. Energy-dispersive X-ray spectroscopy (EDS) images of basalt mineral compounds around maize root. A: secondary electrons image evidencing andesine (Pl), diopside (Px) and smectite (Sm) minerals; Si: silicon map; Al: aluminum map; Fe: iron map; Ca: calcium map; Mg: magnesium map; and K: potassium map.

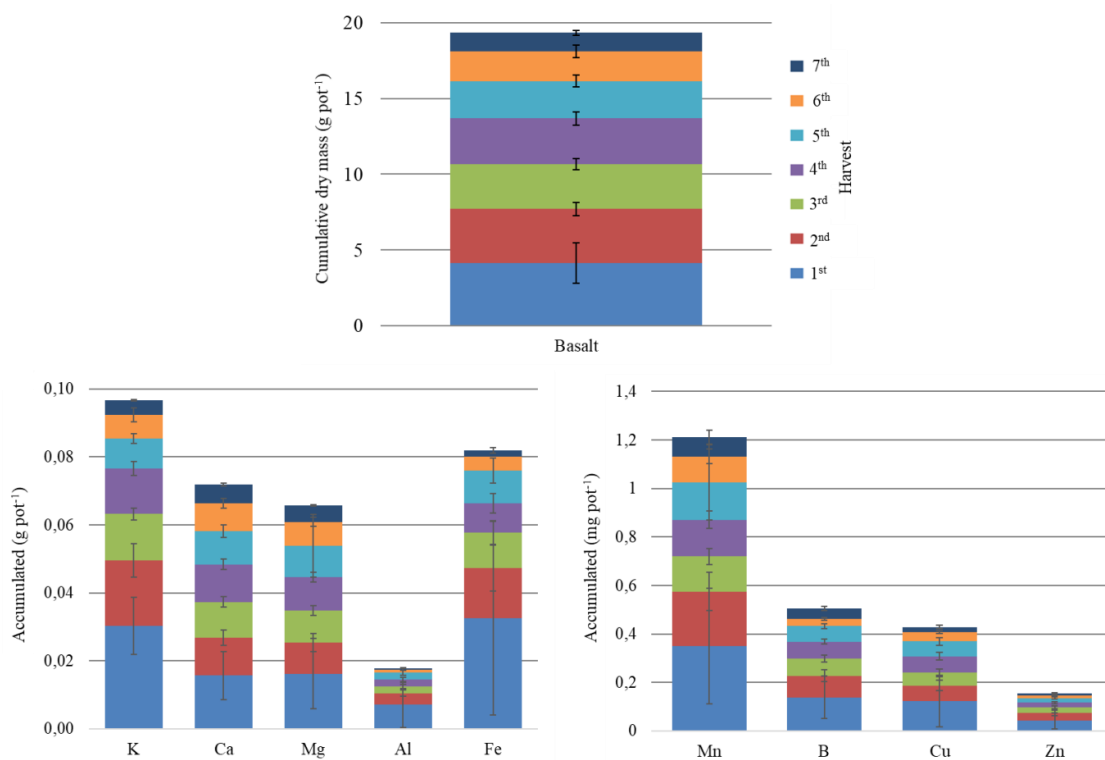


Figure 4. Cumulative dry mass and elements offtake¹by maize cultivated in basalt powder after seven cycles. ¹The number of samples per cycle used to calculate the mean (*n*), from the 1st to the 7th cycle, were: $n = 24 - i$; where $i = \text{cycle number} * -3$. Error bars for each cycle were the standard deviation of *n*.

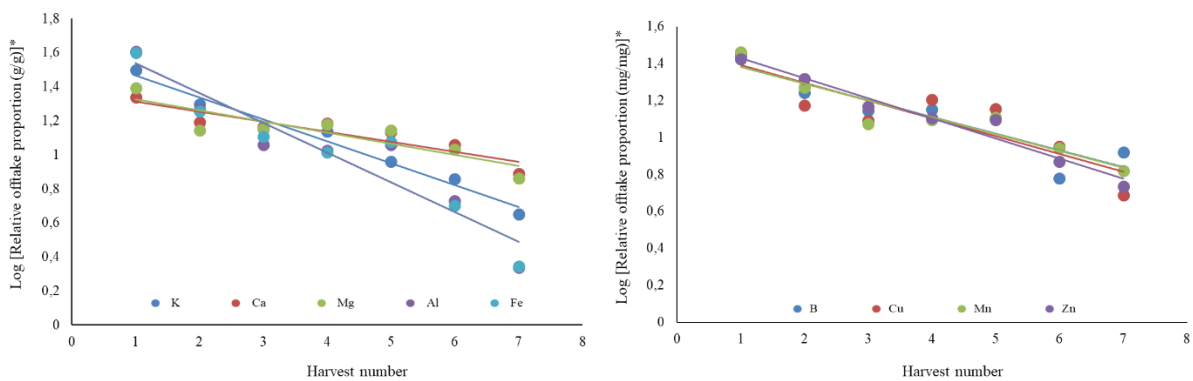


Figure 5. Elements offtake ratio from basalt by maize. *Relative offtake proportion = $\text{Log} \left[\frac{\text{offtake} \cdot 100}{\sum_{c=7}^1 \left(\frac{\text{offtake}}{c} \right)} \right]$; *c* = harvest number.

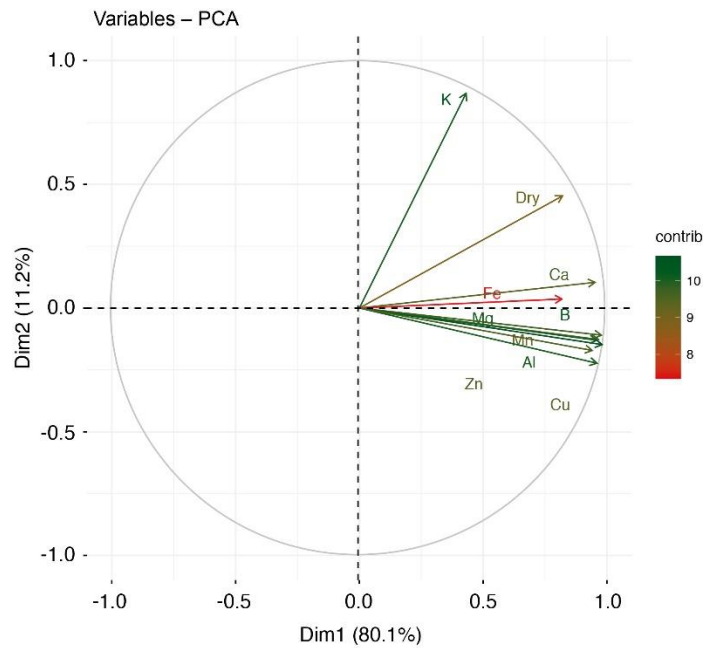


Figure 6. Principal component analysis of K, Ca, Mg, Fe, Al, Mn, B, Cu, and Zn maize offtake from basalt and cumulative Dry (= maize dry matter); Dim = dimension; Contrib = contribution.

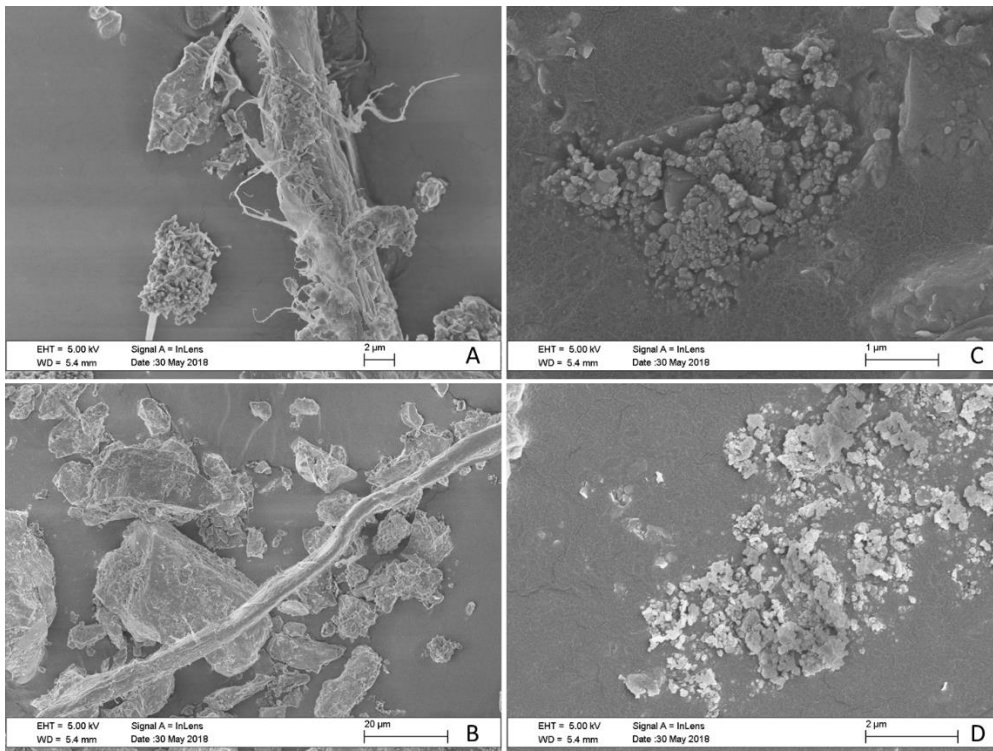


Figure 7. Scanning electron microscopy images of basalt samples after seven maize growth cycles. A and B: interaction of roots with basalt minerals; C and D: deposits of low crystallinity minerals.

CHAPTER 3. SILICATE MINERALS AS A SOURCE OF NUTRIENTS TO MAIZE GROWN SUCCESSIVELY

Luise Lottici Krahl^{a*}, Leonardo Fonseca Valadares^b, José Carlos Sousa-Silva^c, Giuliano Marchi^c and Éder de Souza Martins^c.

^a Universidade de Brasília, Área Universitária, 01, Vila Nossa Senhora de Fátima, CEP: 73345-010 - Planaltina - DF, Brazil. E-mail: luisekrah1@yahoo.com.br

^b Embrapa Agroenergia, Parque Estação Biológica - PqEB s/n°. Caixa Postal 40.315, CEP: 70770-901 - Brasília - DF, Brazil. E-mail: leonardo.valadares@embrapa.br

^c Embrapa Cerrados, Rodovia BR-020, Km 18, Caixa Postal 08223, CEP: 73310-970 – Planaltina - DF, Brazil. E-mail: jose.sousa-silva@embrapa.br, giuliano.marchi@embrapa.br, eder.martins@embrapa.br

*Corresponding author.

E-mail address: luisekrah1@yahoo.com.br (L.L. Krahl).

Chapter submitted as an article for the journal *Pesquisa Agropecuária Brasileira*.

Abstract – Some powders of silicate rocks containing the mineral biotite are considered agrominerals as they, during the weathering process in the rhizosphere of plants, may supply nutrients such as K, Ca, Mg, Fe and Mn to plants in the short term. In this study, the ability of maize (*Zea mays* L.) to take up nutrients from biotite schist and biotite syenite was investigated. Powders were characterized chemical, physical and mineralogically, and the availability of elements released from minerals to plants was studied. Plant and rock materials were evaluated at the end of successive growing cycles. Biotite schist and biotite syenite rocks provided nutrients to maize plants which were related to minerals presenting oxidizable Fe and Mn in its structure, such as biotite, chlorite, and clinopyroxene. Some fine particles of these minerals undergo a congruent dissolution, solubilizing its elements, which are made available to plant uptake.

Keywords: bioweathering, biotite, nutrient availability, congruent dissolution.

Introduction

Weathering of silicate minerals is perceived as a slow process. New evidences show that certain minerals in rocks might weather in a shorter-term than the expected, mainly when ground rocks are placed under the influence of the rhizosphere of plants (Manning et al., 2017; Basak, 2018; Ciceri and Allanore, 2019). Thus, many studies have addressed the ability of different silicate minerals to provide nutrients to plants in a short time scale (Hinsinger et al., 1993; Li et al., 2015; Manning et al., 2017; Ciceri et al., 2019). Most of these studies have reported not only incongruent dissolution micas, but also the congruent dissolution of finer fractions of minerals.

Dissolution rates on plant-induced weathering of minerals, depends, primarily, on the kind of mineral, of grinding process, and plant species. Dissolution rates are faster in minerals presenting low Al and Si in its structure, as well as high content of oxidizable Fe and Mn, alkali and alkaline earth cations, such as K, Ca and Mg. Particles may also be selected during the grinding process, generating materials with a diverse chemical composition from the original rock. Usually a fine powder is obtained as a by-product from the production of gravel, and artificial sand, as an example, thus particles usually break in the weakest cleavage faces, where the easily weatherable minerals are in a continuous selection process. The plant species also plays a role on dissolution rate, depending on its root activity, the release of organic substances, and the associated microbial populations (Li et al., 2014; Bray et al., 2015; Burghilea et al., 2015).

Mineral dissolution processes in the natural environment involve, therefore, innumerable factors. The main mineral related factors are: area of exposure from minerals, chemical reactions, such as acid-base, oxidation-reduction, and adsorption-desorption-precipitation. Additionally, it can be included: absorption and release of elements by diverse species of plants, and billions of organisms, not to mention chelates, temperature, and humidity, all of them in a dynamic process.

During the incongruent dissolution, the alteration underwent by some minerals, by releasing cations, may produce secondary or clay minerals, like illite or hydrous mica, vermiculite, chlorite, and interstratified minerals (Naderizadeh et al., 2010; Norouzi and Khademi, 2010). Biotite minerals present in rocks such as some schists and syenites, present a relatively fast dissolution rate, although incongruent, and can be a suitable source of K for plants (Burghilea et al., 2015; Li et al., 2015; Manning et al., 2017).

The ability of plant types to uptake K from silicate minerals has been studied previously (Hinsinger et al., 1992; Wang et al., 2000; Norouzi and Khademi, 2010; Li et al., 2015). These

authors showed that the root-induced release of interlayer K came about in a few weeks of growth. Generally, monocotyledons, such as gramineous, exploit better the soil K reserves than dicotyledons. Gramineous species may have evolved, developing a very efficient mechanism to mobilize Fe (Broadley et al., 2012). Most of these studies were focused in K release from minerals. It was found that a significant proportion of K needed by plants may be met from K-rich minerals, which are present in silicate rocks, not only in micas, but also in K-feldspars and their weathering products (Zorb et al., 2014; Basak et al., 2018; Ciceri et al., 2019).

Other nutrients than K, also required for plant growth, such as Ca, Mg, and S, as well as micronutrients, such as Mn, B, Zn, Ni, Cu, and Fe, are abundant either in the structure or in interlayer sites of minerals. These nutrients are released during the dissolution of minerals, however, there is not abundant data on the release of these other nutrients.

The prediction of nutrient availability from rocks passes through the identification of minerals. Some of them are known to be dissolved in the soil in a fast pace under the rhizosphere activity, and to present adequate amounts of nutrients for plant growth. Some chemical extractants have been used to try predicting ground rocks nutrient availability for plants (Li et al., 2014; Basak, 2018), but these methods are still under development, as rock mineralogical, chemical and physical heterogeneity, to the moment, do not allow the use of a single extractant for discovering nutrient availability, and its releasing rates. It is important, however, to test the ground rocks through plant-based extraction of nutrients.

A successive extraction of nutrients from micas, such as biotite, by plants, may shed light on dissolution patterns and nutrient availability along the time. The aim of this work is to assess the nutrient availability to maize grown successively in pure biotite schist and biotite syenite ground rocks.

Materials and methods

Sampling

Biotite schist (BSC) was collected from residue piles in quarries located at the State of Goiás (Navarro et al., 2013b) and biotite syenite (BSY) was collected at the Southeastern of the State of Bahia (Cruz et al., 2016). Samples were air-dried and homogenized using the cone-and-quartering reduction method. This procedure was repeated several times to ensure complete homogenization of material, forming the bulk sample.

Greenhouse experiment

The bulk BSC or BSY samples were placed into 500 mL pots. Two plants of maize (*Zea mays* L.) were grown in seven sets of three pots. Seven extra pots without plants were prepared, as a control treatment. At every 1–2 days all pots were watered with deionized water. Pots were fertilized with nutrient solution ($92.76 \text{ mg pot}^{-1} \text{ NH}_4\text{H}_2\text{PO}_4$) in the 15th and 30th days of growth of each cycle.

At the end of each 45-days cycle, whole plants from all pots were harvested. The rock content from one set of three pots previously grown with plants, and another, from one pot of the control set were removed from the glasshouse. The pots content was used for the laboratory analyses. The remaining sets were re-sown for a new growth cycle.

Plant analyses

The harvested plants were oven dried at 65 °C for 72 hours. The dry biomass was taken. Major (K, Ca, Mg, Al, Fe) and minor elements (B, Cu Mn e Zn) were extracted by $\text{HNO}_3:\text{HClO}_4$ in a digestion block (Embrapa, 2017) and determined by inductively coupled plasma - optical emission spectrometry (ICP-OES).

Elements offtake along the cycles were modeled and the equations were selected according to the analysis of variance (ANOVA) (Supplementary material; Figures S3 - S6; p-values for the coefficients: **p < 0.01, *p < 0.05) and, thereafter, were tested for normality (Shapiro-Wilk), and constant variance test (homoscedasticity), considering p-values < 0.05 significant. These statistical analyses were performed using Sigma Plot 12.0 software (Sigma Plot Software; San Jose, California, USA).

Rock material analyses

Those pots removed from the glasshouse at the end of each growth cycle were dismantled and its contents, bulk samples, were wet sieved to obtain four size fractions: < 53 μm , 53 – 300 μm , 300 – 1000 μm and > 1000 μm (Table 1).

The main chemical elements of BSC and BSY were analyzed using the multi-acid solution method, where: 500 mg of sample was digested in 10:15:10:5 mL of $\text{HCl}:\text{HNO}_3:\text{HF}:\text{HClO}_4$, respectively, determined by ICP-OES (SGS Geosol Laboratórios Ltda). Major elements were determined by wavelength dispersive X-ray fluorescence (XRF) spectroscopy, on fused glass discs, 40 mm-diameter, prepared from 0.8 g of sample powder mixed with 4.5 g lithium tetraborate flux and fused in Pt-5% Au crucibles at 1120 °C (SGS Geosol Laboratórios Ltda) (Supplementary material; Table S1). The analysis was handled

according to certified quality management system ABNT NBR ISO 9001:2008. The loss on ignition was determined after heating samples overnight at 105 °C to remove water. The weight loss was measured after calcination of samples at 1000 °C for approximately 2 hours.

The mineralogical composition of BSC and BSY fractions < 53 µm was analyzed by X-ray diffraction analysis (XRD) using a PANalytical Empyrean (PW3050/60) diffractometer (Mineral Characterization Laboratory at Federal University of Pará), using the powder method in the range of $5^\circ < 2\theta < 75^\circ$. $\text{CoK}\alpha$ radiation (40 kV; 40 mA) was applied, and the 2θ scanning speed was set at $0.02^\circ \text{ s}^{-1}$. Data was acquired using the software X'Pert Data Collector 4.0 and the data were treated on X'Pert HighScore 3.0 (PANalytical). Minerals were identified by comparing the obtained diffractogram with the ICDD-PDF (International Center for Diffraction Data) database.

The Rietveld refinement was performed using the High Score Plus Program (Malvern Panalytical, version 4.7) for quantitative determination of the mineralogical composition in each size fraction of BSC and BSY original samples. The structural models (CIF files) for the identified mineral phases were obtained from the ICSD database. Traditional sequence for such refinements is as follow: scale factor and background, using a polynomial function, besides unit cell parameters for all phases. The W parameter of the Caglioti equation is refined only for the major phases, followed by V and U. Chlorites and micas exhibit strong preferred orientation and the (001) direction must be refined, besides the (100) plane for the feldspars (microcline and albite). Atomic positions were not refined.

Electron probe microanalyses (EPMA) were carried out to identify the biotite mineral within the samples with a JEOL - model Superprobe JXA-8230 (Geosciences Institute of the University of Brasilia), coupled with 5 spectrometers and one EDS (Energy Dispersive Spectrometer) detector, operating with 10 nA of current and 15 kV. The acquisition time was 10 seconds at the peak and 5 seconds at the background and the beam diameter was 1 µm. The instrument was calibrated using natural and synthetic primary standards and the resulting data was processed to calculate the structural formulas of the mineral phases. The analyses involved a total of 25 biotite crystals, 11 of BSC and 14 of BSY (Supplementary material; Tables S2 and S3; Figures S7 and S8).

The morphology of the BSC and BSY bulk samples was examined by scanning electron microscopy (SEM) using a Zeiss field emission microscope model SIGMA HV with the InLens detector (Embrapa Agroenergia). A thin conductive layer of gold (10 nm) was deposited over the samples using the Q150T-ES sputter (Quorum Technologies). The chemical composition of selected mineral particles was evaluated by Energy-dispersive X-ray spectroscopy (EDS).

Results and discussion

The chemical composition (Table 2) and the mineralogical composition (Table 3; Figure 1) of bulk samples and of fractions showed the presence of the mineral biotite in both BSC and BSY. Biotite, although its relatively high content of Si and Al, is the main active mineral prone to release nutrients, such as K during weathering in these two rocks (Table 3, Figure 2). The biotite is a subgroup of the mica group and forms a solid solution series with Fe end members annite [$\text{K Fe}_3 \text{AlSi}_3\text{O}_{10} (\text{OH})_2$] and Mg end member phlogopite [$\text{K Mg}_3 \text{AlSi}_3\text{O}_{10} (\text{OH})_2$]. Variations in Fe and Mg concentrations in natural biotite and the substitution of several other elements in the octahedral and tetrahedral silicate sheets, may lead to differences in weathering rates (Gilkes et al., 1973; Murakami et al., 2003), as it is known that the Fe(II) oxidation is a driving force in primary mineral weathering (Essington, 2015).

The mineral biotite within BSC sample was located in the annite, siderophyllite and phlogopite interface, with the chemical composition $\text{K}_{0.817} \text{Ba}_{0.005} (\text{Mg}_{1.198} \text{Fe}_{1.157} \text{Al}_{0.415} \text{Ti}_{0.088}) (\text{Si}_{2.845} \text{Al}_{1.154} \text{O}_{11}) (\text{OH}_{1.97} \text{F}_{0.02} \text{Cl}_{0.001})$ (Navarro et al., 2013a). The biotite within BSY sample was classified as annite (Tischendorf et al., 2007), a Fe-biotite with the average chemical composition $\text{K}_{0.805} \text{Ba}_{0.022} \text{Na}_{0.011} (\text{Fe}_{1.55} \text{Mg}_{0.785} \text{Ti}_{0.168} \text{Al}_{0.255} \text{Mn}_{0.01}) (\text{Si}_{2.963} \text{Al}_{1.036} \text{O}_{11}) (\text{OH}_{1.949} \text{F}_{0.045} \text{Cl}_{0.005})$. Biotite decreases its stability with increasing iron content, as the oxidation of structural iron destabilizes the mineral (Malmström et al., 1995).

Other minerals of interest found in BSC sample were albite [$\text{Na}(\text{Si}_3\text{Al})\text{O}_8$], a plagioclase feldspar; and chlorite, which have a general chemical composition $(\text{A,B})_{4-6}(\text{Si,Al})_4\text{O}_{10}(\text{OH,O})_8$ (where: A and B in the formula represent ions, which might include: Fe^{2+} , Fe^{3+} , Mg^{2+} , Mn^{2+} , Ni^{2+} , Zn^{2+} , Al^{3+} , Li^+ , or Ti^{4+}). As in the case of biotite, the amount of Fe(II) and its oxidation play a significant role in the chlorite susceptibility to weathering (Malmström et al., 1995). Muscovite [$\text{KAl}_2(\text{AlSi}_3\text{O}_{10}) (\text{OH,F,Cl})_2$], is another K-bearing mineral present in BSC. Biotite, muscovite, and chlorite are all 2:1 phyllosilicate minerals, but biotite and muscovite have K^+ cations in the interlayer, whereas chlorite interlayers contain a Mg-rich, brucite/gibbsite-like, hydroxyinterlayer. Muscovite, because its high content of Al, has greater resistance to alteration than biotite and chlorite.

Most of the BSY sample was composed of K-feldspar (orthoclase and microcline). The orthoclase and microcline are alkaline feldspar minerals with a general chemical composition of KAlSi_3O_8 . Other minerals of interest found in BSY were albite and clinopyroxene. The clinopyroxene is a mafic silicate of a subgroup of the pyroxenes presenting a general chemical composition of ABSi_2O_6 (where: A = Ca^{2+} , Na^+ , and Li^+ ; and B = Mg^{2+} , Fe^{2+} , Fe^{3+} , and Al^{3+}).

Small concentrations of amphibole were also found in the BSY, which have a general composition $A_{0-1}B_2C_5T_8O_{22}(OH,F)_2$ (where: A = Na^+ , K^+ ; B = Ca^{2+} , Na^+ , Mg^{2+} , Fe^{2+} , and also Mn^{2+} , Li^+ ; C = Mg^{2+} , Fe^{2+} , Al^{3+} , Fe^{3+} , and also Mn^{2+} , Zn^{2+} , Cr^{3+} , Li^+ , or Ti^{4+} ; T = Si, Al), which may contribute to plant growth.

Plant-induced transformation of biotite during weathering starts with an expansion of the interlayer distance due to exchange of nonhydrated K^+ by hydrated ions or formation of hydroxypolymer interlayers of units such as $Al_n(OH)_m$. Then, there is an increase in Si/Al ratios in the tetrahedral layer, reducing the layer charge; which is followed by oxidation of octahedral Fe(II), destabilizing the mineral and releasing other elements (Malmström et al., 1995).

Although biotite content in BSY bulk sample was similar than in BSC, the BSY presented 3.5 times more total K_2O . The total amount of K, however, may not reflect its availability, as 52.5% – 64.8% of the BSY is composed of K-feldspar, which is a mineral with high structural stability; as well as albite, which can have, K substituting Na in its structure. The same analysis may be done for BSC, which presents great portion of its K locked in muscovite structure, and probably not available to plants in the short-term.

During the growth cycles, maize plants showed differences in the accumulated biomass: BSC promoted the growth of 15.3% more biomass than BSY (Figure 3). The highest dry matter production was obtained in the first cropping cycle for both crushed rocks, accounting for 23.9 and 20.7%, of the total accumulated during the 7 cycles, respectively, for BSC and BSY. Plant biomass production decreased along each successive cycle according the equations 1 and 2:

$$\text{Dry mass}_{\text{biotite schist}} \text{ (g per pot)} = 6.12^{**} - 1.97^{**} \ln(\text{cycle}), R^2 = 0.95 \quad [\text{Eq. 1}]$$

$$\text{Dry mass}_{\text{biotite syenite}} \text{ (g per pot)} = 4.92^{**} - 0.44^{**} (\text{cycle}), R^2 = 0.80 \quad [\text{Eq. 2}]$$

Although plants were grown in pure rock, they were able to uptake a series of elements, including essential macro and micronutrients for plant growth both from BSC and BSY. The pH of the rock substrates, measured after each cycle, decreased linearly during the growth cycles (Equations 3 and 4). The decrease of the pH was mainly a result of substances released by roots, microorganism interaction, dissolution of CO_2 , and precipitation of the released Al as Al-hydroxide and Al-oxyhydroxide, neutralizing hydroxyls released during the weathering. The pH from the control samples did not change significantly (pH, standard deviation = 8.02, 0.25, and 7.85, 0.25, for BSC and BSY, respectively), along the 7 cycles. The decrease in the pH was, therefore, caused by the increased rate of weathering promoted by plants.

$$\text{pH}_{\text{biotite schist}} = 7.49^{**} - 0.22^{**} (\text{cycle}), R^2 = 0.91 \quad [\text{Eq. 3}]$$

$$\text{pH}_{\text{biotite syenite}} = 7.93^{**} - 0.36^{**} (\text{cycle}), R^2 = 0.88 \quad [\text{Eq. 4}]$$

Concentrations of K in maize plants were found in the range from 18.4 to 36 g K kg⁻¹, and from 13.9 to 26.5 g K kg⁻¹ of dry mass from plants grown in BSC and BSY, respectively. The requirement for optimal maize growth is from 17.5 to 22.5 g K kg⁻¹ in vegetative parts (Malavolta et al., 1997).

Potassium offtake by plants grown in BSC, in the first cycle, corresponded to 21.7% of the total accumulated K, while in the last cycle it was reduced to 10.4% (corresponding to 0.15 and 0.07 g of K pot⁻¹, respectively; Figure 3). Potassium offtake by plants grown in BSY was 18.9% in the first cycle, and 8.5% in the final cycle (corresponding to 0.08 and 0.03 g pot⁻¹, respectively). The decrease in K offtake in plants grown in BSC and BSY, followed the equations 5 and 6, respectively:

$$K_{\text{offtake_biotite schist}} \text{ (g per pot)} = 0.15^{**} - 0.04^{**} \ln(\text{cycle}), \quad R^2 = 0.91 \quad [\text{Eq. 5}]$$

$$K_{\text{offtake_biotite syenite}} \text{ (g per pot)} = 0.09^{**} - 0.007^{*}(\text{cycle}), \quad R^2 = 0.73 \quad [\text{Eq. 6}]$$

The content of Fe₂O₃ in BSY suffered a sort of segregation during fractionation, increasing its content in the smaller size fractions (Table 2). The trend was identified as an increase in biotite in the < 300 μm fractions, by preferential segregation during the milling process. The finest are the most important fractions as, according to Harley and Gilkes (2000); Bray et al. (2015); Basak (2018), the reactivity of BSC is higher in finer fractions, preferentially in those < 53 μm. It is particularly important as a higher structural concentration of Fe(II), and Mg accelerates the alteration and release K from biotite (Murakami et al., 2004), facilitating the formation of secondary minerals (such as hydrobiotite and vermiculite), at least in an early stage. Because vermiculite dissolves at a much slower rate than biotite, Mg-rich biotite (such as the biotite in the BSC) dissolves at a slower rate than Fe-rich biotite. When the biotite is Fe-rich (such as the one present in the BSY), the Fe released into solution is subsequently precipitated in particle surfaces, decreasing biotite weathering and K release rates.

The high initial Fe and Al offtake (Figure 3) suggests an initial dissolution of the fine low crystallinity minerals, in a congruent way, releasing their elements into solution. As dissolution of the easily weatherable minerals proceeds, along the cycles, Fe and Al offtake decreases (Equations 7 – 10), indicating the decrease of easily weatherable mineral surfaces. The offtake data of Fe and Al from BSC and BSY along the cycles was normalized with data of K, Ca and Mg offtake to allow observing their influence on the rate the elements were taken up by plants (Figure 4). The steep curve shapes from BSY show that a higher content of Fe was released from BSY than from BSC along the cycles, as related to K, Ca, and Mg content. The Fe and Al offtake were positively correlated in both rocks (Pearson correlation, $r_{\text{biotite schist}} = 0.99$ and $r_{\text{biotite syenite}} = 0.99$; $p < 0.05$) showing a similar trend (Figure 4). Iron oxidation is, therefore,

a main component responsible for weathering of minerals by plants. The strong correlation indicates that the origin of the Al offtake was from the same mineral or group of minerals containing oxidizable Fe. Minerals containing oxidizable Fe in BSC are biotite and chlorite, while in BSY are, mainly the biotite, and in a smaller extent, the clinopyroxene.

$$Fe_{\text{offtake_biotite schist}} \text{ (g per pot)} = 0.024^{**} - 0.011^{*} \ln(\text{cycle}), R^2 = 0.70 \quad [\text{Eq. 7}]$$

$$Fe_{\text{offtake_biotite syenite}} \text{ (g per pot)} = 0.15^{*} e^{(-0.93^{**} \text{cycle})}, R^2 = 0.90 \quad [\text{Eq. 8}]$$

$$Al_{\text{offtake_biotite schist}} \text{ (g per pot)} = 0.019^{**} - 0.0096^{*} \ln(\text{cycle}), R^2 = 0.73 \quad [\text{Eq. 9}]$$

$$Al_{\text{offtake_biotite syenite}} \text{ (g per pot)} = 0.07^{*} e^{(-1.12^{**} \text{cycle})}, R^2 = 0.92 \quad [\text{Eq. 10}]$$

The EDS analysis shows an indicative that the clinopyroxene in BSY presents Fe and Mg and a high content of Ca; and low Al (Figure 2). Depending on the milling size, and environmental conditions, the clinopyroxene may be easily weathered, and after applied to agricultural soils, may become a source of Fe, Ca and Mg for crops.

Calcium concentration in maize ranged from 2.69 to 0.01 g Ca kg⁻¹ of dry mass in plants grown in BSC and from 2.8 to 1.4 g Ca kg⁻¹ of dry mass in BSY over the cycles. Considering that the Ca requirement for optimum maize growth ranges between 2.5 to 4.0 g Ca kg⁻¹ (Malavolta et al., 1997), BSY provided consistently more Ca than BSC, as presents Ca-rich clinopyroxene, as evidenced by the EDS (Figure 2). The Ca offtake data by plants grown in BSC was a dispersion, showing no relation with crop cycle. In addition, EDS shows a very small concentration of Ca in BSC sample. The Ca offtake by maize plants grown in BSY decreased according to the equation 11:

$$Ca_{\text{offtake_biotite syenite}} \text{ (g per pot)} = 0.11^{**} - 0.004^{**} \ln(\text{cycle}), R^2 = 0.87 \quad [\text{Eq. 11}]$$

In the BSC, contrasting to the low Ca content, Mg presented higher content, mainly in the mineral biotite and in chlorite, as observed in EDS images (Figure 2). The weathering of biotite and clinopyroxene from BSY also provided an appreciable amount of Mg for maize. However, as finer particles are dissolved, presenting a congruent and linear dissolution (Schott et al., 1981), Mg availability for the plants was reduced along the cycles. The reduction in finer particles reflects the decrease of Mg offtake in the plant tissue (Equations 12 and 13).

$$Mg_{\text{offtake_biotite schist}} \text{ (g per pot)} = 0.016^{**} - 0.0074^{*} \ln(\text{cycle}), R^2 = 0.70 \quad [\text{Eq. 12}]$$

$$Mg_{\text{offtake_biotite syenite}} \text{ (g per pot)} = 0.012^{**} - 0.0055^{*} \ln(\text{cycle}), R^2 = 0.75 \quad [\text{Eq. 13}]$$

Magnesium concentration in dry mass ranged from 5.6 to 0.7 g Mg kg⁻¹ in plants grown in BSC and from 5.2 to 0.9 g Mg kg⁻¹ in plants grown in BSY. The reached values are partially in the range of optimal Mg contents; 2.5 to 4.0 g Mg kg⁻¹, in adult plants, and 1.5 g Mg kg⁻¹ in plants of early vegetative growth stage (Hawkesford et al., 2012). Therefore, both powdered rocks may be considered a source of Mg for plants.

The congruent dissolution of fine particles on the surface of biotite minerals was evidenced by SEM images (Figure 5), as demonstrated before by Manning et al. (2017) and Basak (2018). Biotite surfaces from not-weathered, original samples, taken from BSC and from BSY, were covered with fine particles. After 7 crop cycles there was a clear reduction in fine particles covering biotite minerals.

Plants significantly mobilized micronutrients, such as manganese, boron, copper, and zinc from both rocks (Figure 6). Plants and the associated microbiota can significantly increase mobilization for most elements from minerals, and most of these elements comes predominantly from easily dissolved minerals (Burgelea et al., 2018).

Manganese as it occurs with Fe, also oxidizes either after dissolved or within crystals, by solid state diffusion of electrons to electron acceptors in soil solution at the mineral surface (Gilkes and McKenzie, 1988). After oxidized, it remains in the soil, as it presents extremely low solubility as a secondary oxide [about 10^{-28} mol kg⁻¹ at pH 7; Gilkes and McKenzie (1988)]. The Mn concentrations in maize dry mass provided by both rocks were small. In plants grown in BSC, concentrations varied from 122.8 to 43.9 mg Mn kg⁻¹ of dry mass. Most of the plants were within the sufficiency range [50 – 150 mg Mn kg⁻¹; Malavolta et al. (1997)]. Mn offtake decreased from the first to the last cycle, following the equation 14 (Figure 6).

$$\text{Mn}_{\text{offtake_biotite schist}} \text{ (mg per pot)} = 0.59^{**} - 0.24^{**} \ln(\text{cycle}), \quad R^2 = 0.91 \quad [\text{Eq. 14}]$$

In contrast, plants grown in BSY showed higher Mn levels in tissue, ranging from 405.4 to 173.2 mg Mn kg⁻¹ of dry mass, with almost all samples above the critical toxicity concentration (200 mg Mn kg⁻¹; Malavolta et. al., 1997). Although concentrations were high on plant tissue, no symptoms of Mn toxicity were observed in plants grown in BSY samples. Manganese offtake from BSY also decreased from the first to the last cycle, following the equation 15 (Figure 6).

$$\text{Mn}_{\text{offtake_biotite syenite}} \text{ (mg per pot)} = 1.27^{**} - 0.10^*(\text{cycle}), \quad R^2 = 0.71 \quad [\text{Eq. 15}]$$

Plants grown in BSC presented low boron levels, with 62% of the samples below the minimum (15 to 20 mg B kg⁻¹ of dry mass), according to Malavolta et al. (1997). In the course of experiment, B offtake in these plants ranged from 0.06 to 0.04 mg pot⁻¹ (Figure 6), reflecting in almost constant offtake throughout the experiment (Equation 16). All plants grown in BSY presented adequate B levels in tissue and the B offtake decreased from first and the last cycle (Equation 17; Figure 6).

$$\text{B}_{\text{offtake_biotite schist}} \text{ (mg per pot)} = 0.06^{**} - 0.0018(\text{cycle}), \quad R^2 = 0.08 \quad [\text{Eq. 16}]$$

$$\text{B}_{\text{offtake_biotite syenite}} \text{ (mg per pot)} = 0.19^{**} - 0.07^{**} \ln(\text{cycle}), \quad R^2 = 0.79 \quad [\text{Eq. 17}]$$

The Cu concentration in maize grown in BSC was adequate in all samples, from 26.1 to 7.0 mg Cu kg⁻¹ of dry mass (Figure 6). According to Malavolta et al. (1997), the critical concentration of Cu in maize is from 6 to 20 mg Cu kg⁻¹. Copper offtake in BSC decreased from the first to the last cycle following the equation 18:

$$\text{Cu}_{\text{offtake_biotite schist (mg per pot)}} = 0.083^{**} - 0.02^{**}\ln(\text{cycle}), \quad R^2 = 0.59 \quad [\text{Eq. 18}]$$

In maize plants grown in BSY, Cu concentration was adequate in 66% of samples (from 23.3 to 2.9 mg Cu kg⁻¹ of dry mass) and Cu offtake decreased from the first to the last cycle, according the equation 19:

$$\text{Cu}_{\text{offtake_biotite syenite (mg per pot)}} = 0.055^{**} - 0.02^{**}\ln(\text{cycle}), \quad R^2 = 0.91 \quad [\text{Eq. 19}]$$

Concentrations of zinc in maize plants grown in BSC were in the range from 40.7 to 8.1 mg Zn kg⁻¹ of dry mass. The nutrient requirement for optimal maize growth is 15 – 50 mg Zn kg⁻¹ (Broadley et al., 2012). Plants grown in BSY presented Zn concentrations from 54 to 11.4 mg Zn kg⁻¹ of dry mass. Zinc offtake decrease from the first to the last cycle (Figure 6) in plants grown in BSC according the equations 20 and 21:

$$\text{Zn}_{\text{offtake_biotite schist (mg per pot)}} = 0.13^{**} - 0.03\ln(\text{cycle}), \quad R^2 = 0.56 \quad [\text{Eq. 20}]$$

$$\text{Zn}_{\text{offtake_biotite syenite (mg per pot)}} = 0.13^{**} - 0.05^{**}\ln(\text{cycle}), \quad R^2 = 0.87 \quad [\text{Eq. 21}]$$

The availability of nutrients from BSC and BSY was related to the oxidizable iron content in minerals, such as biotite, chlorite, and clinopyroxene, which are also rich in alkali and alkaline earth cations. Along the experiment, the offtake of all elements decreased, indicating that a great part of the small, easily weatherable particles and exposed surfaces of minerals were (congruent or incongruently) dissolved. BSC and BSY, through the dissolution of selected minerals, therefore, provided nutrients to plants.

Conclusions

Biotite schist and biotite syenite are sources of macro and micronutrients for maize plants. Although biotite schist presented considerably less K in its composition than biotite syenite, plants grown in biotite schist produced higher amount of dry mass and accumulated more K and Mg than those grown in biotite syenite. It reflects the weathering process of the biotite mineral, conditioned by Mg and Fe content. Biotite syenite released a higher amount of Fe and Mn than the biotite schist, and the trend was highly correlated with Al offtake by plants, thus dissolution of minerals by plants within the experiment was related to the oxidation of Fe and Mn from selected minerals.

Tables and figures

Table 1. Particle size distribution of crushed rocks powders used in the experiment.

Sample	Particle size distribution (μm)				Total (g pot^{-1})
	< 53	53 - 300	300 - 1000	>1000 - 2000	
-----%-----					
Biotite schist	21.1	17.4	2.4	59.1	546.82
Biotite syenite	11.9	23.2	29.6	35.3	681.02

Table 2. Chemical composition of biotite schist and biotite syenite powder (bulk sample and fractions) determined by XRF and ICP-OES.^a

Sample	Fraction (μm)	SiO ₂	Al ₂ O ₃	Fe ₂ O ₃	CaO	MgO	TiO ₂	P ₂ O ₅	Na ₂ O	K ₂ O	MnO	BaO	Cr ₂ O ₃	Cu	Mo	Zn	LOI ^b
		-----%-----													----- mg kg ⁻¹ -----		
Biotite schist	< 53	59.6	16.1	8.06	2.31	3.84	1.08	0.29	2.57	2.61	0.06	0.06	0.02	104	<3	104	2.18
	53-300	59.7	19	7.74	0.87	3.68	0.57	0.15	1.84	4.14	0.05	0.11	0.02	35	<3	35	2.72
	300 – 1000	67.1	14.4	6.49	1.31	2.38	0.94	0.13	2.23	2.38	0.11	0.05	0.01	73	<3	73	1.59
	>1000	66.4	15.1	7.22	1.54	2.55	0.83	0.17	2.21	2.53	0.16	0.06	0.01	53	<3	53	1.5
	Bulk sample ^c	62.6	16.8	7.8	1.44	3.2	0.86	0.2	1.93	3.19	0.12	0.07	0.02	49	<3	49	2.17
Biotite syenite	< 53	53.4	14.6	10.5	3.38	2.16	2.31	0.61	1.49	9.36	0.17	0.58	0.01	88	<3	88	1.28
	53-300	53.7	14.9	11.1	2.69	2.14	2.32	0.38	1.19	10.7	0.14	0.58	0.01	46	<3	46	0.37
	300 – 1000	57.3	16.1	8.51	1.63	1.72	1.29	0.19	1.15	11.9	0.11	0.58	<0,01	35	<3	35	0.36
	>1000	57.6	16	7.41	1.89	1.54	1.26	0.24	1.38	11.8	0.11	0.6	<0,01	32	<3	32	0.29
	Bulk sample ^c	55.9	16	8.16	2	1.7	1.49	0.24	1.19	11.3	0.11	0.57	<0,01	31	<3	31	0.49

^aSGS Geosol Laboratórios Ltda; ^bLoss on ignition; ^cOriginal sample.

Table 3. Mineralogical composition of biotite schist and biotite syenite powder (bulk samples and fractions) used in the experiment.

Sample	Fraction (μm)	Quartz	Albite	Biotite	Muscovite	Chlorite	Clinopyroxene
Biotite schist	< 53	30.8	27.5	9.3	18.6	11.7	2.0
	53-300	33.4	22.2	10.3	22.5	10.5	1.1
	300 – 1000	38.7	20.7	7.5	17.0	14.4	1.6
	>1000	36.0	24.9	9.2	15.4	13.2	1.3
	Bulk sample ^a	35.7	22.1	11.2	17.9	11.3	1.7
Biotite syenite		K-feldspar ^b	Albite	Biotite	Amphibole	Clinopyroxene	
	< 53	60.3	13.9	10.7	1.9	13.2	
	53-300	52.5	11.0	22.5	4.4	9.4	
	300 – 1000	55.2	13.7	15.5	5.0	10.7	
	>1000	64.8	15.7	10.1	2.4	7.0	
	Bulk sample ^a	58.1	9.3	15.4	3.6	13.5	

^aOriginal sample; ^bOrthoclase and microcline.

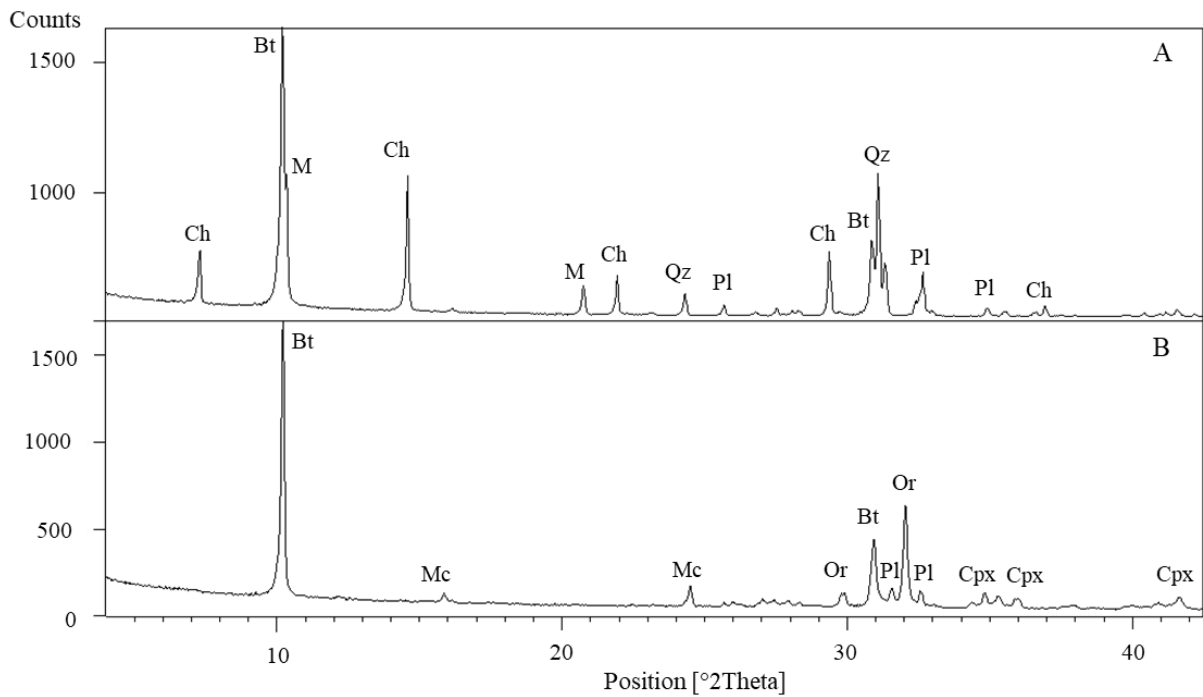


Figure 1. X-ray diffraction patterns of < 53 μm size particles of original samples of biotite schist and biotite syenite. A: X-ray diffraction pattern of biotite schist sample evidencing quartz (Qz), albite (Pl), Biotite (Bt), muscovite (M), chlorite (Ch) and; B: X-ray diffraction pattern of biotite syenite sample evidencing the orthoclase (Or), Microcline (Mc), Biotite (Bt) and clinopyroxene (Cpx).

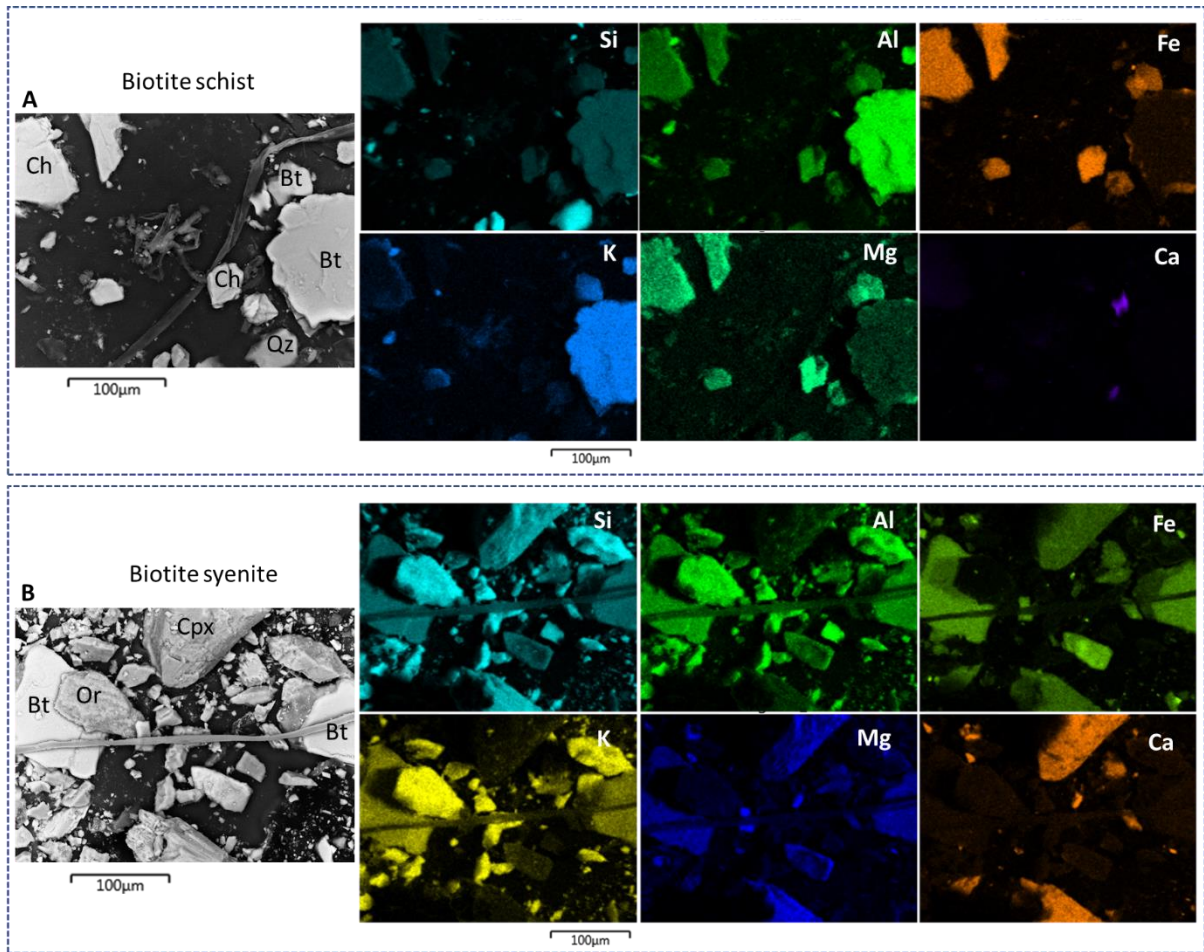


Figure 2. Energy-dispersive X-ray spectroscopy (EDS) images of biotite schist and biotite syenite compounds around the maize root. A: image of secondary electrons of biotite schist sample evidencing quartz (Qz), Biotite (Bt) and chlorite (Ch); B: image of secondary electrons of biotite syenite sample evidencing the orthoclase (Or), Biotite (Bt) and clinopyroxene (Cpx); Si: silicon; Al: aluminum; Fe: iron; K: potassium; Mg: magnesium; and Ca: calcium

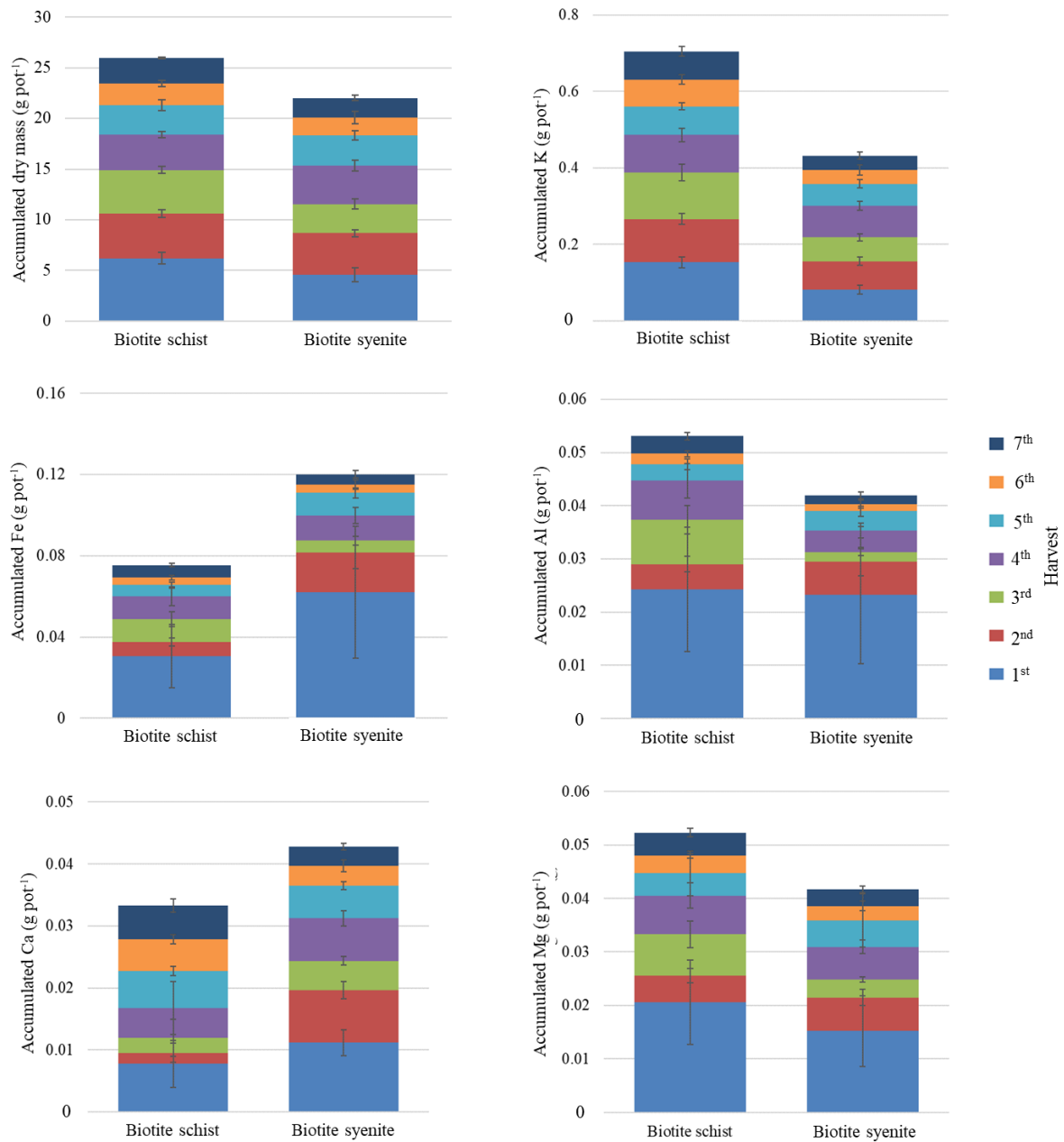


Figure 3. Cumulative dry mass and major elements offtake by maize cultivated in biotite schist and biotite syenite powder after seven cycles.

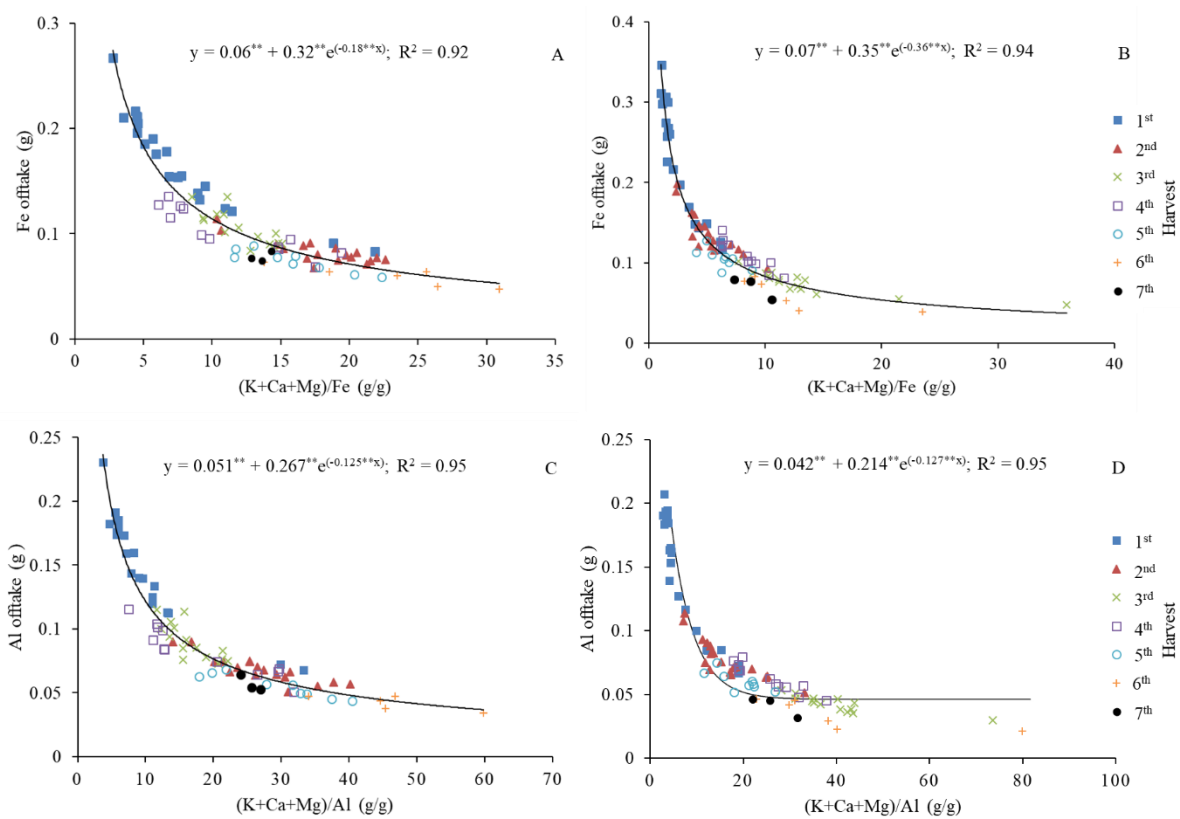


Figure 4. Iron (Fe) offtake as related to iron normalized sum of potassium, calcium and magnesium, extracted by plants from biotite schist (A) and biotite syenite (B); aluminum (Al) offtake as related to aluminum normalized sum of potassium, calcium and magnesium, extracted by plants from biotite schist (C) and biotite syenite (D); $**p < 0.01$.

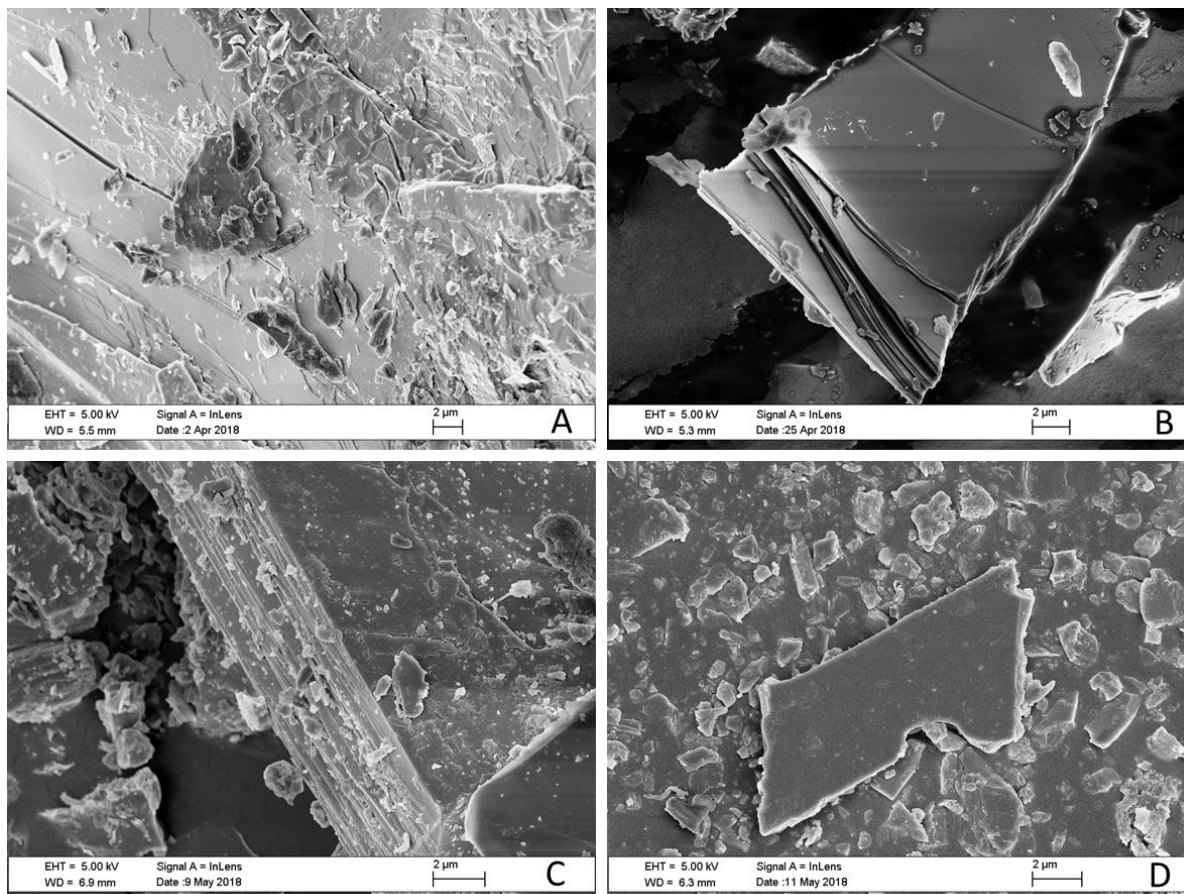


Figure 5. Scanning electron microscopy images of biotite grains from maize growth experiments. A) biotite surface before plant growth on biotite schist. B) biotite surface after plant growth on biotite schist. C) biotite surface before plant growth on biotite syenite. D) biotite surface after plant growth on biotite syenite.

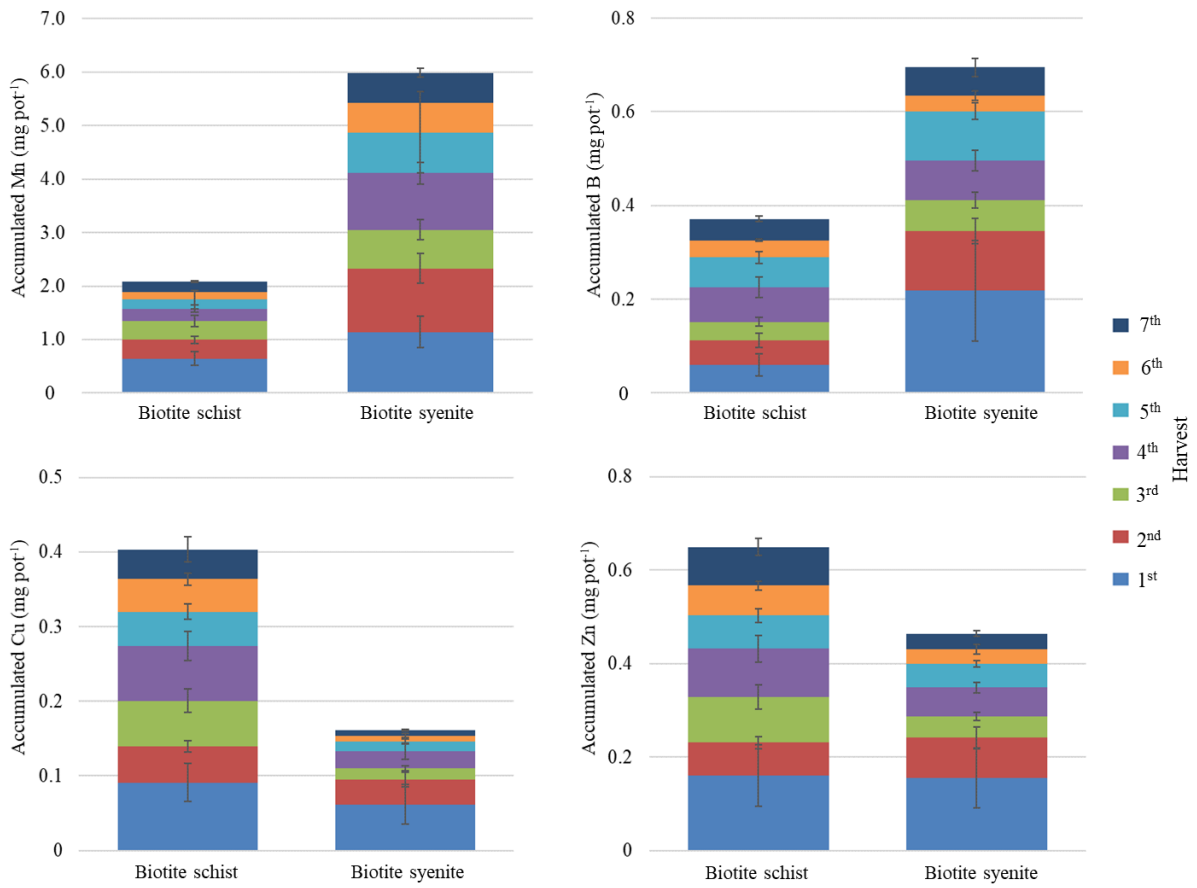


Figure 6 Cumulative micronutrients offtake by maize cultivated in biotite schist and biotite syenite powder after seven cycles

CHAPTER 4. RHIZOSPHERE OF MAIZE INCREASES WEATHERING RATES AND CHARGE OF SILICATE ROCKS

Luise Lottici Krahl^{a*}, Leonardo Fonseca Valadares^b, Simone Patrícia Aranha da Paz^c, Rômulo Simões Angélica^c, José Carlos Sousa-Silva^d, Giuliano Marchi^d and Éder de Souza Martins^d.

^a Universidade de Brasília, Área Universitária, 01, Vila Nossa Senhora de Fátima, CEP: 73345-010 - Planaltina - DF, Brazil. E-mail: luisekrah1@yahoo.com.br

^b Embrapa Agroenergia, Parque Estação Biológica - PqEB s/n°. Caixa Postal 40.315, CEP: 70770-901 - Brasília - DF, Brazil. E-mail: leonardo.valadares@embrapa.br

^c Universidade Federal do Pará, Instituto de Geociências, Caixa Postal 1611, CEP: 66075-110, Belém - PA, Brazil. E-mail: paz@ufpa.br, angelica@ufpa.br

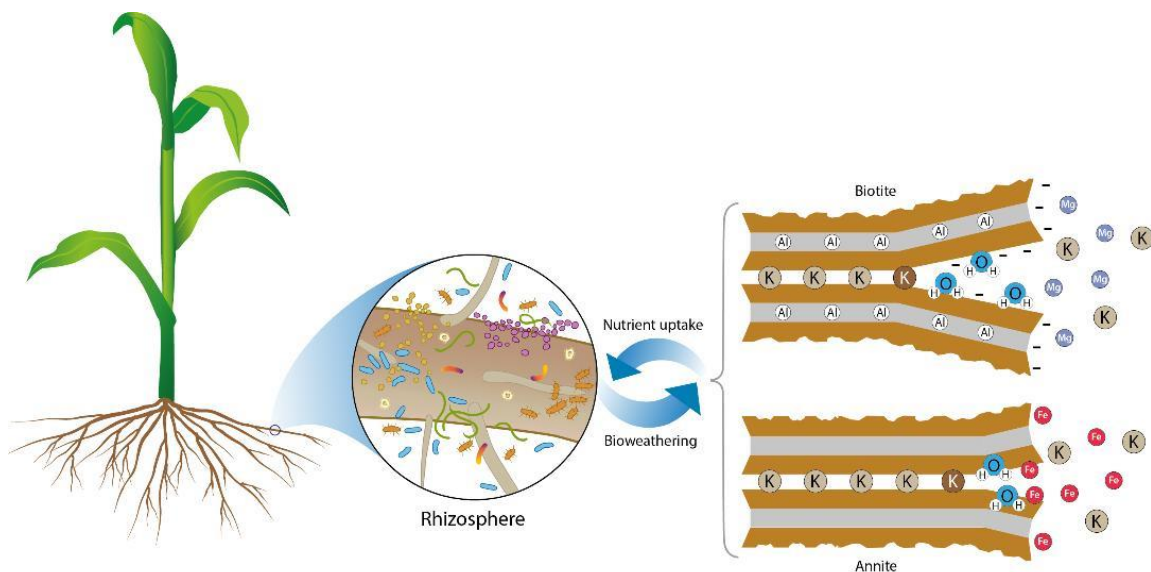
^d Embrapa Cerrados, Rodovia BR-020, Km 18, Caixa Postal 08223, CEP: 73310-970 – Planaltina - DF, Brazil. E-mail: jose.sousa-silva@embrapa.br, giuliano.marchi@embrapa.br, eder.martins@embrapa.br

*Corresponding author.

E-mail address: luisekrah1@yahoo.com.br (L.L. Krahl).

Chapter submitted as an article for the journal *Geoderma*.

Graphical Abstract:



Abstract – The release of elements from some silicate rocks minerals is known to significantly contribute to plant nutrition. The weathering of these rocks can occur in a few days of cropping and can generate different physicochemical properties in the silicate minerals. In this study, the weathering rates of biotite schist and biotite syenite under the influence of maize (*Zea mays* L.) rhizosphere were investigated. Pot experiments were carried out under controlled environmental conditions, where plant and rock materials were evaluated for seven successive growing cycles. Iron and potassium were taken up from biotite schist and biotite syenite during cropping. The dissolution of biotite minerals promoted by maize rhizosphere caused mineralogical changes in rock materials. Interstratified biotite-vermiculite minerals were observed by X-ray diffraction in biotite schist and in biotite syenite. The most significant changes in X-ray diffraction patterns occurred in < 53 μm particle size fraction, but the 53 - 300 μm fractions also changed. The alteration in biotite with low Fe/Mg in octahedral site was responsible for an increase in cation exchange capacity in fractions < 300 μm on biotite schist. However, the biotite weathering process in the biotite syenite, which presents higher Fe/Mg in octahedral sites, did not increased the cation exchange capacity. The formation of materials with permanent cation exchange capacity is particularly important for the management of soils presenting small cation retention capacity, such as tropical Oxisols.

Keywords: bioweathering, K-release, biotite, cation exchange.

Highlights:

- Rhizospheres induce the release of K from biotite schist and biotite syenite.
- Fe and K were extracted by plants from biotite schist and biotite.
- Hydrobiotite was formed from biotite schist and biotite syenite.
- Mineralogical transformation of biotite promoted significant increases in CEC.

Introduction

Aluminosilicate minerals can weather in a period of few days under the influence of the rhizosphere and thus provide nutrients to plants, working as slow release fertilizers (Basak, 2018; Ciceri and Allanore, 2019; Manning et al., 2017). Macro and micronutrients required for plant growth are abundant in these minerals (Basak et al., 2018; Burghilea et al., 2015; Hinsinger et al., 1992; Norouzi and Khademi, 2010), but

the selection of sources for agricultural use does not depend only on the absolute nutrient content, but rather on the rate minerals dissolve and nutrients are available for plants.

Mineral dissolution processes in the natural environment involve innumerable physical and chemical factors, including area of exposure, oxidation-reduction and adsorption-desorption-precipitation reactions (Manning, 2010). Additionally, the root activity is a determining factor affecting dissolution rates of minerals by modifying its environment, absorbing and releasing elements, releasing organic substances, and promoting microbial population growth (Hinsinger et al., 1993; Jones, 1998; Uroz et al., 2009; Wang et al., 2011; Yu, 2018). Above all else, plant-induced weathering rates of silicate rocks depends on the kind and proportion of minerals it contains.

Many studies have addressed the ability of different silicates to provide nutrients to plants in a short time scale, especially on the release of K (Ciceri et al., 2019; Hinsinger et al., 1992; Li et al., 2015; Manning et al., 2017). It was found that a significant proportion of K needed by plants can be extracted from K-rich minerals present in silicate rocks containing micas, K-feldspars and their weathering products (Burghelea et al., 2015; Ciceri et al., 2019; Mohammed et al., 2014 ; Naderizadeh et al., 2010; Zorb et al., 2014).

The release rates of K during mica weathering vary according to its mineralogy. Trioctahedral micas (biotite and phlogopite) exhibit a less stable structure than dioctahedral micas (muscovite), therefore K may be extracted by plants far easier by the former (Li et al., 2015). The release of cations from these trioctahedral micas during the incongruent dissolution may lead to the production of secondary minerals containing 2:1 layers, like illite or hydrous mica, vermiculite, chlorite, and interstratified minerals (Mohammed et al., 2014 ; Naderizadeh et al., 2010; Norouzi and Khademi, 2010).

During the beginning of the natural weathering process of biotite minerals, an expanded interstratified biotite-vermiculite (hydrobiotite) is formed. Hydrobiotite presents a large peak in X-ray analysis, ranging from 10 Å to ~24 Å as a result of the interlayer expansion on the edge of biotite layers. Along the time, it is expected a build up of a peak at 14 Å, reflecting the presence of vermiculite minerals (Fanning et al., 1989; Murakami et al., 2003; Pozzuoli et al., 1992). Both hydrobiotite and vermiculite may contribute to the increase of soil cation exchange capacity (Churchman and Lowe, 2012), especially in soils with low content of 2:1 minerals, and presenting low amount of organic matter. However, the chemical composition, especially the Fe and Mg content of the biotite, as well as the substitution of elements in the octahedral and tetrahedral silicate

sheets (e.g. Si^{4+} by Al^{3+} and Fe^{3+} in tetrahedron site or Al^{3+} by Mg^{2+} in octahedron sites), lead to different weathering rates (Gilkes et al., 1973; Murakami et al., 2003). In oxidizing conditions, reduced iron released from the mineral matrix, if not absorbed by plant roots, or lost by leaching or runoff, rapidly precipitates as amorphous Fe(III) hydroxides. The precipitation of Fe on the surface of transforming minerals probably play a role in delaying the continuity of the weathering process and blocking charged sites formed on mineral surfaces (Bray et al., 2015; Tamrat et al., 2018; Tombolini et al., 2002; Zavarzina et al., 2016).

Biotite bearing rocks, like some schists and syenites, are widely available in tropical environments (Ciceri et al., 2019; Manning et al., 2017; Navarro et al., 2013). These rocks may present a relatively fast dissolution rates in soils agroecosystems being able to release nutrients for plants (Basak et al., 2018; Burghilea et al., 2015; Li et al., 2015; Manning et al., 2017; Wang et al., 2000). Thus, investigations about the weathering of these silicate rocks can provide information on physicochemical parameters, which can improve soil properties, especially for those highly weathered. The aim of this work is to study the weathering products of biotite schist and biotite syenite, as affected by the rhizosphere of maize.

Material and methods

Sampling

Biotite schist (BSC) was collected from residue piles in quarries located at Abadiânia, state of Goiás, Brazil (Navarro et al., 2013) and biotite syenite (BSY) was collected at Ceraíma massif, in the southeastern of the state of Bahia, Brazil (Cruz et al., 2016). Samples (150 kg of each rock) were air-dried and homogenized using the cone-and-quartering reduction method. This procedure was repeated several times to ensure complete homogenization of material, forming the bulk sample.

Greenhouse experiment

The bulk BSC and BSY samples were placed into 500 mL pots. Two plants of maize (*Zea mays* L.) were grown in seven sets of three pots. Seven extra pots without plants were prepared, as a control treatment. At every 1–2 days all pots were watered with deionized water. Pots were fertilized with nutrient solution ($92.76 \text{ mg pot}^{-1} \text{ NH}_4\text{H}_2\text{PO}_4$) in the 15th and 30th days of growth of each cycle.

At the end of each 45-days cycle, whole plants from all pots were harvested. The rock material content from one set of three pots previously grown with plants, and another from one pot of the control set, were removed from the greenhouse. The pots content was used for laboratory analyses. The remaining sets were re-sown for a new growth cycle.

Sample preparation and analyses

The harvested plants were oven dried at 65 °C for 72 hours. Potassium, iron and magnesium in dry biomass (total dry mass comprising leaves shoots and roots) were extracted by HNO₃:HClO₄ in a digestion block (Embrapa, 2017) and determined by inductively coupled plasma - optical emission spectrometry (ICP-OES). Elements offtake along the cycles were modeled and the equations were selected according to the analysis of variance (ANOVA) (Supplementary material; Figures S3 and S5) and, thereafter, were tested for normality (Shapiro-Wilk), and constant variance test (homoscedasticity), considering p-values < 0.05 significant. These statistical analyses were performed using Sigma Plot 12.0 software (Sigma Plot Software; San Jose, California, USA).

The pots removed from the greenhouse at the end of each growth cycle were dismantled and its contents, bulk samples, were wet sieved to obtain four size fractions: < 53 µm, 53 – 300 µm, 300 – 1000 µm and > 1000 µm.

The main chemical elements of BSC and BSY samples were analyzed using wavelength dispersive X-ray fluorescence (XRF) spectroscopy and the multi-acid solution method. Major elements were determined on fused glass discs, 40 mm-diameter, prepared from 0.8 g of sample powder mixed with 4.5 g lithium tetraborate flux and fused in Pt-5% Au crucibles at 1120°C (SGS Geosol Laboratórios Ltda) (Supplementary material; Table S1). The analysis was handled according to certified quality management system ABNT NBR ISO 9001:2008. The multi-acid solution method consisted of digesting 500 mg of sample in 10:15:10:5 mL of HCl:HNO₃:HF:HClO₄, respectively and, afterward minor elements were determined by ICP-OES (SGS Geosol Laboratórios Ltda). The loss on ignition was determined after heating samples overnight at 105 °C to remove water. The weight loss was measured after calcination of samples at 1000 °C for approximately 2 hours.

Electron probe microanalyses (EPMA) were carried out to identify the biotite mineral within the samples with a JEOL (model Superprobe JXA-8230), coupled with 5 spectrometers and one EDS (Energy Dispersive Spectrometer) detector, operating with 10 nA of current and 15 kV. The acquisition time was 10 seconds at the peak and 5

seconds at the background and the beam diameter was 1 μm . The instrument was calibrated using natural and synthetic primary standards and the resulting data was processed to calculate the structural formulas of the mineral phases. The analyses involved a total of 25 biotite crystals, 11 of BSC and 14 of BSY (Supplementary material; Tables S2 and S3; Figures S7 and S8).

The mineralogical composition of BSC and BSY fractions before and after every crop cycle was analyzed by X-ray diffraction analysis (XRD) using a PANalytical Empyrean (PW3050/60) diffractometer, using the powder method in the range of $5^\circ < 2\theta < 75^\circ$. $\text{CoK}\alpha$ radiation (40 kV; 40 mA) was applied, and the 2θ scanning speed was set at $0.02^\circ \text{ s}^{-1}$. Data was acquired using the software X'Pert Data Collector 4.0 and was treated on X'Pert HighScore 3.0 (PANalytical). Minerals were identified by comparing the obtained diffractogram with the ICDD-PDF (International Center for Diffraction Data) database.

The transformation rate of biotite into hydrobiotite for both BSC and BSY was estimated using the following equation:

$$\text{Hydrobiotite: biotite ratio per cycle (\%)} = \left(\frac{\text{Hydrobiotite peak area}}{\text{Hydrobiotite peak area} + \text{biotite peak area}} \right) \cdot 100 \quad [\text{Eq. 1}]$$

The peak area was used to estimate a ratio for the biotite:muscovite ratio from BSC by the equation:

$$\text{Biotite: muscovite ratio per cycle (\%)} = \left(\frac{\text{biotite peak area}}{\text{biotite peak area} + \text{muscovite peak area}} \right) \cdot 100 \quad [\text{Eq. 2}]$$

The Rietveld refinement was performed using the High Score Plus Program (Malvern Panalytical, version 4.7) for quantitative determination of the mineralogical composition in each size fraction of BSC and BSY original samples. The structural models (CIF files) for the identified mineral phases were obtained from the ICSD database. Traditional sequence for such refinements is as follow: scale factor and background, using a polynomial function, besides unit cell parameters for all phases. The W parameter of the Caglioti equation is refined only for the major phases, followed by V and U. Chlorites and micas exhibit strong preferred orientation and the (001) direction must be refined, besides the (100) plane for the feldspars (microcline and albite). Atomic positions were not refined.

The morphology of the BSC and BSY on $< 53 \mu\text{m}$ samples was examined by scanning electron microscopy (SEM) on a Zeiss SIGMA HV field emission microscope model using the InLens detector. Samples were pulverized over conductive double-face

carbon tape fixed on SEM stubs. A thin conductive layer of gold (10 nm) was deposited over the samples using the Q150T-ES sputter (Quorum Technologies).

The cation exchange capacity (CEC) of BSC and BSY after each growth cycle was determined by the method BS EN ISO 11260 (2011), where: 3.5 g of sample were placed in 50 mL polyethylene tubes, and leached with 30 mL 0.1 mol L⁻¹ barium chloride dihydrate for 1 h. Tubes were centrifuged and the supernatant was removed. The procedure was repeated three times. Samples were, then, equilibrated with 30 mL 0.01 mol L⁻¹ barium chloride solution, and shaken for 12 h. Tubes were centrifuged and the supernatants were removed. Subsequently, 30 mL 0.02 mol L⁻¹ magnesium sulfate heptahydrate was added and shaken for 12 h. Tubes were centrifuged and supernatant was collected for analysis. The excess magnesium was determined by flame atomic absorption spectrometry (FAAS AA-6300 Shimadzu). Each treatment was repeated 3 times. The Texas Montmorillonite (STx-1), Gonzales County, Texas, USA, was used as a standard reference for the measured CEC. The amount of STx-1 used in the CEC analysis was 1g.

Results and discussion

The bulk samples and fractions (Table 1) chemical and mineralogical composition (Tables 2 and 3) showed the presence of the mineral biotite in both BSC and BSY. In these rocks, the mineral biotite is the main active mineral likely to weather, releasing nutrients, such as K, Ca, Mg, Fe and Mn (Table 3).

The mineral biotite analyzed showed great variation in the MgO and FeO contents between the rocks (Figure 1). The biotite within BSC samples presents higher MgO and Al₂O₃ contents in octahedral sites, referred henceforth as Mg-biotite. According to Tischendorf et al. (2007) classification was located in the annite, siderophyllite and phogopite interface, with the chemical composition K_{0.817} Ba_{0.005} (Mg_{1.198} Fe_{1.157} Al_{0.415} Ti_{0.088}) (Si_{2.845} Al_{1.154} O₁₁) (OH_{1.97} F_{0.02} Cl_{0.001}). In BSY samples, the mineral biotite was classified as annite (Tischendorf et al., 2007), a Fe-biotite with the chemical composition K_{0.805} Ba_{0.022} Na_{0.011} (Fe_{1.55} Mg_{0.785} Ti_{0.168} Al_{0.255} Mn_{0.01}) (Si_{2.963} Al_{1.036} O₁₁) (OH_{1.949} F_{0.045} Cl_{0.005}).

The pH of the bulk sample, measured after each cycle, decreased linearly after each growth cycle (Equations 3 and 4). The pH of the control samples did not change significantly (pH, standard deviation = 8.0, 0.2, and 7.8, 0.2, for BSC and BSY,

respectively; **p < 0.01), along the 7 cycles. The pH decrease was, therefore, promoted by the rhizosphere of plants during weathering.

$$\text{pH}_{\text{biotite schist}} = 7.49^{**} - 0.22^{**} (\text{cycle}), \quad R^2 = 0.91 \quad [\text{Eq. 3}]$$

$$\text{pH}_{\text{biotite syenite}} = 7.93^{**} - 0.36^{**} (\text{cycle}), \quad R^2 = 0.88 \quad [\text{Eq. 4}]$$

At nearly neutral pH, the weathering of biotite involves the oxidation of structural Fe(II) and the exchange of interlayer K for ions in the external solution, while at acidic pH it proceeds through a near-congruent dissolution (Malmström and Banwart, 1997; Ryu et al., 2016; Voinot et al., 2013).

Nutrient release and mineralogical changes of biotite schist and biotite syenite

During the growth cycles, maize plants showed differences in potassium offtake according to the substrate and crop cycle. The accumulated potassium offtake by plants grown successively during 315 days in BSC was 0.704 g of K pot⁻¹ and in BSY was 0.431 g of K pot⁻¹. Potassium offtake by plants was higher in the first cycle for both rocks and then, decrease along the cycles according to the equations 5 and 6 (Supplementary material; Figure S3 and S5; **p < 0.01, *p < 0.05):

$$K_{\text{offtake_biotite schist}} (\text{g per pot}) = 0.15^{**} - 0.04^{**} \ln(\text{cycle}), \quad R^2 = 0.91 \quad [\text{Eq. 5}]$$

$$K_{\text{offtake_biotite syenite}} (\text{g per pot}) = 0.09^{**} - 0.007^{*} (\text{cycle}), \quad R^2 = 0.73 \quad [\text{Eq. 6}]$$

The potassium mobilization by plants was rock specific, but not related to the total concentration of this element in the rocks. Although biotite and the total K contents in the BSY bulk sample were higher than in BSC (Tables 2 and 3), the total K offtake was lower in plants grown in BSY. The mineral biotite present in BSC is more susceptible to weathering than the biotite and K-feldspars found in the BSY. As K-bearing minerals, orthoclase and microcline, which comprises 60.3% of the BSY, are minerals of high structural stability. This finding shows that the K availability depends on biotite mineralogy and its chemical composition.

Even though, an important parameter in the dissolution rate and nutrient release of primary minerals is the grain size and its relationship with the exposed reactive surface of minerals and with the chemical composition. The availability of K from K-rich silicate minerals can be substantially altered by milling that can transform minerals structural K into available forms and increase the percentage of finer fractions in the milled material

(Madaras et al., 2013). The smallest grain sizes are the most reactive fractions (Basak, 2018; Bray et al., 2015).

Therefore, nutrient release from ground rock fertilizer are dependent on the grain size and also on the density of surface defects of the material. The understanding of these mechanisms may help in the development of preparative treatments for silicate rock powders to allow greater dissolution and nutrient availability (Harley and Gilkes, 2000). Thus, the reactivity of BSC and BSY will be higher in the finer fractions, preferentially in those $< 53 \mu\text{m}$. This trend was verified by the XRD analysis: after 315 days of growth, the greatest pattern changes occurred in the finer size fraction ($< 53 \mu\text{m}$; Figure 2). The formation of interstratified mica-vermiculite, even for the coarser particle size fraction ($53 - 300 \mu\text{m}$), was also observed for BSC and BSY (Figure 2). This upshot shows that coarser particles are not chemically inert in short time scale as it was generally believed. The practical use of this information is that great part of the BSC and BSY applied to agricultural soils ($> 80\%$ w/w) should be milled $< 300 \mu\text{m}$.

The X-ray diffraction patterns of particles smaller than $53 \mu\text{m}$ of BSC and BSY detected mineralogical transformations occurring right after the first 45 days cycle (Figure 3). This result confirms that the finer particle size fraction contains the most reactive particles in the bulk sample. The XRD pattern of the $< 53 \mu\text{m}$ collected from pots without plants (control samples) after 315 days of incubation were similar to the XRD results of the original material (before the experiment) for both BSC and BSY. There was no evidence of weathering on the control samples and for this reason, the maize rhizosphere was the responsible for the weathering observed in the rock materials.

The XRD pattern from the BSC after each of the 7 cycles (totaling 315 days) showed progressive process of vermiculitization (Figure 3). The edges of the mineral biotite expanded and, consequently, a large peak for the formed hydrous mica was detected. A hydrobiotite, a precursor of vermiculite, is a mica that has gained water by losing a part of its K content. The hydrobiotite peak at 14.8 \AA emerged gradually, as roots extracted K from biotite interlayers. The observed result is consistent with the work conducted by Mohammed et al. (2014) where a corresponding appearance of the 14.8 \AA peak in weathered biotite was classified as a clear, defined, 002 vermiculite peak.

Similar results were obtained for BSY, with a 14.5 \AA peak, also indicating the beginning of the hydrobiotite formation from the weathering of biotite (Figure 3). Similarly, the appearance of this peak in phlogopite and biotite weathered by the rhizosphere of alfalfa for 90 days was interpreted by Norouzi and Khademi (2010) as

reflections from the 001 planes of a typical vermiculite. Although BSY was mostly constituted by a K-feldspar, the change in the XRD pattern was attributed only to the biotite as it was a short experiment. Feldspars are known to be more resistant to weather than biotite, however, it does not form a new crystalline phase.

The XRD peak areas of biotite and hydrobiotite were used to estimate their relative percentages over time (Figures 4 and 5). The decrease in the biotite peak area was related to the formation of hydrobiotite in BSC along the time (Figure 4A; Equation 1). Thus, the hydrobiotite formation rate was negatively correlated with biotite on the < 53 μm size fractions (Pearson correlation, $r = -0.88$; $p < 0.05$). This result indicated that the incongruent dissolution of biotite was the source for the appearance of hydrobiotite in BSC samples.

However, the dissolution of biotite in BSC samples was estimated using the muscovite [$\text{KA}_2(\text{AlSi}_3\text{O}_{10})(\text{OH},\text{F},\text{Cl})_2$] as an internal standard (Figure 5; Equation 2). Likewise, biotite, muscovite is a K-bearing mineral, however, muscovite has a higher content of Al than biotite, thus presenting high resistance to weathering. The internal standard for the BSY, on the other hand, a K-feldspar (a high resistant mineral), did not allow to correlate the biotite and hydrobiotite ratios. Therefore, the dissolution rate of the mineral biotite in BSY samples was not estimated.

For the BSY samples, the formation of hydrobiotite was slower than with BSC. Hydrobiotite formation was relatively faster in the initial crop cycles but slowed down during the experiment (Figure 4B; Equation 1). The magnesium and Fe(II) contents on biotite mineral structure of the BSY, with high Fe/Mg in octahedral site, may explain the slow pace of hydrobiotite formation rate. Some authors denote the variations in Fe and Mg contents, and the substitution rate of elements in the octahedral and tetrahedral silicate sheets, to differences in the weathering rate of biotite minerals (Li et al., 2015; Madaras et al., 2013; Murakami et al., 2003; Naderizadeh et al., 2010). Therefore, plants mobilized Mg and Fe differently from BSC and BSY. These differences in element mobilization were related to dissolution kinetics of minerals specific to different rock types, specially biotite. After 315 days, plants accumulated 0.052 and 0.041 mg of Mg pot^{-1} , and 0.07 and 0.12 mg of Fe pot^{-1} , for BSC and BSY, respectively (Supplementary material; Figure S3 and S5).

The oxidation of octahedral Fe in biotite may be an important mechanism in the mineral which prevents the release of the interlayered K (Murakami et al., 2003). According to Barshad and Kishk (1969) and Gilkes et al. (1972), as the weathering

proceeds, the Fe-rich biotite such as the one found in BSY becomes more stable and the weathering process slow down. The authors showed that biotite dissolution rates decrease with an increasing oxidation of the iron held in octahedrally coordinated sites. As a matter of fact, Fe(II) leaves the network and oxide to Fe(III), getting out from the mineral structure, which enhances the weathering. After this stage, biotite weathering rate decreases, exactly as occurred in the present experiment for BSY samples (Figure 4). The difference in OH orientation has also been cited as the cause of higher potassium retention in Fe-rich biotites after structural Fe(II) oxidation (Barshad and Kishk, 1969; Gilkes et al., 1972, 1973).

While Fe(II) oxidation is the dawn of the weathering process, for BSC (with low Fe/Mg in biotite octahedral site), a higher Mg content in biotite composition accelerates the alteration that leads to vermiculite, as discussed by Murakami et al. (2003). The authors pointed out that vermiculite formation via layer-by-layer transformation occurs even in the early stage of dissolution for Mg-rich biotite and phlogopite, but this process does not occur for Fe-rich biotite.

Even though the XRD analysis of both kinds of biotite showed they did not dissolve congruently throughout the experiment, a detailed observation of grain surfaces by SEM (Figure 6) supports the idea that biotite experienced a congruent dissolution of the fine-grained particles, similarly as demonstrated by Manning et al. (2017) and Basak (2018). The surfaces of biotite mineral from control samples after 7 cycles (without plants) from BSC and BSY were covered with fine particles. On the other hand, on the surfaces of the biotite mineral particles, which were submitted to the growth of plants during 7 cycles, it was observed a reduction in the amount of fine particles covering them.

Effect of weathering promoted by maize rhizosphere on cation exchange capacity (CEC)

Values for CEC of the STx-1 (average±standard deviation, n = 12) were 66.8 ± 4.05 $\text{cmol}_c \text{ kg}^{-1}$. The measured values are lower than the published values found for the clay mineral, using other methodologies [$84.4 \text{ cmol}_c \text{ kg}^{-1}$ (van Olphen and Fripiat, 1979); $83.3 \text{ cmol}_c \text{ kg}^{-1}$ (Battaglia et al., 2004); $89 \text{ cmol}_c \text{ kg}^{-1}$ (Borden and Giese, 2001)]. Choo and Bai (2016) also commented on CEC values for the STx-1 using $\text{BaCl}_2/\text{MgSO}_4$ method to be lower (data was not shown) than the published values using other methodologies.

Cation exchange capacity analyses for the studied rock materials were obtained from the non-weathered samples and throughout the experiment after interaction with

maize rhizosphere only for those samples that showed evidences of hydrobiotite in X-ray diffractograms. Although coarser fractions of BSY formed hydrobiotite after the seven growth cycles (Figure 2), the fraction $< 53 \mu\text{m}$ did not had its CEC modified along the experiment ($\text{CEC} = 3.73 \pm 0.93 \text{ cmol}_c \text{ kg}^{-1}$, $n = 24$, in 7 cycles), not justifying further analyses of coarser BSY fractions. Murakami et al. (2003) revealed that the bulk biotite solution is supersaturated with respect to Fe and Al oxide-hydroxides very early during its dissolution. Iron is probably in the amorphous form and disperse as fine-grained microcrystalline oxides on the surface and edges of oxidized biotite (Bray et al., 2015; Murakami et al., 2004; Tamrat et al., 2018; Zavarzina et al., 2016). The charge properties of BSY, therefore, may have been altered after Fe oxides were formed in its surface (Scott and Amonette, 1988).

Nevertheless, fractions $< 53 \mu\text{m}$ and $53 - 300 \mu\text{m}$ from BSC showed presence of hydrobiotite in XRD (Figure 2) and were analyzed for CEC. Along the cycles of growth, the BSC showed a progressive increase in the CEC, which started to increase in the first cycle (Figure 7), and not after decades, as it was supposed to happen following laboratory data without the presence of plants or organic ligands (e.g. Malmström and Banwart, 1997; Bray et al., 2015). The CEC on the fractions $< 53 \mu\text{m}$ and $53 - 300 \mu\text{m}$ increased along the experiments, respectively from 1.48 and 2.77 $\text{cmol}_c \text{ kg}^{-1}$ to 8.91 and 7.13 $\text{cmol}_c \text{ kg}^{-1}$ after 315 days of continuous growth. Moreover, the CEC on the fraction $< 53 \mu\text{m}$ and the hydrobiotite formation rate were positively correlated (Pearson correlation, $r = 0.92$; $p < 0.05$; Figures 4A and 7). The slope of the CEC equations for each fraction is close to each other, thus the rate of CEC increase is similar for the two fractions under the action of the rhizosphere. The slope of the straight line formed of CEC along the growth cycles also suggests that higher values of CEC would be attained, granted that more cycles were provided.

The CEC presented in the fractions $< 300 \mu\text{m}$ after the 7 growth cycles suggests that the BSC has the potential to increase the CEC from soils with very low CEC, but only recommended after increases in soil quality are thoroughly assured. As a parameter, highly weathered soils, as Oxisols, are characterized by relatively low $\text{CEC}_{\text{pH } 7.0}$ values ($7.6 \pm 5.9 \text{ cmol}_c \text{ kg}^{-1}$, from Essington, 2003; $7.1 \pm 4.0 \text{ cmol}_c \text{ kg}^{-1}$, $n=23$, from Marchi et al., 2015, for representative Oxisols of the Brazilian Cerrado). Other assumption is that both BSC and BSY may weather at diverse rate after applied and mixed to agricultural soils than by plants growing in pure rock materials, and due to the intense exposition of

the material and presence of innumerable other compounds and biota, the limitations seen during the BSY weathering in the present experiment may not happen in soils.

Conclusions

This study provides evidence of the bioweathering on milled rock materials. The growth experiments showed that the maize rhizosphere has induced the release of interlayer K from biotite in BSC and BSY as soon as 45 days growing period. In these experiments, the only source of K were the crushed rocks and as a consequence of the processes on rhizosphere and the uptake activity of the plants, an interstratified biotite-vermiculite (hydrobiotite) was formed in the < 300 μm size fractions.

This result indicates that the initial release of K occurred by congruent dissolution from the finer particles of low crystallinity due to an action of plant intervention, as observed in SEM images. But during the experiment, the XRD patterns showed that the weathering of the minerals also happened incongruently. In BSC, the weathering process formed hydrobiotite which was the responsible for the increase the cation exchange capacity in the < 300 μm size fractions. The Fe(II) oxidation in the mineral of biotite in the BSY has generated a stable weathering environment, preventing further K release and the formation of charge.

Tables and figures

Table 1. Particle size distribution of crushed rocks powders used in the experiment.

Sample	Particle size distribution (μm)				Total (g pot^{-1})
	< 53	53 - 300	300 - 1000	>1000 - 2000	
-----%-----					
Biotite schist	21.1	17.4	2.4	59.1	546.82
Biotite syenite	11.9	23.2	29.6	35.3	681.02

Table 2. Chemical composition of biotite schist and biotite syenite powder (bulk sample and fractions) determined by XRF and ICP-OES.^a

Sample	Fraction (μm)	SiO ₂	Al ₂ O ₃	Fe ₂ O ₃	CaO	MgO	TiO ₂	P ₂ O ₅	Na ₂ O	K ₂ O	MnO	BaO	Cr ₂ O ₃	Cu	Mo	Zn	LOI ^b
		-----%-----													----- mg kg ⁻¹ -----		
Biotite schist	< 53	59.6	16.1	8.06	2.31	3.84	1.08	0.29	2.57	2.61	0.06	0.06	0.02	104	<3	104	2.18
	53-300	59.7	19	7.74	0.87	3.68	0.57	0.15	1.84	4.14	0.05	0.11	0.02	35	<3	35	2.72
	300 – 1000	67.1	14.4	6.49	1.31	2.38	0.94	0.13	2.23	2.38	0.11	0.05	0.01	73	<3	73	1.59
	>1000	66.4	15.1	7.22	1.54	2.55	0.83	0.17	2.21	2.53	0.16	0.06	0.01	53	<3	53	1.5
	Bulk sample ^c	62.6	16.8	7.8	1.44	3.2	0.86	0.2	1.93	3.19	0.12	0.07	0.02	49	<3	49	2.17
Biotite syenite	< 53	53.4	14.6	10.5	3.38	2.16	2.31	0.61	1.49	9.36	0.17	0.58	0.01	88	<3	88	1.28
	53-300	53.7	14.9	11.1	2.69	2.14	2.32	0.38	1.19	10.7	0.14	0.58	0.01	46	<3	46	0.37
	300 – 1000	57.3	16.1	8.51	1.63	1.72	1.29	0.19	1.15	11.9	0.11	0.58	<0,01	35	<3	35	0.36
	>1000	57.6	16	7.41	1.89	1.54	1.26	0.24	1.38	11.8	0.11	0.6	<0,01	32	<3	32	0.29
	Bulk sample ^c	55.9	16	8.16	2	1.7	1.49	0.24	1.19	11.3	0.11	0.57	<0,01	31	<3	31	0.49

^aSGS Geosol Laboratórios Ltda; ^bLoss on ignition; ^cOriginal sample.

Table 3. Mineralogical composition of biotite schist and biotite syenite powder (bulk samples and fractions) used in the experiment.

Sample	Fraction (μm)	Quartz	Albite	Biotite	Muscovite	Chlorite	Clinopyroxene
Biotite schist	< 53	30.8	27.5	9.3	18.6	11.7	2.0
	53-300	33.4	22.2	10.3	22.5	10.5	1.1
	300 – 1000	38.7	20.7	7.5	17.0	14.4	1.6
	>1000	36.0	24.9	9.2	15.4	13.2	1.3
	Bulk sample ^a	35.7	22.1	11.2	17.9	11.3	1.7
Biotite syenite		K-feldspar ^b	Albite	Biotite	Amphibole	Clinopyroxene	
	< 53	60.3	13.9	10.7	1.9	13.2	
	53-300	52.5	11.0	22.5	4.4	9.4	
	300 – 1000	55.2	13.7	15.5	5.0	10.7	
	>1000	64.8	15.7	10.1	2.4	7.0	
	Bulk sample ^a	58.1	9.3	15.4	3.6	13.5	

^aOriginal sample; ^bOrthoclase and microcline.

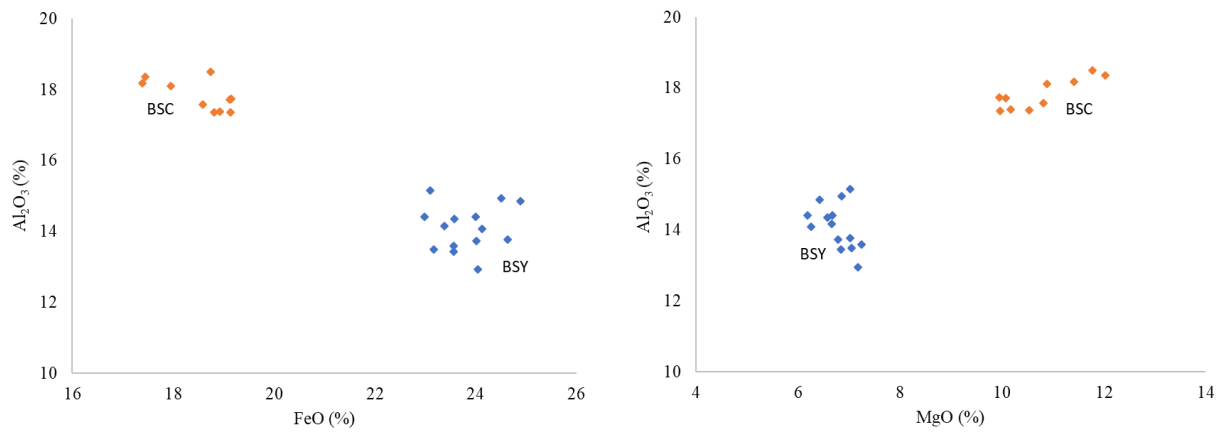


Figure 1. Differentiation of biotite mineral within biotite schist samples (BSC) and biotite syenite samples (BSY) by MgO x Al₂O₃ and FeO x Al₂O₃ ratios.

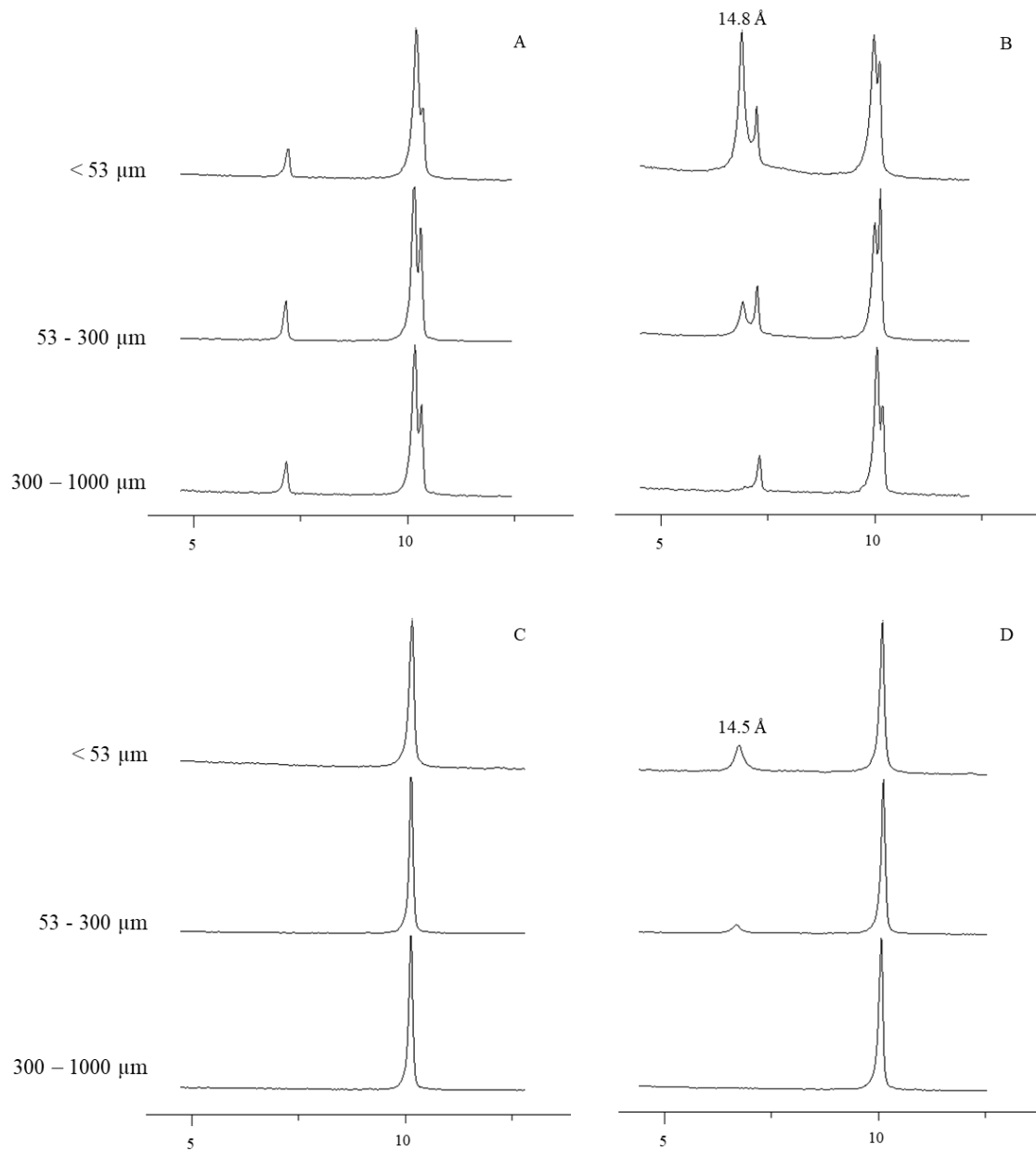


Figure 2. X-ray diffraction patterns of three size particles of biotite schist original samples (A), biotite schist samples after 315 days of interaction with maize rhizosphere (B), biotite syenite original samples (C), and biotite syenite samples after 315 days of interaction with maize rhizosphere (D).

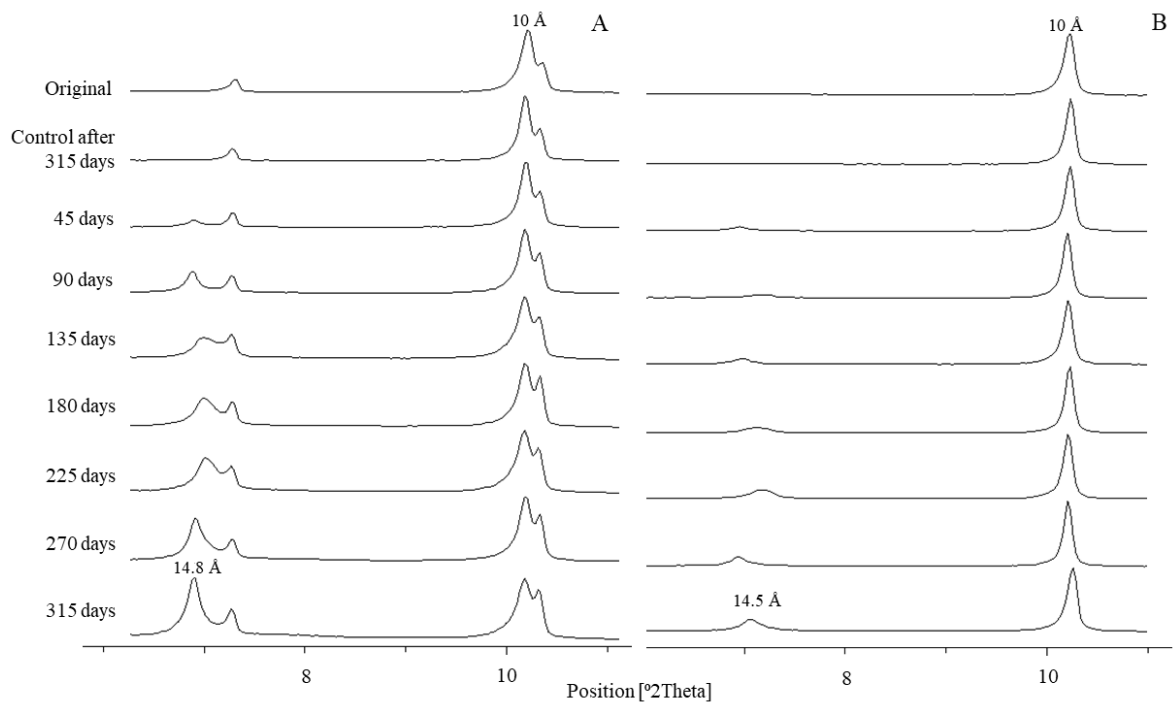


Figure 3. X-ray diffraction patterns of < 53 μm size particles of biotite schist (A) and biotite syenite (B) after interaction with maize rhizosphere.

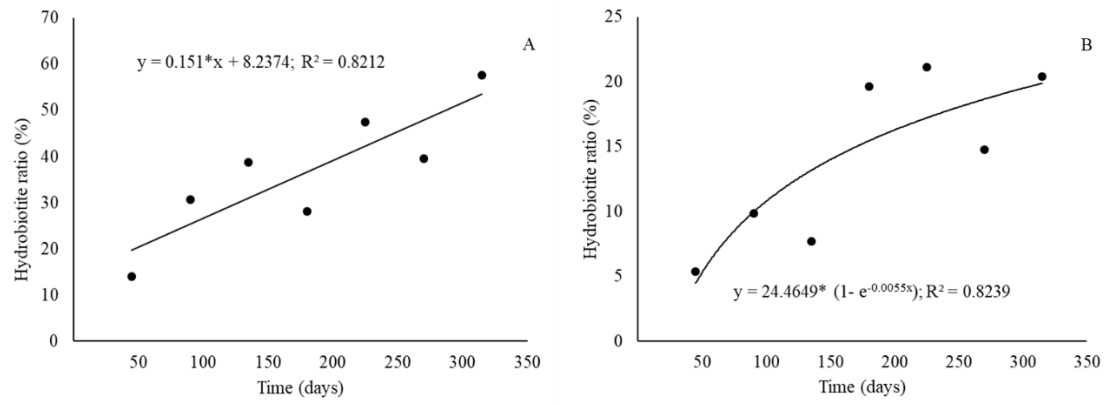


Figure 4. Hydrobiotite formation verse time: (A) biotite schist and (B) biotite syenite.

*Statistically significant at $p < 0.05$.

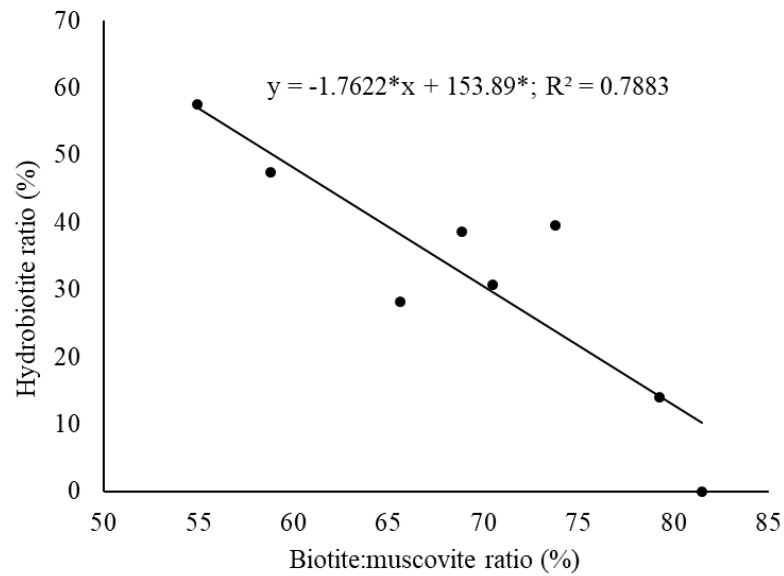


Figure 5. Relationship between biotite intensity XRD peaks and hydrobiotite formation in biotite schist. *Statistically significant at $p < 0.05$.

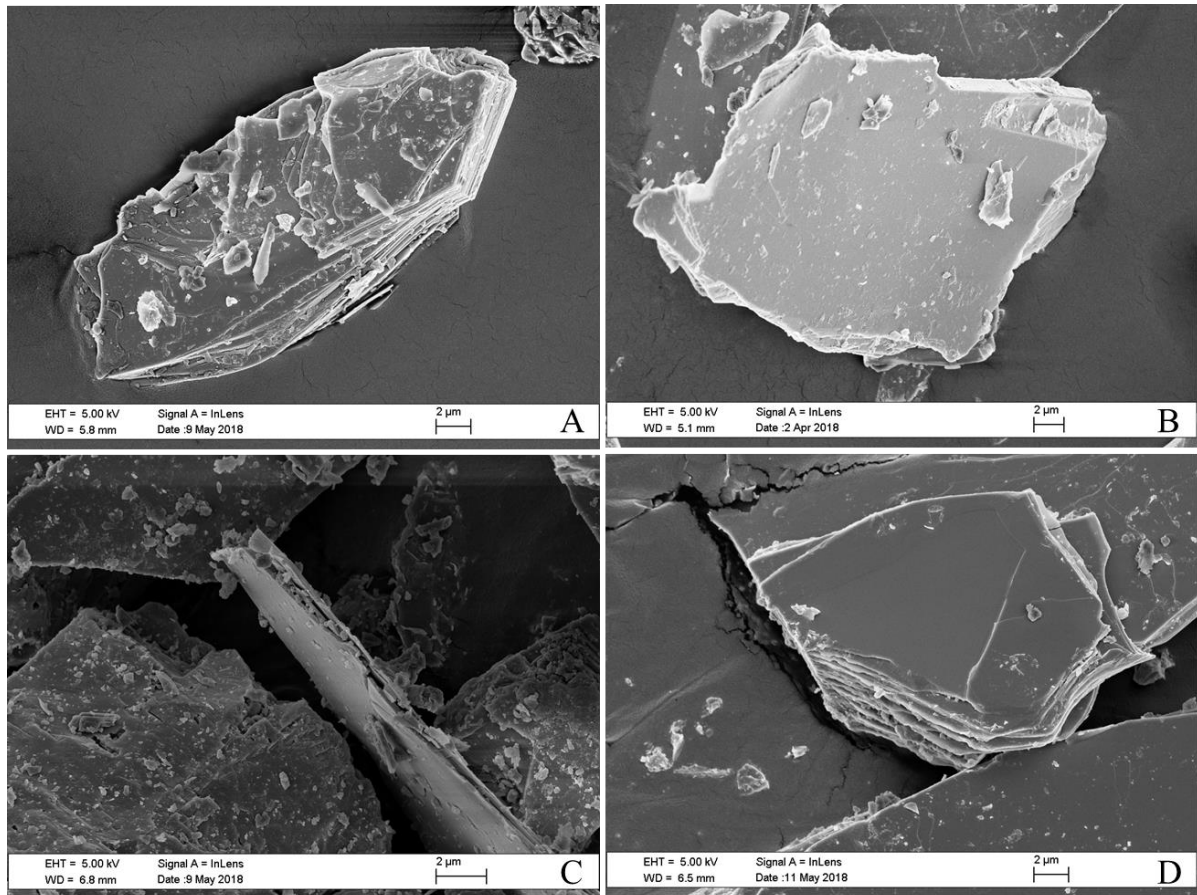


Figure 6. SEM images of biotite grains from maize growth experiments. Biotite surface without plant growth (A) and after plant growth (B) on biotite schist. Biotite surface without plant growth (C) and after plant growth (D) on biotite syenite.

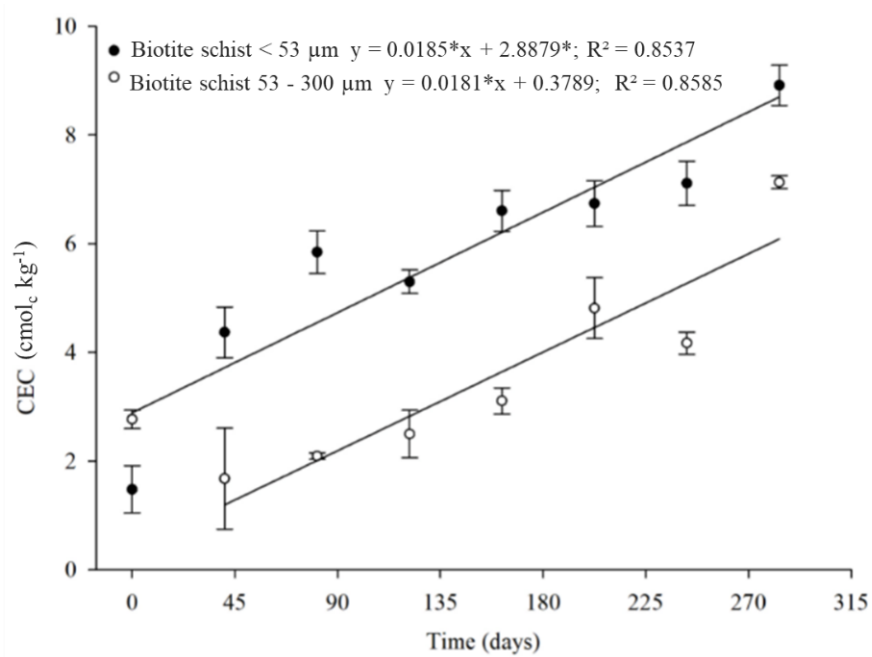


Figure 7. Cation exchange capacity (CEC) of <53 μm and 53 - 300 μm size particles of biotite schist during 315 days (7 cycles) of interaction with maize rhizosphere.

*Statistically significant at $p < 0.05$

CHAPTER 5. REMARKS AND FUTURE RESEARCH DIRECTIONS

Evaluation of the work

This work demonstrated that basalt, biotite schist, and biotite syenite rocks can act as a readily available source of nutrients for plants. Multi-element offtake by maize indicated that the plant plays an important role in the mineral dissolution. The offtake rates of macro and micronutrients could be interpreted in terms of chemical and mineralogical composition from studied rocks which allowed to identify the weathering process of minerals (Chapters 2 and 3). The plant as an extractor may guide new studies with agrominerals in the plant growing environment (Figure 1).

The main contribution of this study was the increase in mineral CEC from biotite schist bioweathering (Chapter 4) in the experimental conditions established. Those are not high values of mineral CEC, but the implications of these results for agrominerals research are relevant because it indicates a perspective for the silicate agrominerals as soil remineralizers.

The CEC reached was the result of a purpose for studying the bioweathering processes from a silicate rock within a short timescale, and are not intended to guide to recommendations for field application. This CEC disregards soil factors, microorganisms, and climate with their possible interactions (Figure 1).

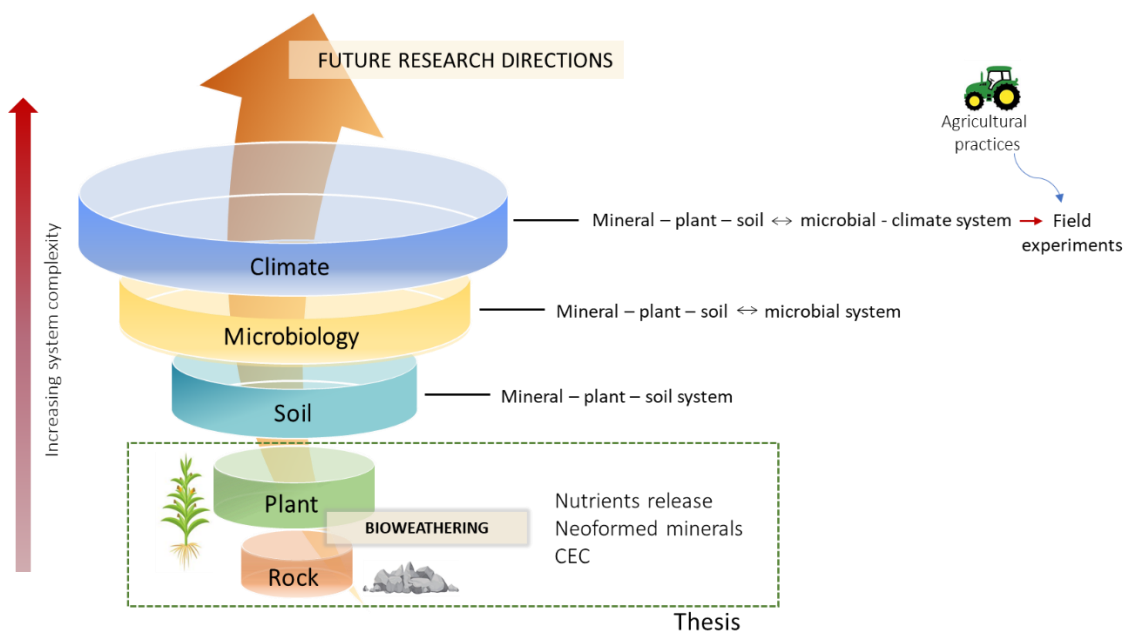


Figure 1. Experimental approach for using silicates as agrominerals.

Future research directions

Although the results provide insights on bioweathering rates of silicates agrominerals, the weathering in the agricultural systems occur in different environments and conditions, which must be addressed.

On a field scale, a range of factors can affect the dissolution process and rates of the silicate agrominerals. The effect of these silicates applied in agricultural soils as fertilizers or remineralizers will depend on soil characteristics, crop type, climate (temperature, precipitation), and management factors. More laboratory studies, greenhouse, and field experiments are needed to test the dissolution kinetics of these agrominerals in such complex natural systems (Figure 1).

Chemical, physical, and biological modification processes in the agrosystems could improve the effectiveness of silicates agrominerals. Active plant metabolism, as well as soil microbial action, have the potential to increase the weathering process greatly. These various processes can contribute to the mobilization of different elements from silicate minerals, with potentially important consequences for nutrient availability. It may also reflect in the soil quality, especially on building up of cation exchange capacity, by the formation of secondary minerals and low-crystallinity stages.

Potential of silicate agrominerals as a regulator of soil carbon storage

Most studies of silicate agrominerals have focused on its potential as an alternative fertilizer or soil amendments. However, other benefits of applying crushed rocks to agricultural soils are emerging. The possibility of these agrominerals for stabilizing carbon has also come into focus recently (Figure 2).

There are two paths to stabilize C in the soil: as soil organic carbon (SOC), mainly in soil organic matter (SOM), and as soil inorganic carbon (SIC). Silicate applications, besides the potential mentioned, could influence SOC - as affected by the soil mineral phases (Kleber et al., 2015; Sarkar et al., 2018; Singh et al., 2017; Wang et al., 2018), and SIC (Beerling et al., 2018, Hartmann et al. 2013; Kantola et al., 2017; Moosdorf et al., 2014; Strefler et al., 2018). Generally, the discussion on soil carbon sequestration has focused on SOC because its levels can change in response to land management in fast ways (Singh et al., 2018).

Researches demonstrated that the adsorption to soil minerals and occlusion within soil aggregates might stabilize SOM against decomposition (Angst et al., 2018; Kleber et al., 2015; Sarkar et al., 2018; Singh et al., 2017). The type and amount of clay minerals

are reported to provide a strong influence on SOM stabilization in soils related to their structure and physicochemical characteristics (Angst et al., 2018; Kleber et al., 2015; Singh et al., 2017; Wang et al., 2018). Soils with higher clay contents, generally, can protect more organic carbon from mineralization through a relation among physical, biological, and chemical mechanisms (Angst et al., 2018; Han et al., 2015; Sarkar et al., 2018). The large specific surface area and higher charge (CEC) both in smectites and vermiculites (2:1 expansive layers type) favor a higher sorption capacity and a greater ability to protect SOM. Besides allophane and imogolite types of clay minerals can strongly adsorb SOM through this mechanism.

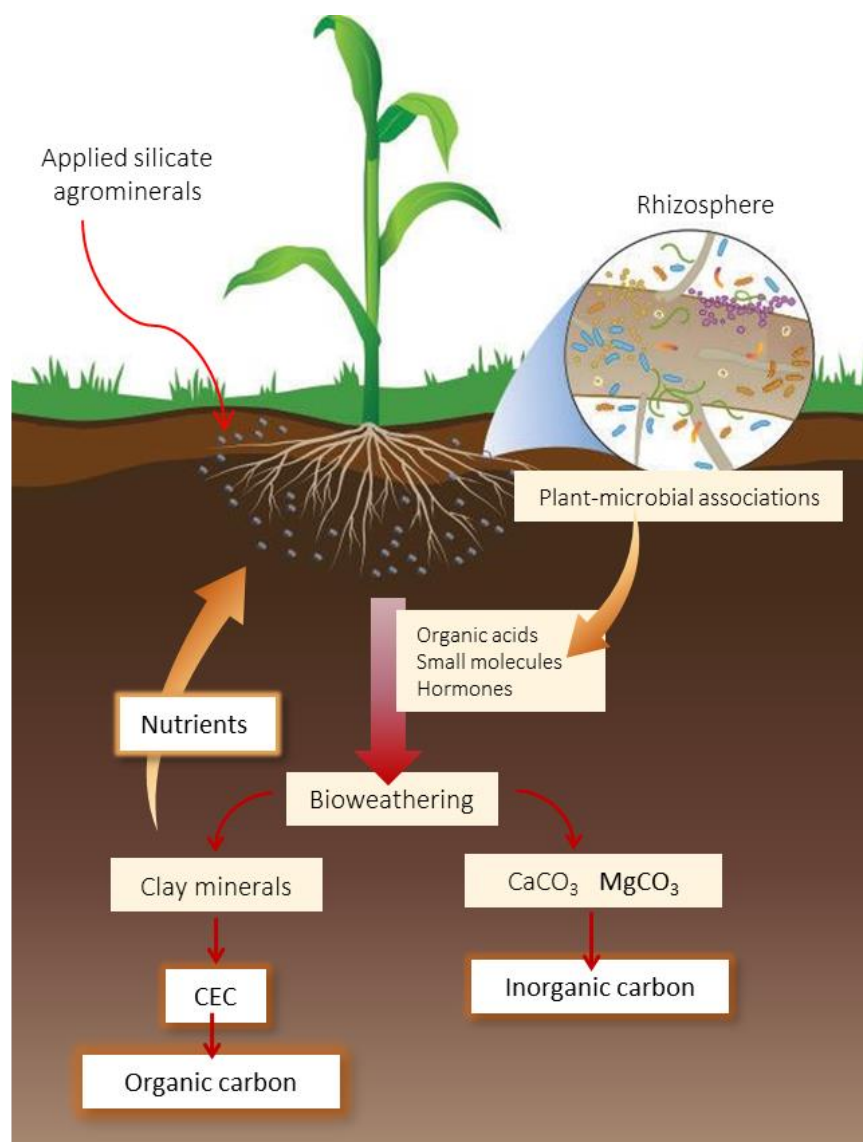


Figure 2. Potential effects of weathering of crushed silicate rocks as agrominerals.

Associations of organic matter with pedogenic minerals (named mineral– organic associations) in the soil is one of the factors defining the long-term retention of SOC. Such mineral organic associations limit microbial and enzymatic access and are quantitatively the most important mechanism protecting SOC from microbial use for centuries or millennia (Keiluweit et al., 2015). The conditions needed to formation of mineral– organic associations will be most abundant in regions with soil moisture supply for produce high plant biomass, that is, under conditions of intensive weathering, low pH and soil formation, such as the tropical environment (Kleber et al., 2015; Sarkar et al., 2018). However, unlike other climate zones, the rate of natural rock weathering in the tropics is limited by the supply of fresh mineral surfaces.

In these tropical environments, applications of silicate rocks in agricultural soils can add raw minerals to the system (Figure 2). Besides improving soil quality, this is a promising alternative to stabilize the SOM by the bioweathering process and newly formed minerals (Edwards et al., 2017; Beerling et al., 2018). These newformed minerals (vermiculites, smectites, amorphous phases, and low crystallinity minerals) with high CEC can lead adsorption or occlusion of SOM and can contribute to SOC stabilization.

As soils have an enormous carbon storage capacity (more than three times the amount of carbon stored in the atmosphere as CO₂), it has been suggested that with appropriate changes in management practices, the soil could represent an important sink for atmospheric CO₂ (Johns, 2017; Singh et al., 2018). Recent studies also highlight the potential of applying crushed silicate rock as a soil amendment for carbon sequestration, as dissolved inorganic carbon - DIC (Beerling et al., 2018, Hartmann et al. 2013; Kantola et al., 2017; Lefebvre et al., 2019; Moosdorf et al., 2014; Renforth, 2012; Strefler et al 2018).

The dissolution of silicate minerals, generally, releases cations such as Ca²⁺ and Mg²⁺ into the solution and thereby consumes CO₂, regulating the atmospheric CO₂ on geologic timescales. These slow natural process can be accelerated by amending soils with some crushed silicate rocks - as *enhanced weathering* - EW (Beerling et al., 2018, Hartmann et al. 2013; Kantola et al., 2017; Lefebvre et al., 2019; Moosdorf et al., 2014; Renforth, 2012; Strefler et al 2018), capturing and storing DIC in soil minerals and weathering process. The process takes CO₂ into the solution to form carbonate ions (CO₃²⁻) and bicarbonate (HCO₃⁻), increasing the alkalinity and pH of natural waters. Some products of mineral dissolution would precipitate in soils as CaCO₃, which sequester carbon in mineral form (Hartmann et al., 2013) or be taken up by ecosystems (Figure 2).

Large parts of the terrestrial surface are managed for agriculture and this may offer an opportunity to deploy means of carbon sequestration at scale within a decade or two (Beerling et al., 2018). The highest CO₂ sequestration potential is expected from ultramafic rocks with low silica content, dominated by Mg-rich olivine variety with 1.1 t CO₂ per t of rock, and mafic rocks such as the basalt with 0.3 t CO₂ per t of rock (Beerling et al., 2018; Hartmann et al., 2013; Renforth, 2012), without considering the effect of biological metabolisms. These arguments point out that a globally increased application of agrominerals into soils may be driven by the quest for mitigating climate change.

Potential application areas need to provide a suitable environment for chemical weathering and be accessible for terrestrial material spreading. Suitable environments are moist and warm, based on the assumption that moisture is needed for dissolution reactions and temperature increases chemical weathering rates (Moosdorf et al., 2014). The best-suited locations are warm and humid areas, particularly in India, Brazil, South-East Asia, and China, where almost 75% of the global potential can be realized (Strefler et al., 2018).

These silicate minerals weathering under laboratory conditions is well documented, little experimental data are available under field conditions. Poorly constrained kinetic parameters of mineral dissolution or precipitation in the field soil-water-plant system hampers accurate prediction of the effectiveness of applying agrominerals for mitigating climate change (Zhang et al., 2019).

The silicate agrominerals have large process and uses but a great challenge is due to low solubility, which need large amounts of rock. If they are not available close to the agricultural areas, it might be uneconomic and unfitted as a whole to extract and transport large volumes of these materials (Lefebvre et al., 2019; van Straaten, 2006). Therefore, basic studies must be encouraged, according to the socioeconomic characteristics on local practices to increase accuracy.

REFERENCES

- ABNT NBR ISO 9001:2018, Sistemas de Gestão da Qualidade – Requisitos.
- Akter, M., Akagi, T., 2005. Effect of Fine Root Contact on Plant-Induced Weathering of Basalt. *Soil Sci. Plant Nutr.* 51, 861-871. <https://doi.org/10.1111/j.1747-0765.2005.tb00121.x>.
- Anda, M., Shamshuddin, J., Fauziah, C.I., 2015. Improving chemical properties of a highly weathered soil using finely ground basalt rocks. *Catena.* 124, 147-161. <https://doi.org/10.1016/j.catena.2014.09.012>.
- Angst, G., Messinger, J., Greiner, M., Häusler, W., Hertel, D., Kirfel, K., Kögel-Knabner, I., Leuschner, C., Rethemeyer, J., Mueller, C.W., 2018. Soil organic carbon stocks in topsoil and subsoil controlled by parent material, carbon input in the rhizosphere, and microbial-derived compounds. *Soil Biol. Biochem.* 122, 19-30. <https://doi.org/10.1016/j.soilbio.2018.03.026>.
- Azevedo, A.C., Kämpf, N., Bohnen, H., 1996. Alterações na dinâmica evolutiva de Latossolo Bruno pela calagem. *Rev. Bras. Cienc. Solo.* 20, 191-198. <https://doi.org/10.1590/S0100-06832000000200006>.
- Anda, M., Shamshuddin, J., Fauziah, C.I., 2015. Improving chemical properties of a highly weathered soil using finely ground basalt rocks. *Catena.* 124, 147-161. <https://doi.org/10.1016/j.catena.2014.09.012>.
- Baggio, S.B., Hartmann, L.A., Bello, R.M.S., 2016. Paralavas in the Cretaceous Paraná volcanic province, Brazil – A genetic interpretation of the volcanic rocks containing phenocrysts and glass. *An. Acad. Bras. Ciênc.* 88, 2167-2193. <https://doi.org/10.1590/0001-3765201620150088>.
- Bakker, E., Lanson, B., Findling, N., Wander, M.M., Hubert, F., 2019. Mineralogical differences in a temperate cultivated soil arising from different agronomic processes and plant K-uptake. *Geoderma.* 347, 210-219. <https://doi.org/10.1016/j.geoderma.2019.04.010>.
- Barshad, I., Kishk, F.M., 1969. Chemical composition of soil vermiculite clays as related to their genesis. *Contrib. Mineral. Petrol.* 24, 136-155. <https://doi.org/10.1007/BF00376887>.
- Basak, B.B., 2018. Waste Mica as Alternative Source of Plant-Available Potassium: Evaluation of Agronomic Potential Through Chemical and Biological Methods. *Nat. Resour. J.* 27, 1-13. <https://doi.org/10.1007/s11053-018-9430-3>.
- Basak, B.B., Sarkar, B., Sanderson, P., Naidu, R., 2018. Waste mineral powder supplies plant available potassium: Evaluation of chemical and biological interventions. *J. Geochem. Explor.* 186, 114-120. <https://doi.org/10.1016/j.gexplo.2017.11.023>.
- Battaglia, S., Leoni, L., Sartori, F., 2004. Determinazione della Capacità di Scambio Cationico delle argille attraverso l'analisi in fluorescenza X di pastiglie di polvere. *Atti Soc. Tosc. Sci. Nat.* 109, 103-113.

- Beerling, D.J., Leake, J.R., Long, S.P., Scholes, J.D., Ton, J., Nelson, P.N., Bird, M., Kantzas, E., Taylor, L.L., Sarkar, B., Kelland, M., DeLucia, E., Kantola, I., Müller, C., Rau, G., Hansen, J., 2018. Farming with crops and rocks to address global climate, food and soil security. *Nature plants*. 4, 138-147.
<https://doi.org/10.1038/s41477-018-0108-y>.
- Berner, R.A., Schott, J., 1982. Mechanism of pyroxene and amphibole weathering II. Observations of soil grains. *Am. J. Sci.* 282, 1214-1231.
<https://doi.org/10.2475/ajs.282.8.1214>.
- Berner, R.A., Berner, E.K., 1997. Silicate Weathering and Climate. In: Ruddiman, W.F.(Ed.). *Tectonic Uplift and Climate Change*. Boston, Massachusetts: Springer, pp. 353-365. https://doi.org/10.1007/978-1-4615-5935-1_15.
- Borden, D., Giese, R.F., 2001. Baseline studies of the Clay Minerals Society Source Clays: Cation exchange capacity measurements by the Ammonia-Electrode Method. *Clays Clay Miner.* 49, 444-445.
<https://doi.org/10.1346/CCMN.2001.0490510>.
- Bowen, N.L., 1922. The Reaction Principle in Petrogenesis. *J. Geol.* 30, 177-198.
- Bray, A.W., Oelkers, E.H., Bonneville, S., Wolff-Boenisch, D., Potts, N.J., Fones, G., Benning, L.G., 2015. The effect of pH, grain size, and organic ligands on biotite weathering rates. *Geochim. Cosmochim. Acta.* 164, 127-145.
<https://doi.org/10.1016/j.gca.2015.04.048>.
- Broadley, M., Brown, P., Cakmak, I., Rengel, Z., Zhao, F., 2012. Function of Nutrients: Micronutrients. In: Marschner, P. (Ed.). *Marschner's Mineral Nutrition of Higher Plants*. London: Academic Press, pp. 191-248.
<https://doi.org/10.1016/B978-0-12-384905-2.00007-8>.
- BS EN ISO 11260, 2011. Soil Quality: determination of Effective Cation Exchange Capacity and Base Saturation Level using Barium Chloride Solution. B. Standards
- Buol, S.W., Eswaran, H., 1999. Oxisols. *Adv. Agron.* 68, 151-195.
[https://doi.org/https://doi.org/10.1016/S0065-2113\(08\)60845-7](https://doi.org/https://doi.org/10.1016/S0065-2113(08)60845-7).
- Burghilea, C., Zaharescu, D.G., Dontsova, K., Maier, R., Huxman, T., Chorover, J., 2015. Mineral nutrient mobilization by plants from rock: influence of rock type and arbuscular mycorrhiza. *Biogeochemistry*. 124, 187-203.
<https://doi.org/10.1007/s10533-015-0092-5>.
- Burghilea, C.I., Dontsova, K., Zaharescu, D.G., Maier, R.M., Huxman, T., Amistadi, M.K., Hunt, E., Chorover, J., 2018. Trace element mobilization during incipient bioweathering of four rock types. *Geochim. Cosmochim. Acta.* 234, 98-114.
<https://doi.org/10.1016/j.gca.2018.05.011>.
- Burke, B.C., Heimsath, A.M., White, A.F., 2007. Coupling chemical weathering with soil production across soil-mantled landscapes. *Earth Surf. Processes. Landforms.* 32, 853 - 873. <https://doi.org/10.1002/esp.1443>.

- Campos, M., Campos, R., 2017. Applications of quartering method in soils and foods. *Int. J. Eng. Res. Appl.* 7, 35-39. <https://doi.org/10.9790/9622-0701023539>.
- Carvalho, A.M., Burle, M.L., Pereira, J., Silva, M.A., 1999. Manejo de adubos verdes no cerrado. Brasília, Embrapa Cerrados. Circular Técnica, 4.
- Chaturika, J.A.S., Indraratne, S.P., Dandeniya, W.S., Kumaragamage, D., 2015. Beneficial management practices on growth and yield parameters of maize (*Zea mays*) and soil fertility improvement. *Trop. Agric. Res.* 27, 59-74. <https://doi.org/10.4038/tar.v27i1.8154>.
- Choo, K.Y., Bai, K., 2016. The effect of the mineralogical composition of various bentonites on CEC values determined by three different analytical methods. *Appl. Clay Sci.* 126, 153-159. <https://doi.org/10.1016/j.clay.2016.03.010>.
- Churchman, G.J., Lowe, D.J., 2012. Alteration, formation, and occurrence of minerals in soils. In: Huang, P.M., Li, Y., Sumner, M.E. (Eds.). *Handbook of Soil Sciences*, 1. Boca Raton: CRC Press, pp. 20.1-20.72. <https://doi.org/10.1201/b11267>.
- Ciceri, D., Allanore, A., 2019. Local fertilizers to achieve food self-sufficiency in Africa. *Sci. Total Environ.* 648, 669-680. <https://doi.org/10.1016/j.scitotenv.2018.08.154>.
- Ciceri, D., Close, T.C., Barker, A.V., Allanore, A., 2019. Fertilizing properties of potassium feldspar altered hydrothermally. *Commun. Soil Sci. Plant Anal.* 50, 482-491. <https://doi.org/10.1080/00103624.2019.1566922>.
- Colombo, C., Palumbo, G., He, J.-Z., Pinton, R., Cesco, S., 2014. Review on iron availability in soil: interaction of Fe minerals, plants, and microbes. *J. Soils Sed.* 14, 538-548. <https://doi.org/10.1007/s11368-013-0814-z>.
- Cruz, S.C.P., Barbosa, J.S.F., Pinto, M.S., Peucat, J.J., Paquette, J.L., de Souza, J.S., Martins, V.D., Chemale, F., Carneiro, M.A., 2016. The Siderian-Orosirian magmatism in the Gavião Paleoplate, Brazil: U-Pb geochronology, geochemistry and tectonic implications. *J. S. Am. Earth Sci.* 69, 43-79. <https://doi.org/10.1016/j.jsames.2016.02.007>.
- Deer, W.A., Howie, R.A., Zussman, J. *An Introduction to the Rock-Forming Minerals*. London, U.K.: Mineralogical Society of Great Britain and Ireland, 2013. <https://doi.org/10.1180/DHZ>.
- Dohnalkova, A., Arey, B., Varga, T., Miller, M., Kovarik, L., 2017. Imaging and Analytical Approaches for Characterization of Soil Mineral Weathering. *Microsc. Microanal. Microstruct.* 23, 2172-2173. <https://doi.org/10.1017/S1431927617011527>.
- Dontsova, K., Zaharescu, Dragos, Henderson, W., Vergheze, S., Perdrial, Nicolas, Hunt, E., Chorover, J., 2014. Impact of organic carbon on weathering and chemical denudation of granular basalt. *Geochim. Cosmochim. Acta.* 139, 508-526. <https://doi.org/10.1016/j.gca.2014.05.010>.

- Edwards, D.P., Lim, F., James, R.H., Pearce, C.R., Scholes, J., Freckleton, R.P., Beerling, D.J., 2017. Climate change mitigation: potential benefits and pitfalls of enhanced rock weathering in tropical agriculture. *Biol Lett.* 13, 1-7. <https://doi.org/10.1098/rsbl.2016.0715>.
- Eggleton, R.A., Foudoulis, C., Varkevisser, D., 1987. Weathering of basalt: changes in rock chemistry and mineralogy. *Clays Clay Miner.* 35, 161-169. <https://doi.org/10.1346/CCMN.1987.0350301>.
- Embrapa. Manual de métodos de análise de solo. Rio de Janeiro: Centro Nacional de Pesquisa de Solos, 2017.
- Essington, M.E. Soil and water chemistry: an integrative approach. Boca Raton: CRC PRESS, 2003. <https://doi.org/10.1201/b12397>.
- Fageria, N.K., Stone, L.F., 1999. Manejo da acidez dos solos de cerrado e de várzea do Brasil. Santo Antônio de Goiás, Embrapa-CNPAF. Documentos,92.
- Fanning, D.S., Keramidas, V.Z., El-Desoky, M.A., 1989. Micas In: Dixon, J.B., Weed, S.B. (Eds.). Madison, Wisconsin: SSSA, pp. 551-634.
- Fischer, G., Nachtergaele, O. F., Prieler, S., van Velthuisen, H., Verelst, L.; Wiberg, D., 2008. HWSD: Global total cultivated land. Land Use Change and Agriculture Program, International Institute for Applied Systems Analysis (IIASA).
- Franzosi, C., Castro, L.N., Celeda, A.M., 2014. Technical evaluation of glauconies as alternative potassium fertilizer from the Salamanca Formation, Patagonia, Southwest Argentina. *Nat. Resour. Res.* 23, 311-320. <https://doi.org/10.1007/s11053-014-9232-1>.
- Gilkes, R.J., McKenzie, R.M., 1988. Geochemistry of manganese in soil. In: Graham, R.D., Hannan, R.J., Uren, N.C. (Eds.). *Manganese in Soils and Plants*, 1. Netherlands: Kluwer academic publishers. pp. 23-34. <https://doi.org/10.1007/978-94-009-2817-6>.
- Gilkes, R.J., Young, R.C., Quirk, J.P., 1972. The oxidation of octahedral iron in biotite. *Clays Clay Miner.* 20, 303-315. <https://doi.org/10.1346/CCMN.1972.0200507>.
- Gilkes, R.J., Young, R.C., Quirk, J.P., 1973. Artificial Weathering of Oxidized Biotite: I. Potassium Removal by Sodium Chloride and Sodium Tetraphenylboron Solutions. *Soil Sci. Soc. Am. Proc.* 37, 25- 28. <https://doi.org/10.2136/sssaj1973.03615995003700010013x>.
- Goedert, W.J., 1983. Management of the Cerrado soils of Brazil: a review. *J. Soil Sci.* 34, 405-428. <https://doi.org/10.1111/j.1365-2389.1983.tb01045.x>.
- Han, L., Sun, K., Jin, J., Xing, B., 2016. Some concepts of soil organic carbon characteristics and mineral interaction from a review of literature. *Soil Biol. Biochem.* 94, 107-121. <https://doi.org/10.1016/j.soilbio.2015.11.023>.

- Harley, A.D., Gilkes, R.J., 2000. Factors influencing the release of plant nutrient elements from silicate rock powders: a geochemical overview. *Nutr. Cycl. Agroecosyst.* 56, 11-36. <https://doi.org/10.1023/A:100985930>.
- Hartemink, A.E., 2002. Soil Science in Tropical and Temperate Regions - Some Differences and Similarities. *Adv. Agron.* 77, 269-292. [https://doi.org/10.1016/S0065-2113\(02\)77016-8](https://doi.org/10.1016/S0065-2113(02)77016-8).
- Hartmann, J., West, A.J., Renforth, P., Köhler, P., De La Rocha, C.L., Wolf-Gladrow, D.A., Dürr, H.H., Scheffran, J., 2013. Enhanced chemical weathering as a geoengineering strategy to reduce atmospheric carbon dioxide, supply nutrients, and mitigate ocean acidification. *Rev. Geophys.* 51, 113-149. <https://doi.org/10.1002/rog.20004>.
- Hawkesford, M., Horst, W., Kichey, T., Lambers, H., Schjoerring, J., Møller, I.S., White, P., 2012. Functions of Macronutrients. In: Marschner, P. (Ed.). *Marschner's Mineral Nutrition of Higher Plants*. London: Academic Press, pp. 135-189. <https://doi.org/10.1016/B978-0-12-384905-2.00006-6>.
- Hinsinger, P., Barros, O.N.F., Benedetti, M.F., Noack, Y., Callot, G., 2001. Plant-induced weathering of a basaltic rock: Experimental evidence. *Geochim. Cosmochim. Acta.* 65, 137-152. [https://doi.org/10.1016/S0016-7037\(00\)00524-X](https://doi.org/10.1016/S0016-7037(00)00524-X).
- Hinsinger, P., Elsass, F., Jaillard, B., Robert, M., 1993. Root induced irreversible transformation of a trioctahedral mica in the rhizosphere of rape. *J. Soil Sci.* 44, 535-545. <https://doi.org/10.1111/j.1365-2389.1993.tb00475.x>
- Hinsinger, P., Jaillard, B., Dufey, J.E., 1992. Rapid weathering of a trioctahedral mica by the roots of ryegrass. *Soil Sci. Soc. Am. J.* 56, 977-982. <https://doi.org/10.2136/sssaj1992.03615995005600030049x>.
- Jones, D.L., 1998. Organic acids in the rhizosphere – a critical review. *Plant Soil.* 205, 25-44. <https://doi.org/10.1023/A:1004356007312>.
- Jones, D.L., Darah, P.R., Kochian, L.V., 1996. Critical evaluation of organic acid mediated iron dissolution in the rhizosphere and its potential role in root iron uptake. *Plant Soil.* 180, 57-66. <https://doi.org/10.1007/BF00015411>.
- Kalinowski, B.E., Schweda, P., 1996. Kinetics of muscovite, phlogopite, and biotite dissolution and alteration at pH 1-4, room temperature. *Geochim. Cosmochim. Acta.* 60, 367-385. [https://doi.org/10.1016/0016-7037\(95\)00411-4](https://doi.org/10.1016/0016-7037(95)00411-4).
- Kamprath, E.J., 1984. Crop response to lime on soils in the tropics. In: Adams, F. (Ed.). *Soil acidity and liming, 2*. Madison: American Society of Agronomy, pp.349-368.
- Kantola, I.B., Masters, M.D., Beerling, D.J., Long, S.P., DeLucia, E.H., 2017. Potential of global croplands and bioenergy crops for climate change mitigation through dep. *Biol. Lett.* 13, 1-7. <https://doi.org/10.1098/rsbl.2016.0714>.

- Karathanasis, A.D., 2002. Mineral Equilibria in Environmental Soil Systems. In: Dixon, J.B., Schulze, D.G. (Eds.). *Soil Mineralogy with Environmental Applications*, 7. Madison, Wisconsin: SSSA, pp. 109-151. <https://doi.org/10.2136/sssabookser7.c4>.
- Keiluweit, M., Bougoure, J.J., Nico, P.S., Pett-Ridge, J., Weber, P.K., Kleber, M., 2015. Mineral protection of soil carbon counteracted by root exudates. *Nat. Clim. Change*. 5, 588-595. <https://doi.org/10.1038/NCLIMATE2580>.
- Kleber, M., Eusterhues, K., Keiluweit, M., Mikutta, C., Mikutta, R., Nico, P.S., 2015. Mineral-Organic Associations: formation, properties, and relevance in soil environments. *Adv. Agron.* 130, 1-140. <https://doi.org/10.1016/bs.agron.2014.10.005>.
- Kong, M., Huang, L., Li, L., Zhang, Z., Zheng, S., Wang, M.K., 2014. Effects of oxalic and citric acids on three clay minerals after incubation. *Appl. Clay Sci.* 99, 207-214. <https://doi.org/10.1016/j.clay.2014.06.035>.
- Lasaga, A.C., 1995. Fundamental approaches in describing mineral dissolution and precipitation rates. *Rev. Mineral. Geochem.* 31, 21-86.
- Lefebvre, D., Goglio, P., Williams, A., Manning, D.A.C., Carlos de Azevedo, A., Bergmann, M., Meersmans, J., Smith, P., 2019. Assessing the potential of soil carbonation and enhanced weathering through Life Cycle Assessment: A case study for Sao Paulo State, Brazil. *J. Clean Prod.* 233, 468-481. <https://doi.org/10.1016/j.jclepro.2019.06.099>.
- Leonardos, O.H., Theodoro, S.H., Assad, M.L., 2000. Remineralization for sustainable agriculture: A tropical perspective from a Brazilian viewpoint. *Nutr. Cycl. Agroecosys.* 56, 3-9. <https://doi.org/10.1023/A:1009855409700>.
- Li, J., Zhang, W., Li, S., Li, X., Lu, J., 2014. Effects of citrate on the dissolution and transformation of biotite, analyzed by chemical and atomic force microscopy. *Appl. Geochem.* 51, 101-108. <https://doi.org/10.1016/j.apgeochem.2014.10.001>.
- Li, T., Wang, H., Wang, J., Zhou, Z., Zhou, J., 2015. Exploring the potential of phyllosilicate minerals as potassium fertilizers using sodium tetraphenylboron and intensive cropping with perennial ryegrass. *Sci Rep.* 5, 1-7. <https://doi.org/10.1038/srep09249>.
- Li, T., Wang, H., Zhou, Z., Chen, X., Zhou, J., 2015. A nano-scale study of the mechanisms of non-exchangeable potassium release from micas. *Appl. Clay Sci.* 118, 131-137. [https://doi.org/DOI: 10.1016/j.clay.2015.09.013](https://doi.org/DOI:10.1016/j.clay.2015.09.013).
- Liu, X., Burras, C.L., Kravchenko, Y.S., Duran, A., Huffman, T., Morris, H., Studdert, G., Zhang, X., Cruse, R.M., Yuan, X., 2002. Overview of Mollisols in the world: Distribution, land use and management. *Can. J. Soil Sci.* 92, 383-402. <https://doi.org/10.4141/CJSS2010-058>.
- Loughnan, F.C. *Chemical Weathering of Silicates*. New York: Elsevier, 1969.

- Machado, R.V., Andrade, F.V., Passos, R.R., Ribeiro, R.C.C., Mendonça, E.S., Mesquita, L.F., 2015. Characterization of ornamental rock residue and potassium liberation via organic acid application. *Rev. Bras. Cienc. Solo.* 40, 1-13. <https://doi.org/10.1590/18069657rbc20150153>.
- Madaras, M., Mayerová, M., Kulhánek, M., Koubová, M., Faltus, M., 2013. Waste silicate minerals as potassium sources: a greenhouse study on spring barley. *Arch. Agron. Soil Sci.* 59, 671-683. <https://doi.org/10.1080/03650340.2012.667079>.
- Malavolta, E., Vitti, G.C., Oliveria, S.A. Avaliação do estado nutricional das plantas: princípios e aplicações. Piracicaba: POTAFOS, 1997.
- Malmström, M., Banwart, S., 1997. Biotite dissolution at 25°C: The pH dependence of dissolution rate and stoichiometry. *Geochim. Cosmochim. Acta.* 61, 2779-2799. [https://doi.org/10.1016/S0016-7037\(97\)00093-8](https://doi.org/10.1016/S0016-7037(97)00093-8).
- Malmström, M., Banwart, S., Duro, L., Wersin, P., Bruno, J., 1995. Biotite and chlorite weathering at 25° C: the dependence of pH and (bi)carbonate on weathering kinetics, dissolution stoichiometry, and solubility; and the relation to redox conditions in granitic aquifers. Stockholm: Swedish Nuclear Fuel and Waste Management Co.
- Manning, D.A.C., 2010. Mineral sources of potassium for plant nutrition. A review. *Agron. Sustain. Dev.* 30, 281-294. <https://doi.org/10.1051/agro/2009023>.
- Manning, D.A.C., 2015. How will minerals feed the world in 2050? *P. Geologist Assoc.* 126, 14-17. <https://doi.org/10.1016/j.pgeola.2014.12.005>.
- Manning, D.A.C., Baptista, J., Limon, M.S., Brandt, K., 2017. Testing the ability of plants to access potassium from framework silicate minerals. *Sci. Total Environ.* 574, 476-481. <https://doi.org/10.1016/j.scitotenv.2016.09.086>.
- Marchi, G., Vilar, C.C., O'Connor, G., Silva, M.L.N., 2015. Surface Complexation Modeling in variable charge soils: charge characterization by potentiometric titration. *Rev. Bras. Cienc. Solo.* 39, 1387-1394. <https://doi.org/10.1590/01000683rbc20140528>.
- Miranda, L.N., Miranda, J.C.C., Rein, T.A., Gomes, A.C., 2005. Utilização de calcário em plantio direto e convencional de soja e milho em Latossolo Vermelho. *Pesq. Agropec. Bras.* 40, 563-572. <https://doi.org/10.1590/S0100-204X2005000600006>.
- Mohammed, S.M.O., Brandt, K., Gray, N.D., White, M.L., Manning, D.A.C., 2014. Comparison of silicate minerals as sources of potassium for plant nutrition in sandy soil. *Eur. J. Soil Sci.* 65, 653-662. <https://doi.org/10.1111/ejss.12172>
- Moosdorf, N., Renforth, P., Hartmann, J., 2014. Carbon dioxide efficiency of terrestrial enhanced weathering. *Environ. Sci. Technol.* 48, 4809-4816. <https://doi.org/10.1021/es4052022>.

- Moraes, L.C.d., Seer, H.J., Marques, L.S.M., 2018. Geology, geochemistry and petrology of basalts from Paraná Continental Magmatic Province in the Araguari, Uberlândia, Uberaba and Sacramento regions, Minas Gerais state, Brazil. *Braz. J. Geol.* 48, 221-241. <https://doi.org/10.1590/2317-4889201820170091>.
- Murakami, T., Ito, J., Utsunomiya, S., Kasama, T., Kozai, N., Ohnuki, T., 2004. Anoxic dissolution processes of biotite: implications for Fe behavior during Archean weathering. *Earth. Planet. Sci. Lett.* 224, 117-129. <https://doi.org/10.1016/j.epsl.2004.04.040>.
- Murakami, T., Utsunomiya, S., Yokoyama, T., Kasama, T., 2003. Biotite dissolution processes and mechanisms in the laboratory and in nature: Early stage weathering environment and vermiculitization. *Am. Mineral.* 88, 377-386. <https://doi.org/10.2138/am-2003-2-314>.
- Naderizadeh, Z., Khademi, H., Arocena, J.M., 2010. Organic matter induced mineralogical changes in clay-sized phlogopite and muscovite in alfalfa rhizosphere. *Geoderma.* 159, 296-303. <https://doi.org/10.1016/j.geoderma.2010.08.003>.
- Navarrete, J.U., Cappelle, I.J., Schnittker, K., Borrok, D.M., 2013. Bioleaching of ilmenite and basalt in the presence of iron-oxidizing and iron-scavenging bacteria. *Int. J. Astrobiol.* 12, 123-134. <https://doi.org/10.1017/S1473550412000493>.
- Navarro, G.R.B., Zanardo, A., Conceição, F.T., 2013a. Metamorphic evolution and P-T path of gneisses from Goiás Magmatic Arc in southwestern Goiás State. *Braz J Geol.* 43, 301-315. <https://doi.org/10.5327/Z2317-48892013000200008>.
- Navarro, G.R.B., Zanardo, A., Da Conceição, F.T., 2013b. O Grupo Araxá na região sul-sudoeste do Estado de Goiás. *Geologia USP. Série Científica.* 13, 5-28. <https://doi.org/10.5327/Z1519-874X2013000200002>
- Norouzi, S., Khademi, H., 2010. Ability of alfalfa (*Medicago sativa* L.) to take up potassium from different micaceous minerals and consequent vermiculitization. *Plant Soil.* 328, 83-93. <https://doi.org/10.1007/s11104-009-0084-0>.
- Nunes, J.M.G., Kautzmann, R.M., Oliveira, C., 2014. Evaluation of the natural fertilizing potential of basalt dust wastes from the mining district of Nova Prata (Brazil). *J. Clean Prod.* 84, 649-656. <https://doi.org/10.1016/j.jclepro.2014.04.032>.
- Oelkers, E.H., Declercq, J., Saldi, G.D., Gislason, S.R., Schott, J., 2018. Olivine dissolution rates: A critical review. *Chem. Geol.* 500, 1-19. <https://doi.org/j.chemgeo.2018.10.008>.
- Palandri, J.L., Kharaka, Y.K., 2004. A compilation of rate parameters of water-mineral interaction kinetics for application to geochemical modelling. Menlo Park, California: U.S. Geological Survey.

- Pozzuoli, A., Vila, E., Franco, E., Ruiz-Amil, A., 1992. Weathering of biotite to vermiculite in Quaternary lahars from Monti Ernici, Central Italy. *Clay Miner.* 27, 175-184. <https://doi.org/10.1180/claymin.1992.027.2.03>.
- Rada, N., 2013. Assessing Brazil's Cerrado agricultural miracle. *Food Policy.* 38, 146-155. <https://doi.org/10.1016/j.foodpol.2012.11.002>.
- Raheb, A., Heidari, A., 2011. Clay mineralogy and its relationship with potassium forms in some paddy and non-paddy soils of northern Iran. *Aust. J. Agr. Resour. Ec.* 2, pp. 169-175
- Ramezani, A., Dahlin, A.S., Campbell, C.D., Stephen, H., Mannerstedt-Fogelfors, B., Öborn, I., 2013. Addition of a volcanic rockdust to soils has no observable effects on plant yield and nutrient status or on soil microbial activity. *Plant Soil.* 367, 419-436. <https://doi.org/10.1007/s11104-012-1474-2>.
- Ramos, C.G., Medeiros, D.S., Gomez, L., Oliveira, L.F.S., Schneider, I.A.H., Kautzmann, R.M., 2019. Evaluation of soil re-mineralizer from by-product of volcanic rock mining: experimental proof using black oats and maize crops. *Nat. Resour. Res.*, 1-18. <https://doi.org/10.1007/s11053-019-09529-x>.
- Ramos, C.G., Querol, X., Oliveira, M.L.S., Pires, K., Kautzmann, R.M., Oliveira, L.F.S., 2015. A preliminary evaluation of volcanic rock powder for application in agriculture as soil a remineralizer. *Sci. Total Environ.* 512-513, 371-380. <https://doi.org/10.1016/j.scitotenv.2014.12.070>
- Reatto, A., Martins, E.S., 2005. Classes de solo em relação aos controles de paisagem do Bioma Cerrado. In: Scariot, A., Silva, J.C.S., Felfilli, J.M., (Eds.). *Cerrado: Ecologia, Biodiversidade e Conservação*. Brasília: Ministério do Meio Ambiente, pp. 47-59.
- Renforth, P., 2012. The potential of enhanced weathering in the UK. *Int. J. Greenh. Gas Control.* 10, 229–243. <https://doi.org/10.1016/j.ijggc.2012.06.011>.
- Resk, D.V.S., Ferreira, E.A.B., Figueiredo, C.C., Zinn, Y.L., 2008. Dinâmica da matéria orgânica no Cerrado. In: Santos, G.A., Silva, L.S., Canellas, L.P., Camargo, F.A.O. (Eds.). *Fundamentos da matéria orgânica do solo: ecossistemas tropicais e subtropicais*. Porto Alegre: Editora Cinco Continentes, pp. 359-417
- Rudmin, M., Oskina, Y., Banerjee, S., Mazurov, A., Soktoev, B., Shaldybin, M., 2018. Roasting-leaching experiments on glauconitic rocks of Bakchar ironstone deposit (Western Siberia) for evaluation their fertilizer potential. *Appl. Clay Sci.* 162, 121-128. <https://doi.org/10.1016/j.clay.2018.05.033>.
- Ryu, J., Vigier, N., Decarreau, A., Lee, S., Lee, K., Song, H., Petit, S., 2016. Experimental investigation of Mg isotope fractionation during mineral dissolution and clay formation. *Chem. Geol.* 445, 135-145. <https://doi.org/10.1016/j.chemgeo.2016.02.006>.
- Samal, D., Kovar, J.L., Steingrobe, B., Sadana, U.S., Bhadoria, P.S., Claassen, N., 2010. Potassium uptake efficiency and dynamics in the rhizosphere of maize (*Zea mays* L.), wheat (*Triticum aestivum* L.), and sugar beet (*Beta vulgaris* L.)

- evaluated with a mechanistic model. *Plant Soil*. 332, 105-121.
<https://doi.org/10.1007/s11104-009-0277-6>.
- Sanchez, P.A. *Properties and Management of Soils in the Tropics*. Cambridge; New York: Cambridge University Press, 2019.
<https://doi.org/10.1017/9781316809785>.
- Sarkar, B., Singh, M., Mandal, S., Churchman, G.J., Bolan, N.S., 2018. Clay Minerals - Organic Matter Interactions in Relation to Carbon Stabilization in Soils. In: Garcia, C., Nannipieri, P., Hernandez, T. (Eds.). *The Future of Soil Carbon*. 71-86. London: Academic Press Elsevier. <https://doi.org/10.1016/B978-0-12-811687-6.00003-1>.
- Schaetzl, R., Anderson, S. *Soils: Genesis and Geomorphology*. New York: Cambridge University Press, 2005.
- Schott, J., Berner, R.A., Sjöberg, E.L., 1981. Mechanism of pyroxene and amphibole weathering - I. Experimental studies of iron-free minerals. *Geochim. Cosmochim. Acta*. 45, 2123-2135. [https://doi.org/10.1016/0016-7037\(81\)90065-X](https://doi.org/10.1016/0016-7037(81)90065-X).
- Schulze, D.G., 2002. An Introduction to Soil Mineralogy. In: Dixon, B., Schulze, D.G. (Eds.). *Soil Mineralogy with Environmental Applications*, 7. Madison, Wisconsin: SSSA, pp. 1-35. <https://doi.org/10.2136/sssabookser7.c1>.
- Scott, A.D., Amonette, J., 1988. Role of Iron in Mica Weathering. In: Stucki, J.W., Goodman, B.A., Schwertmann, U. (Eds.). *Iron in Soils and Clay Minerals*, 217. Dordrecht, Netherlands: Springer, pp. 537-623. [10.1007/978-94-009-4007-9_16](https://doi.org/10.1007/978-94-009-4007-9_16).
- Shafar, J.M., Noordin, W.D., Zulkefly, S., Shamshuddin, J., Hanafi, M.M., 2017. Improving soil chemical properties and growth performance of *Hevea brasiliensis* through basalt application. *Proc. Int. Rubber Conf.*, Bali, Indonesia. <https://doi.org/10.22302/ppk.procirc2017.v1i1.483>.
- Shirale, A.O., Meena, B.P., Gurav, P.P., Srivastava, S., Biswas, A.K., Thakur, J.K., Somasundaram, J., Patra, A.K., Rao, A.S., 2019. Prospects and challenges in utilization of indigenous rocks and minerals as source of potassium in farming. *J. Plant Nutr.* 42, 2682-2701. <https://doi.org/10.1080/01904167.2019.1659353>.
- Silva, R.C.S., 2016. *Intemperismo de minerais de um remineralizador*. PhD. Escola Superior de Agricultura Luiz de Queiroz, Piracicaba, pp. 183.
- Silva, R.C.S., Cury, M.E., Ieda, J.J.C., Sermarini, R.A., Azevedo, A.C., 2017. Chemical attributes of a remineralized Oxisol. *Ciência Rural*. 47, 1-10.
<https://doi.org/10.1590/0103-8478cr20160982>.
- Singh, M., Sarkar, B., Biswas, B., Bolan, N.S., Churchman, G.J., 2017. Relationship between soil clay mineralogy and carbon protection capacity as influenced by temperature and moisture. *Soil Biol. Biochem.* 109, 95-106.
<https://doi.org/10.1016/j.soilbio.2017.02.003>.

- Singh, M., Sarkar, B., Sarkar, S., Churchman, G.J., Bolan, N.S., Mandal, S., Menon, M., Purakayastha, T.J., Beerling, D.J., 2018. Stabilization of Soil Organic Carbon as Influenced by Clay Mineralogy. *Adv. Agron.* 148, 33-84. <https://doi.org/10.1016/bs.agron.2017.11.001>.
- Sousa, D.M.G., Lobato, E. Cerrado: correcao do solo e adubacao. Planaltina, DF: Embrapa Cerrados: Embrapa Informação Tecnológica, 2004.
- Souza, E.D., Costa, S.E.V.G.A., Anghinoni, I., Carvalho, P.C.F., Andrigueti, M.C., E., 2009. Estoques de carbono orgânico e de nitrogênio no solo em sistema de integração lavoura-pecuária em plantio direto, submetido a intensidades de pastejo. *Rev. Bras. Ciênc. Solo.* 33, 1829-1836. <https://doi.org/10.1590/S0100-06832009000600031>.
- Streffer, J., Amann, T., Bauer, N., Kriegler, E., Hartmann, J., 2018. Potential and costs of carbon dioxide removal by enhanced weathering of rocks. *Environ. Res. Lett.* 13, 1-9. <https://doi.org/10.1088/1748-9326/aaa9c4>.
- Tamrat, W.Z., Rose, J., Grauby, O., Doelsch, E., Levard, C., Chaurand, P., Basile-Doelsch, I., 2018. Composition and molecular scale structure of nanophases formed by precipitation of biotite weathering products. *Geochim. Cosmochim. Acta.* 229, 53-64. <https://doi.org/10.1016/j.gca.2018.03.012>.
- Tischendorf, G., Forster, H.J., Gottesmann, B., Rieder, M., 2007. True and brittle micas: composition and solid-solution series. *Mineral Mag.* 71, 285-320. <https://doi.org/10.1180/minmag.2007.071.3.285>.
- Tombolini, F., Brigatti, M.F., Marcelli, A., Cibin, G., Mottana, A., Giuli, G., 2002. Local and average Fe distribution in trioctahedral micas: Analysis of Fe K-edge XANES spectra in the phlogopite–annite and phlogopite–tetraferriphlogopite joins on the basis of single-crystal XRD refinements. *Eur. J Mineral.* 14, 1075-1085. <https://doi.org/10.1127/0935-1221/2002/0014-1075>.
- United States Department of Agriculture (USDA), 2006. *Soil Taxonomy: A Basic System of Soil Classification for Making and Interpreting Soil Surveys*.
- Uroz, S., Calvaruso, C., Turpault, M.-P., Frey-Klett, P., 2009. Mineral weathering by bacteria: ecology, actors and mechanisms. *Trends Microbiol.* 17, 378-387. <https://doi.org/10.1016/j.tim.2009.05.004>.
- Uroz, S., Kelly, L.C., Turpault, M.-P., Lepleux, C., Frey-Klett, P., 2015. The Mineralosphere Concept: Mineralogical Control of the Distribution and Function of Mineral-associated Bacterial Communities. *Trends Microbiol.* 23, 751-762. <https://doi.org/10.1016/j.tim.2015.10.004>.
- van Dam, N.M., Bouwmeester, H.J., 2016. Metabolomics in the rhizosphere: tapping into belowground chemical communication. *Trends Plant Sci.* 21, 256-265. <https://doi.org/10.1016/j.tplants.2016.01.008>.
- van Olphen, H., Fripiat, J.J., 1979. *Data Handbook for Clay Materials and Other Non-Metallic Minerals*, vol 131. Oxford.

- van Straaten, P., 2006. Farming with rocks and minerals: challenges and opportunities. *An. Acad. Bras. Ciênc.* 78, 731-747. <https://doi.org/10.1590/S0001-37652006000400009>.
- Voinot, A., Lemarchand, D., Collignon, C., Granet, M., Chabaux, F., Turpault, M.P., 2013. Experimental dissolution vs. transformation of micas under acidic soil conditions: clues from boron isotopes. *Geochim. Cosmochim. Acta.* 117, 144-160. <https://doi.org/10.1016/j.gca.2013.04.012>.
- Wang, H.Y., Shen, Q.H., Zhou, J.M., Wang, J., Du, C.W., Chen, X.Q., 2011. Plants use alternative strategies to utilize nonexchangeable potassium in minerals. *Plant Soil.* 343, 209-220. <https://doi.org/10.1007/s11104-011-0726-x>.
- Wang, J.G., Zhang, F.S., Cao, Y.P., Zhang, X.L., 2000. Effect of plant types on release of mineral potassium from gneiss. *Nutr. Cycl. Agroecosyst.* 56, 37-44. <https://doi.org/10.1023/A:1009826111929>.
- Wang, X., Yoo, K., Wackett, A.A., Gutknecht, J., Amundson, R., Heimsath, A., 2018. Soil organic carbon and mineral interactions on climatically different hillslopes. *Geoderma.* 322, 71-80. <https://doi.org/10.1016/j.geoderma.2018.02.021>.
- West, A.J., Galy, A., Bickle, M., 2005. Tectonic and climatic controls on silicate weathering. *Earth Planet. Sci. Lett.* 235, 211-228. <https://doi.org/10.1016/j.epsl.2005.03.020>.
- White, A.F., Brantley, S.L., 1995. *Chemical Weathering of Silicate Minerals*. Vol 31. Washington, D.C.: Mineralogical Society of America.
- White, A.F., Brantley, S.L., 2003. The effect of time on the weathering of silicate minerals: why do weathering rates differ in the laboratory and field? *Chem. Geol.* 202, 479-506. <https://doi.org/10.1016/j.chemgeo.2003.03.001>.
- White, R.A., Rivas-Ubach, A., Borkum, M.I., Koberl, M., Bilbao, A., Colby, S.M., Hoyt, D.W., Bingol, K., Kim, Y.-M., Wendler, J.P., Hixson, K.K., Jansson, C., 2017. The state of rhizospheric science in the era of multi-omics: A practical guide to omics technologies. *Rhizosphere.* 3, 212-221. <https://doi.org/10.1016/j.rhisph.2017.05.003>.
- Wilcke, W., Lilienfein, J., 2005. Nutrient Leaching in Oxisols Under Native and Managed Vegetation in Brazil. *Soil Sci. Soc. Am. J.* 69, 1152-1161. <https://doi.org/10.2136/sssaj2004.0350>.
- Wilson, M.J., 2004. Weathering of the primary rock-forming minerals: Processes, products and rates. *Clay Miner.* 39, 233-266. <https://doi.org/10.1180/0009855043930133>.
- Yu, G., 2018. Root Exudates and Microbial Communities Drive Mineral Dissolution and the Formation of Nano-size Minerals in Soils: Implications for Soil Carbon Storage. In: Giri, B., Prasad, R.A.V. (Eds.). *Root Biology*, 52. Springer International Publishing, pp. 143-166. https://doi.org/10.1007/978-3-319-75910-4_5.

- Yu, G., Xiao, J., Hu, S., Polizzotto, M.L., Zhao, F.-J., Mcgrath, S.P., Li, H., Ran, W., Shen, Q., 2017. Mineral availability as a key regulator of soil carbon storage. *Environ. Sci. Technol.* 51, 4960-4969. <https://doi.org/10.1021/acs.est.7b00305>.
- Zavarzina, D.G., Chistyakova, N.I., Shapkin, A.V., Savenko, A.V., Zhilina, T.N., Kevbrin, V.V., Alekseeva, T.V., Mardanov, A.V., Gavrilov, S.N., Bychkov, A.Y., 2016. Oxidative biotransformation of biotite and glauconite by alkaliphilic anaerobes: The effect of Fe oxidation on the weathering of phyllosilicates. *Chem. Geol.* 439, 98-109. <https://doi.org/10.1016/j.chemgeo.2016.06.015>.
- Zhang, G., Kang, J., Wang, T., Zhu, C., 2018. Review and outlook for agromineral research in agriculture and climate mitigation. *Soil Res.* 56, 113-122. <https://doi.org/10.1071/SR17157>.
- Zorb, C., Senbayram, M., Peiter, E., 2014. Potassium in agriculture—status and perspectives. *J. Plant Physiol.* 171, 656-669. <https://doi.org/10.1016/j.jplph.2013.08.008>.

SUPPLEMENTARY MATERIAL

Table S1. Reporting limits for the elements determined by XRF and ICP-OES (SGS Geosol Laboratórios Ltda).

Element	Lower limit	Unit
SiO ₂	0.1	%
Al ₂ O ₃	0.1	%
Fe ₂ O ₃	0.01	%
CaO	0.01	%
MgO	0.1	%
TiO ₂	0.01	%
P ₂ O ₅	0.01	%
Na ₂ O	0.1	%
K ₂ O	0.01	%
MnO	0.01	%
BaO	0.01	%
Cr ₂ O ₃	0.01	%
Cu	3	mg kg ⁻¹
Mo	3	mg kg ⁻¹
Zn	3	mg kg ⁻¹

Table S2. Chemical composition of biotite crystals on biotite schist rock samples determined by EPMA.

Sample	SiO₂	TiO₂	Al₂O₃	FeO	MnO	MgO	CaO	K₂O	BaO	F	Cl	ZnO	H₂O
1	38.28	1.599	17.389	18.92	0.016	10.168	0	8.649	0.264	0.264	0.003	0.07	3.88
2	38.371	1.778	17.745	19.147	0.099	9.954	0.046	8.47	0.005	0.005	0.029	0	4.02
3	37.633	1.73	17.369	18.808	0.115	10.537	0	8.757	0.174	0.008	0.013	0.06	4.00
4	37.405	1.731	18.18	17.396	0.107	11.42	0	8.913	0	0	0.011	0	4.04
5	38.319	1.547	18.355	17.452	0.148	12.027	0	8.755	0.094	0.094	0	0.129	4.00
6	38.509	1.261	18.505	18.738	0.082	11.775	0.03	8.445	0.102	0	0.03	0	4.03
7	37.123	1.656	17.576	18.592	0.066	10.816	0	8.093	0.26	0.14	0.007	0.02	3.95
8	38.775	1.262	17.362	19.142	0.041	9.958	0	8.585	0.348	0.176	0.019	0	3.93
9	37.931	1.647	17.719	19.119	0.099	10.074	0.024	8.374	0.399	0.397	0.011	0.01	3.81
10	38.474	1.468	18.11	17.957	0.082	10.879	0	8.728	0.245	0.091	0.008	0	3.99
11	33.223	0.78	20.225	19.476	0.115	11.93	0.355	3.4	0.072	0	0.005	0	4.10

Table S3. Chemical composition of biotite crystals on biotite syenite rock samples determined by EPMA.

Sample	SiO ₂	TiO ₂	Al ₂ O ₃	FeO	MnO	MgO	CaO	K ₂ O	BaO	F	Cl	Cr ₂ O ₃	H ₂ O
	-----%												
1	37.622	3.686	12.941	24.049	0.115	7.174	0.002	7.899	1.196	0.201	0.066	0.085	3.75
2	36.421	2.671	14.941	24.515	0.134	6.86	0	8.236	0.292	0.203	0.059	0.075	3.76
3	37.481	2.801	13.73	24.009	0.117	6.784	0	7.913	0.652	0.187	0.023	0	3.79
4	38.321	2.86	14.081	24.122	0.087	6.259	0.015	7.885	0.245	0.183	0.052	0.042	3.81
5	37.935	2.762	14.85	24.895	0.192	6.42	0.001	8.055	0.399	0.12	0.022	0.149	3.83
6	38.45	2.964	13.592	23.571	0.197	7.24	0.034	8.409	0.865	0.27	0.025	0	3.75
7	38.351	3.383	13.484	23.171	0.246	7.051	0	8.031	1.019	0.17	0.045	0.136	3.80
8	38.05	3.291	13.442	23.562	0.256	6.84	0	8.101	1.433	0.19	0.063	0.062	3.76
9	38.503	2.766	14.346	23.578	0.117	6.571	0.019	8.127	1.111	0.055	0.04	0.071	3.86
10	38.222	2.415	13.777	24.636	0.147	7.015	0.061	7.796	0.187	0.149	0.049	0	3.82
11	38.402	2.906	14.414	22.981	0.011	6.679	0	8.045	1.349	0.114	0.043	0.04	3.84
12	38.372	2.526	15.152	23.1	0.122	7.027	0.019	8.407	0.471	0.199	0.011	0.061	3.82
13	38.435	2.584	14.159	23.384	0.306	6.665	0	8.318	0.897	0.354	0.035	0.01	3.71
14	38.903	2.779	14.413	24.002	0.084	6.189	0	8.506	0.243	0.189	0.036	0.154	3.81

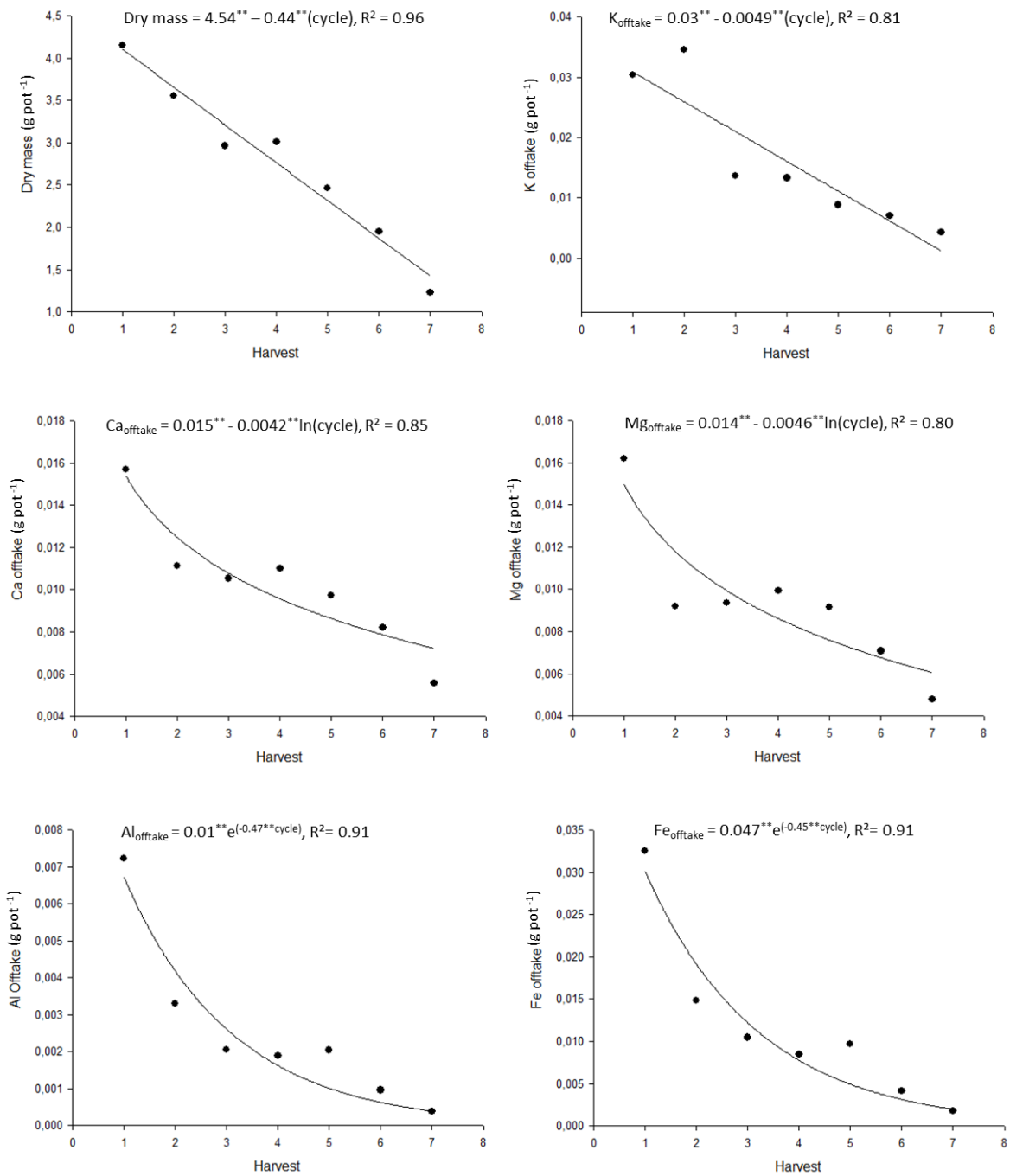


Figure S1. Dry mass and major elements offtake (plant element concentration x dry mass) along the cycles by maize cultivated in basalt rock, selected according to the analysis of variance (ANOVA). Harvest = crop cycle; ** $p < 0.01$.

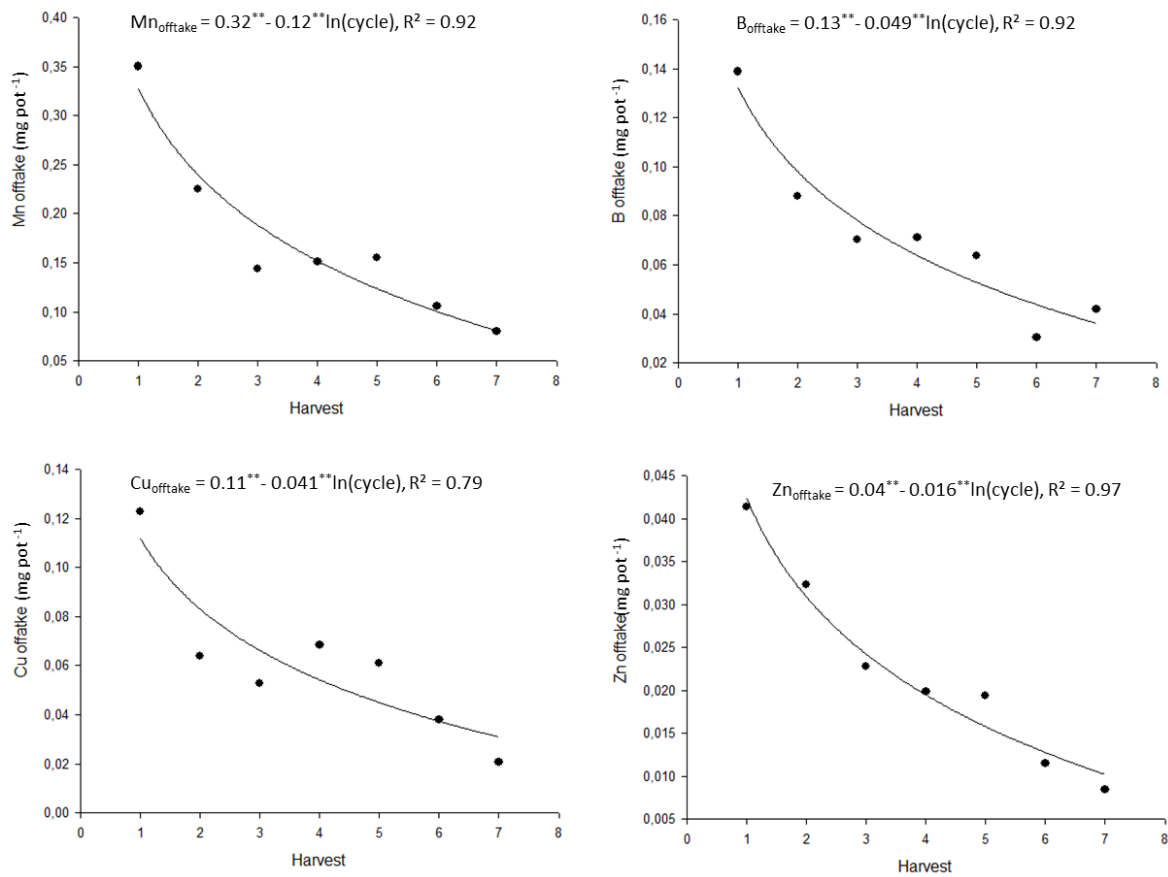


Figure S2. Dry mass and minor elements offtake (plant element concentration x dry mass) along the cycles by maize cultivated in basalt rock, selected according to the analysis of variance (ANOVA). Harvest = crop cycle; ** p < 0.01.

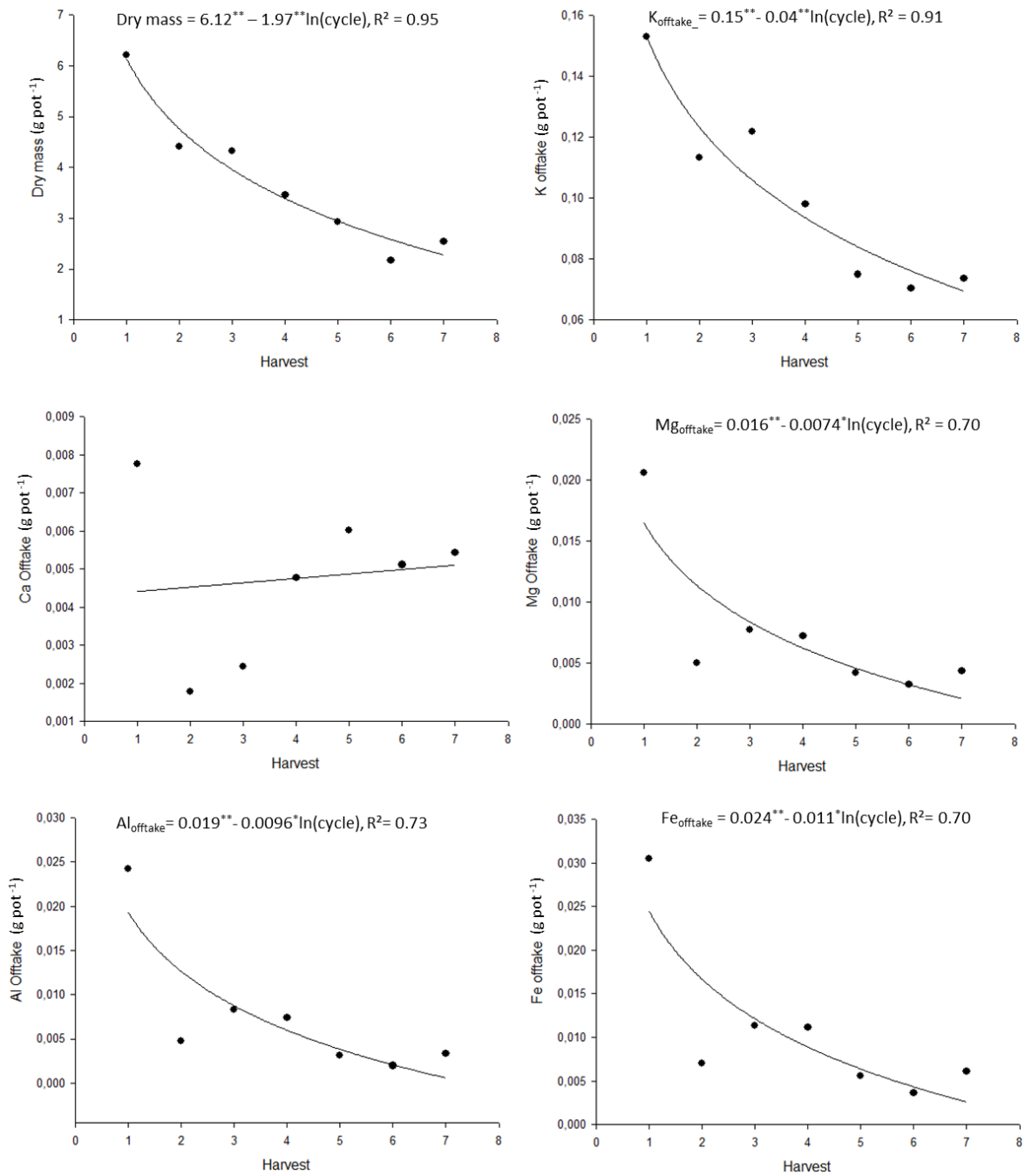


Figure S3. Dry mass and major elements offtake (plant element concentration x dry mass) along the cycles by maize cultivated in biotite schist, selected according to the analysis of variance (ANOVA). Harvest = crop cycle; ** p < 0.01; * p < 0.05.

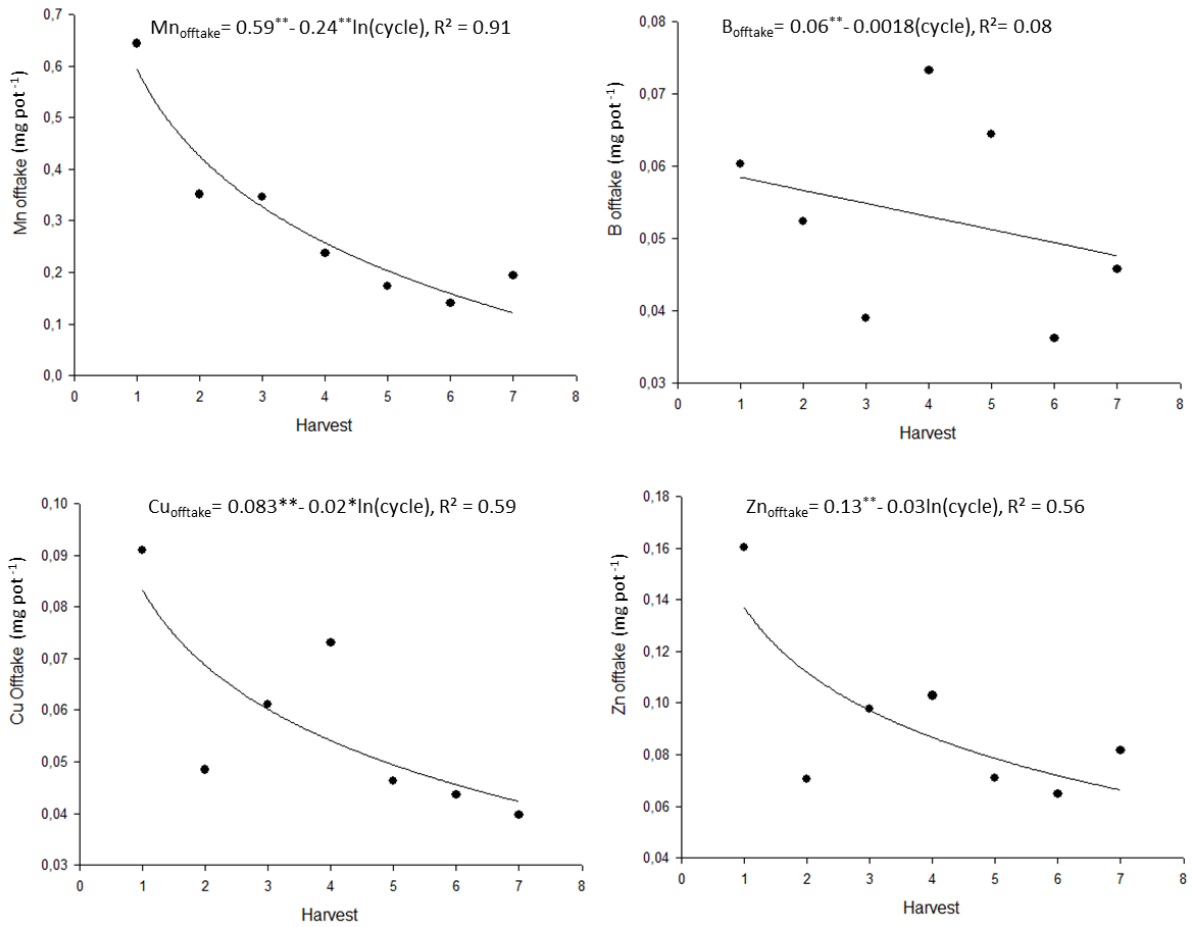


Figure S4. Minor elements offtake (plant element concentration x dry mass) along the cycles by maize cultivated in biotite schist, selected according to the analysis of variance (ANOVA). Harvest = crop cycle; ** p < 0.01; * p < 0.05.

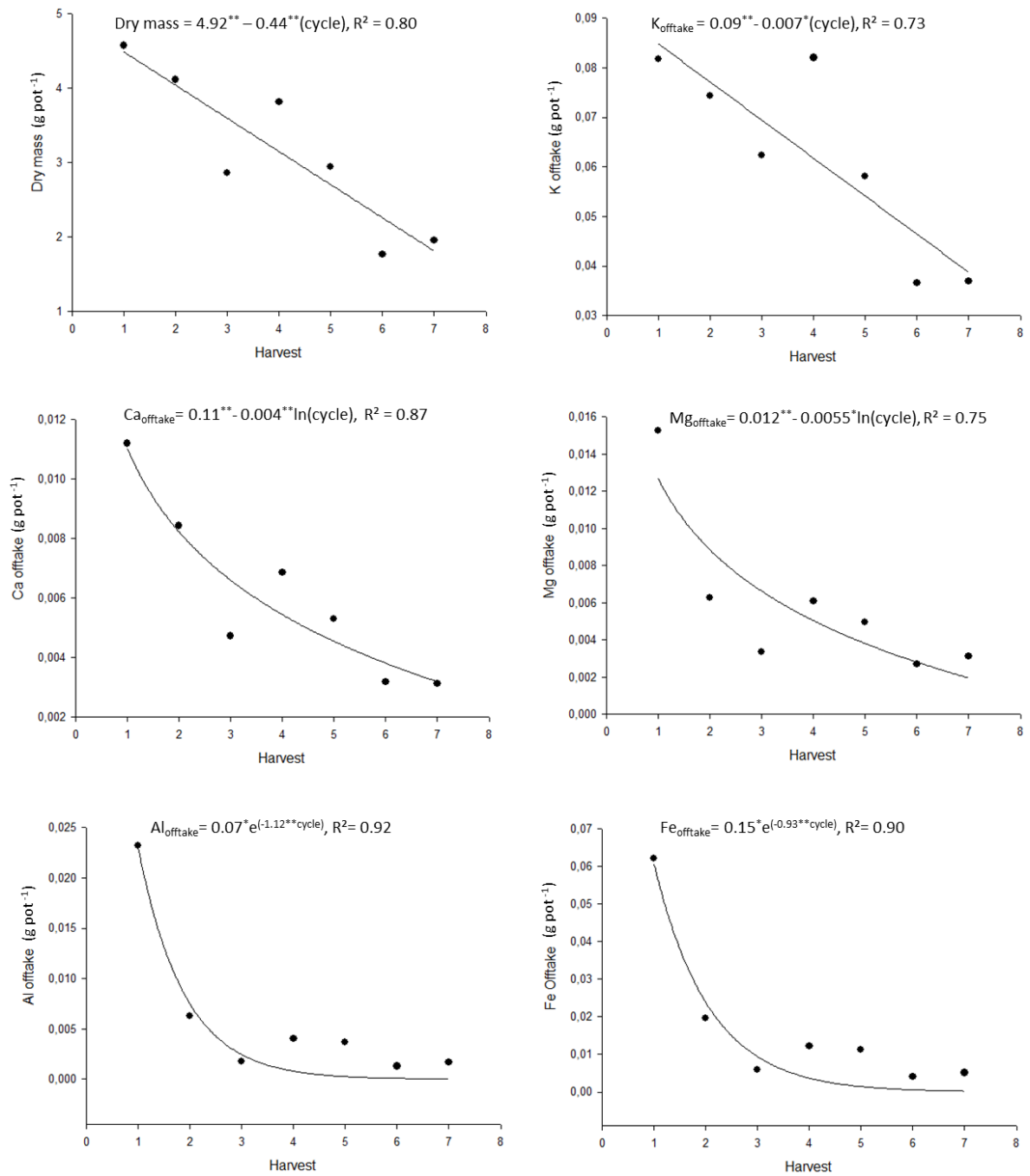


Figure S5. Dry mass and major elements offtake (plant element concentration x dry mass) along the cycles by maize cultivated in biotite syenite, selected according to the analysis of variance (ANOVA). Harvest = crop cycle; ** $p < 0.01$; * $p < 0.05$.

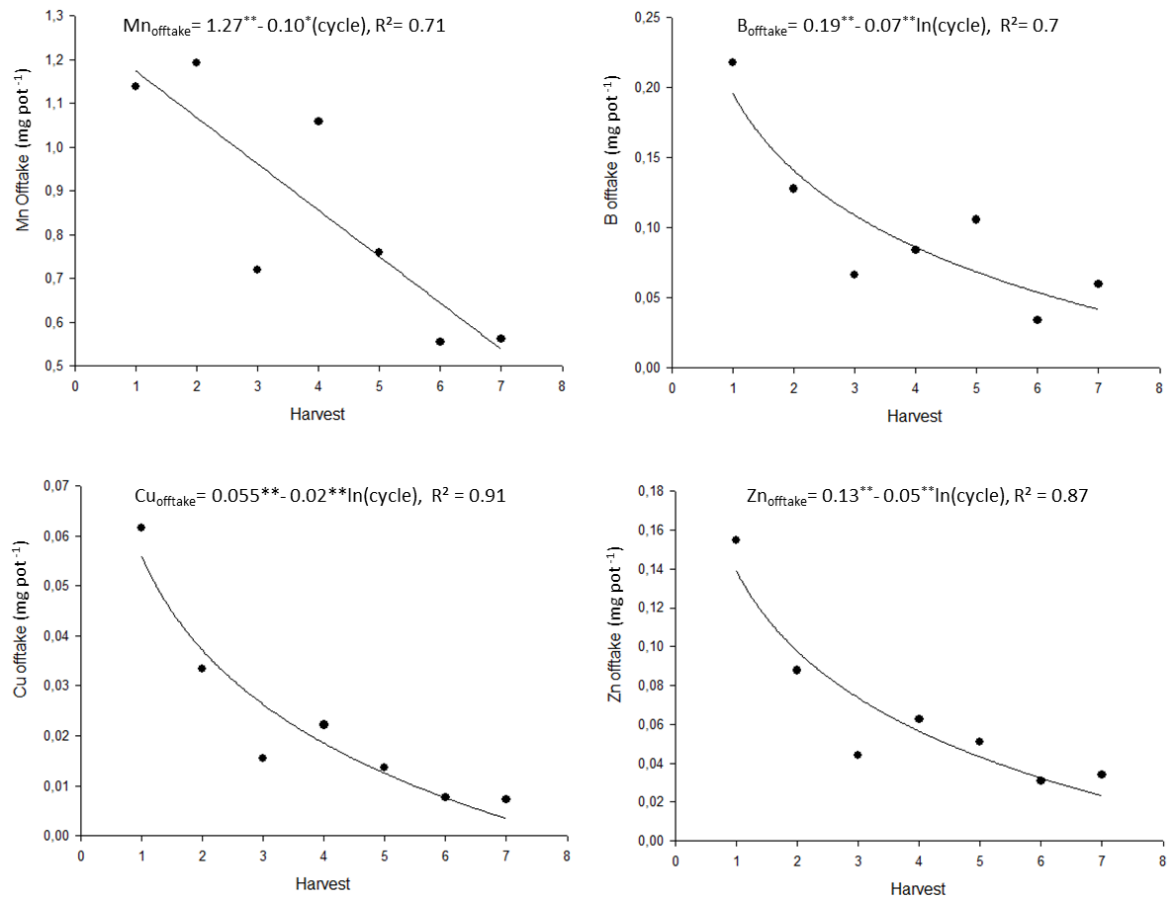


Figure S6. Minor elements offtake (plant element concentration x dry mass) along the cycles by maize cultivated in biotite syenite, selected according to the analysis of variance (ANOVA). Harvest = crop cycle; ** p < 0.01; * p < 0.05.

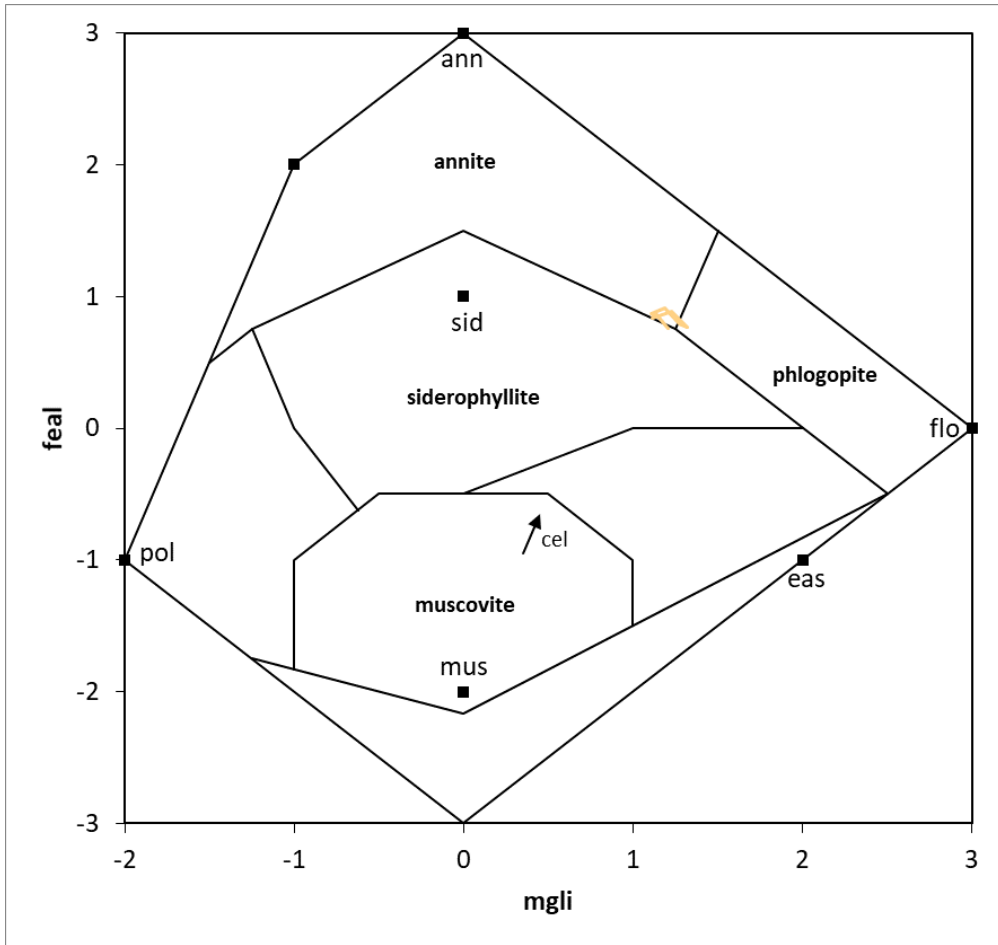


Figure S7. Classification diagram of biotite crystals on biotite schist samples obtained by EPMA.

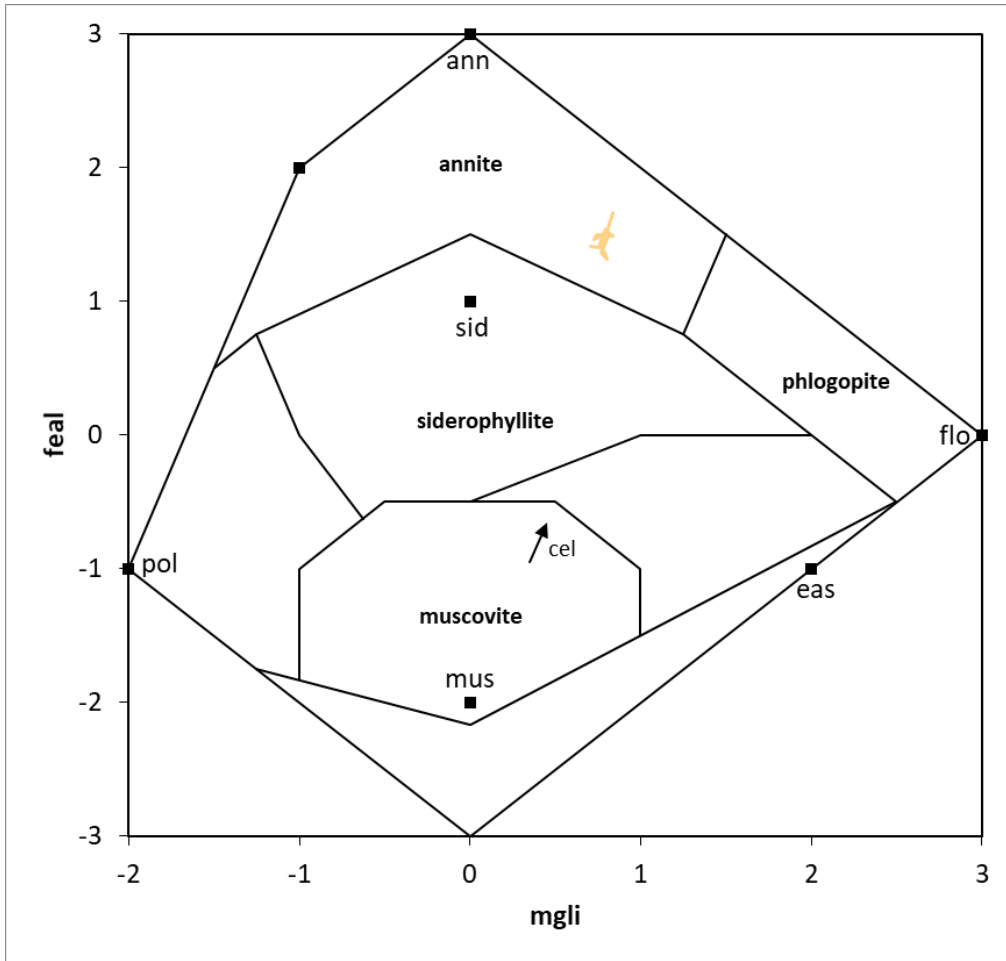


Figure S8. Classification diagram of biotite crystals on biotite syenite samples obtained by EPMA.